

	Short Stable Cavities Preliminary Design	Date 2024-05-22 VIR-0461A-24 Page 1 of 101
---	--	--



Short Stable Cavities Preliminary Design

VIR-0461A-24

The Virgo Collaboration

Document Control

Rel.	Date	Changes / Notes
VIR-0461A-2 4	2024-05-2 2	Document approved after circulation among authors and SSMs. Preliminary design document built on conceptual design document (VIR-0026A-24) and Q&A (VIR-0082A-24) document from IRC
Approval	Approved on 2024-05-22 by A. Rocchi	

Table of Contents

- List of Acronyms..... 4**
- 1. Introduction..... 6**
 - 1.1. Scope of the document..... 6
 - 1.2. Motivations..... 6
 - 1.3. Optical requirements..... 8
 - 1.3.1. Gouy phase..... 8
 - 1.3.2. Aberrations..... 9
 - 1.4. Displacement noise requirements..... 10
 - 1.4.1. Introduction..... 10
 - 1.4.2. Requirements for AdV+ Phase II..... 10
 - 1.4.3. Requirements for Virgo_nEXT i.e. postO5..... 12
- 2. Short Stable Recycling Cavities..... 15**
 - 2.1. Layout..... 15
 - 2.2. Optical configuration..... 17
 - 2.2.1. Principle..... 17
 - 2.2.2. Short cavity layout..... 18
 - 2.3. Auxiliary beams..... 30
 - 2.3.1. Overview..... 30
 - 2.3.2. Beam images..... 31
 - 2.4. Modulation frequencies and Gouy phases..... 34
 - 2.4.1. Introduction..... 34
 - 2.4.2. Modulation frequencies..... 34
 - 2.4.3. Gouy phase inside PR cavity..... 35
 - 2.4.4. Gouy phase inside SR cavity..... 36
 - 2.4.5. Summary..... 38
 - 2.5. Interferometer sensing and control..... 39
 - 2.5.1. Microscopic length and control sidebands..... 39
 - 2.5.2. Simulation of the error signals..... 40
 - 2.5.3. Angular Control..... 44
 - 2.6. Thermal effects..... 45
 - 2.6.1. Introduction..... 45
 - 2.6.2. Thermal effects evaluation..... 45
 - 2.6.3. OSCAR simulations..... 47
 - 2.6.4. Comparison with marginally stable configuration..... 49

2.6.5. OSCAR results with 80 W of input power.....	49
2.7. Mirrors.....	51
2.7.1. Introduction.....	51
2.7.2. PRM1/SRM1.....	51
2.7.3. PRM2/SRM2.....	52
2.7.4. PRM3/SRM3.....	53
2.8. Thermal control: PRM3/SRM3.....	55
2.9. Injection: SIB1.....	56
2.9.1. General considerations.....	56
2.9.2. SIB1 considerations.....	57
2.9.3. PR bench considerations.....	58
2.9.4. Mode-Matching Telescope.....	58
2.10. Detection: SDB1.....	60
2.10.1. Introduction.....	60
2.10.2. Possible optical scheme for the SRB and SDB1 benches.....	61
2.10.3. Mode-Matching Telescope.....	65
2.10.4. Compatibility with future upgrades.....	66
2.11. Detection: Pick-off.....	67
2.11.1. Path for the extraction of the power recycling cavity pick-off.....	67
2.11.2. Mode-Matching Telescope.....	67
2.12. Suspensions.....	69
2.12.1. Introduction.....	69
2.12.2. Technology.....	69
2.12.3. Suspensions for SRM3/PRM3 and SRM2/PRM2.....	74
2.12.4. Suspensions for SIB1, PRM1, SDB1, SRM1 optical benches.....	77
2.13. Vacuum.....	84
2.13.1. General Overview.....	84
2.13.2. Tanks.....	85
2.13.3. Pumps & Materials.....	87
2.13.4. Dust Control.....	87
2.13.5. Tanks structure.....	88
2.14. Infrastructure.....	94
2.14.1. Introduction.....	94
2.14.2. Description of the needed modification works.....	95
3. Costs.....	99
4. Schedule.....	99
5. Risk assessment.....	100



List of Acronyms

ACL	Algorithms for Control and Locking
AdV+	Advanced Virgo Plus
AoI	Angle of Incidence
AR	Anti-Reflecting
BS	Beam Splitter
CARM	Common Arm Length
CEB	Central Building
CITF	Central Interferometer
CP	Compensation Plate
DAQ	Data Acquisition
DARM	Differential Arm Length
DOF	Degree Of Freedom
EMS	Environmental Monitoring System
ETM	End Test Mass
FEA	Finite Element Analysis
FP	Fabry-Perot
FSR	Free Spectral Range
GAS	Geometric Anti-Springs
GW	Gravitational Wave
HOM	Higher Order Modes
HR	High Reflectivity
HVAC	Heating, Ventilation and Air Conditioning
IMC	Input Mode Cleaner
INJ	Injection
IPC2	Input Power Control 2
ISC	Interferometer Sensing and Control
ITF	Interferometer
ITM	Input Test Mass



IVC	Intermediate Vacuum Chamber
LVDT	Linear Variable Differential Transformer
MICH	Michelson Length
OMC	Output Mode Cleaner
OPL	Optical Path Length
PRC	Power Recycling Cavity
PRM	Power Recycling Mirror
PSTAB	Power Stabilization
PZT	Piezo-electric Transducer
RFC	Reference Cavity
RH	Ring Heater
RoC	Radius of Curvature
RTPC	Real-Time PC
SAT	Super Attenuators
SB	SideBand
SBE	Suspended Benches
SDB1	Suspended Detection Bench 1
SIB1	Suspended Injection Bench 1
SIB2	Suspended Injection Bench 2
SIN	Squeezing Injection
SLC	Stray Light Control
SPOB	Suspended Pick-Off Bench
SRC	Signal Recycling Cavity
SRM	Signal Recycling Mirror
SSFS	Second Stage Frequency Stabilization
TCS	Thermal Compensation System
TEM	Transverse Electromagnetic Mode
TOLM	Timing and Optical Link Module
VAC	Vacuum

	Short Stable Cavities Preliminary Design	Date 2024-05-22 VIR-0461A-24 Page 6 of 101
---	--	--

1. Introduction

1.1. Scope of the document

Scope of this document is to provide an overview of the design and construction of stable recycling cavities in Virgo in view of the next observing run (O5). It serves as a foundational guide outlining the initial concepts, requirements, and strategies for the proposed project. The document is intended to provide stakeholders, team members, and other involved parties with a clear understanding of the project's motivations, objectives, and initial design considerations.

The document is not meant to reach the level of maturity expected in a Technical Design Report, as the primary focus of the AdV+ Project in the coming months will be its preparation.

1.2. Motivations

The commissioning of Advanced Virgo Plus has shown the difficulties of using marginally stable recycling cavities in a dual-recycled interferometer. These difficulties originate from two main issues.

Due to the degeneracy of the cavities, the high order modes (HOMs) of the modulation sidebands are resonant in the power recycling (PRC) and signal recycling (SRC) cavities. This situation makes them very sensitive to small wave-front deformations, originating from mirror imperfections, thermal effects and misalignments (as the HOMs created by these defects are amplified). It is not just a matter of scalar losses affecting the recycling gains of the sidebands and so the signal-to-noise ratio of the locking & alignment signals. The field's wave-fronts are deformed in a way that it is difficult to predict, depending on the exact shape of the mirror's surface or thermal deformations. The consequence is that many of the locking and alignment error signals carried by interference between the modulation sidebands and the carrier field are unreliable. In particular, their zero cannot be trusted since they are affected by offsets that can change during the commissioning and operation of the interferometer (see [VIR-0047B-23](#), [VIR-1361A-21](#), [VIR-0039A-23](#)). Due to these offsets the coupling of demodulation noises is largely increased.

Using resonant sidebands extraction with the signal recycling mirror requires the carrier to be anti-resonant in the SRC. As a consequence, the HOMs of the carrier are all resonant in this cavity. Since the field exiting the interferometer from the beam-splitter mainly consists of HOMs originating from the imperfect interference between the two interferometer arm cavities, these imperfections get amplified by the SRC and degrade the interferometer contrast (see [VIR-0923A-22](#) and [VIR-0972A-22](#)). It has been found to be an order of magnitude larger than during O3 ($1-C \sim 10^{-3}$), meaning that the total power on the dark fringe is about 100 times larger than the power on the TEM00 which is carrying the gravitational

	Short Stable Cavities Preliminary Design	Date 2024-05-22 VIR-0461A-24 Page 7 of 101
---	--	--

wave (GW) signal. This favors the transmission of input beam noises to the output port. Moreover, the losses originating from the SRC degeneracy also affect the squeezing performances, which are very sensitive to losses (see [VIR-0239A-23](#)). It has indeed not been possible to obtain a significant improvement in the sensitivity by injecting a squeezed beam in the interferometer.

Other issues related to marginally stable cavities, e.g. the risks related to the extraction of spurious beams originating from secondary faces of input test masses, beam splitter and compensation plates, are described in the document “The need for stable recycling cavities in Virgo-nEXT” ([VIR-0047B-23](#)).

The issues discussed above get worse as the power is increased, which makes reaching the design value of the input power for Advanced Virgo (125 W) not realistic.

This situation motivates the proposal to adopt stable recycling cavities and implement them after O4.

	Short Stable Cavities Preliminary Design	Date 2024-05-22 VIR-0461A-24 Page 8 of 101
---	--	--

1.3. Optical requirements

1.3.1. Gouy phase

The defining feature of stable recycling cavities is that the transverse mode fields (TEM_{mn} modes) have a different resonance condition than the TEM₀₀ carrier field. This is in contrast to the marginally stable cavities currently implemented in Virgo, where the higher-order modes are practically co-resonant with the carrier. The lack of such mode discrimination leads to observed problems in the operational stability: large increase of the contrast defect due to the enhancement of HOMs, offsets on control signals (due to sidebands higher order modes) which vary with thermal effects leading to entanglement of ISC and TCS tunings.

The way to achieve mode discrimination is by introducing an overall Gouy phase shift for a round-trip in the cavity. Gouy phase is an additional phase shift that a focussed Gaussian beam incurs when compared to a plane-wave approximation, and is mostly accumulated around the focus (90 deg of this phase shift happens within the Rayleigh range before and after the point of focus):

$$\phi_G = - \arctan \left(\frac{z}{z_R} \right).$$

Higher-order modes incur an integer multiple of this Gouy phase shift, according to

$$\phi = (m + n + 1)\phi_G.$$

Therefore, the resonance condition of higher order modes changes. In practice, the Gouy phase shift should be at least so large that the resonance peaks of subsequent modes are well separated, and at the same time should avoid hitting numbers that divide 180 deg with a low multiplier, as otherwise low-ordered higher order modes would again become co-resonant with the carrier. A Gouy phase somewhere between 15 deg and 30 deg is generally aimed for, with the exact value to be determined considering the carrier and sideband resonance conditions (see Section on "Modulations frequencies and Gouy phases".)

Since a beam waist is necessary to accumulate significant Gouy phase, any stable recycling cavity implementation has to include focussing elements. Two main approaches exist, as e.g. discussed in [Arain, Müller; <https://doi.org/10.1364/OE.16.010018>]. In the simplest case, a single concave mirror can focus the beam down to a waist, with the actual recycling mirror placed at the right location just in front of the waist, at approximately the Rayleigh range. To not have a too hard focus (and correspondingly high

	Short Stable Cavities Preliminary Design	Date 2024-05-22 VIR-0461A-24 Page 9 of 101
---	--	--

beam intensities) at the recycling mirror, the focal length of the focusing mirror needs to be quite large, approaching 100 m. This configuration is therefore called the “long” solution.

The other option is to focus the beam much stronger, but implement a second, convex mirror, which defocuses the beam again. In effect, this shrinks down the necessary path length to get to a similarly sized focus, at the expense of an additional optical element. This is the “short” solution. For achieving a particular Gouy phase, the two options perform in exactly the same way.

1.3.2. Aberrations

Necessarily, the two configurations employ curved mirror surfaces that are hit under an angle; a single such surface in the case of the long solution, and two such surfaces for the short solution. This leads to astigmatism, i.e. the focal plane in the sagittal and tangential direction is no longer coincident and the beam becomes elliptical. As a consequence, the mode matching between arm cavities (which are anastigmatic) and the recycling cavities, as well as the injection and detection systems, will be degraded. In addition, a different focus in the two directions also leads to a different Gouy phase and thus to a mode resonance splitting. Therefore, this effect should be kept to a minimum; in the design phase we have targeted a maximum (additional) loss of 1000 ppm due to astigmatism, with impact on e.g. alignment control still to be evaluated. In the long configuration, the long distances and relatively large focal lengths involved naturally reduce the amount of astigmatism. In the short configuration, angles of incidence are larger and focal lengths are shorter, potentially leading to large astigmatic loss. However, as will be shown in the optical layout for this configuration, a particular arrangement of the optics can be used ([VIR-NOT-LAS-1390-12](#)) where astigmatism introduced by the first optical element is almost completely cancelled by the second element.

	Short Stable Cavities Preliminary Design	Date 2024-05-22 VIR-0461A-24 Page 10 of 101
---	--	---

1.4. Displacement noise requirements

1.4.1. Introduction

The motion of mirrors forming the recycling cavities can show up in the gravitational wave channel depending on the coupling of the recycling cavity lengths to the variation of power on the dark fringe. The detailed calculation shows that the coupling is much larger for the signal recycling mirrors than for the power recycling mirrors. In the following of this section we will thus limit ourselves to the case of the signal recycling mirrors and we will deduce the displacement noise requirements for these mirrors. The requirements for the power recycling mirror are less stringent by a factor which depends on interferometer imperfections like the common mode rejection factor, the finesse asymmetry etc. At this stage we will apply the requirements for the signal recycling mirrors also to the power recycling mirrors. If necessary the latter can be relaxed.

1.4.2. Requirements for AdV+ Phase II

The coupling of the signal recycling cavity length (SRCL) to the interferometer output signal is driven by the amplitude of the local oscillator used to detect the gravitational wave signal and settled by the so-called differential arm (DARM) offset. This local oscillator field reaches the signal recycling mirror and part of it is reflected back toward the interferometer. The phase of this field varies with the SRCL i.e with the signal recycling mirrors displacement noise. The resonance condition of this field in the signal recycling cavity is such that when these field fluctuations reach the beam splitter and interfere with the main beam coming from the power recycling cavity, they induce anti correlated power fluctuations at the input of the arm cavities. The latter produce a fluctuating radiation pressure in the arms that is differential, so a noise in the gravitational wave channel. This noise increases linearly with the power stored in the arm cavity and with the settled differential arm length creating the local oscillator. Instead it decreases with the mirror inertia so it is inversely proportional to the mass x frequency². The exact calculation gives the following relationship between the SRCL variation δl_{SRCL} and the gravitational wave channel:

$$h(f) = \frac{6 \cdot 10^{-4}}{L} \left(\frac{40 \text{ kg}}{M} \right) \left(\frac{10 \text{ Hz}}{f} \right)^2 \left(\frac{P_{arm}}{400 \text{ kW}} \right) \left(\frac{DARM}{1 \text{ pm}} \right) \delta l_{SRCL}(f) \quad (1)$$

Where L is the arm length, M the mirror mass, f the frequency, P_{arm} the power stored in the interferometers arm and DARM the offset in the arm differential length settled to create the local oscillator field at the interferometer output (see [LIGO-T080192](#) and [LIGO-T010007](#)). This relation has been also verified using the Optickle software. The SRCL to h(f) transfer function obtained with Optickle

is shown in the Figure below, with formula (1) shown in red and the Optickle simulation in blue, for $P_{arm} = 400$ kW and $DARM = 1$ pm. Note that the numerical simulation deviates above 300 Hz from formula (1) due to the combined SR and arm cavity pole.

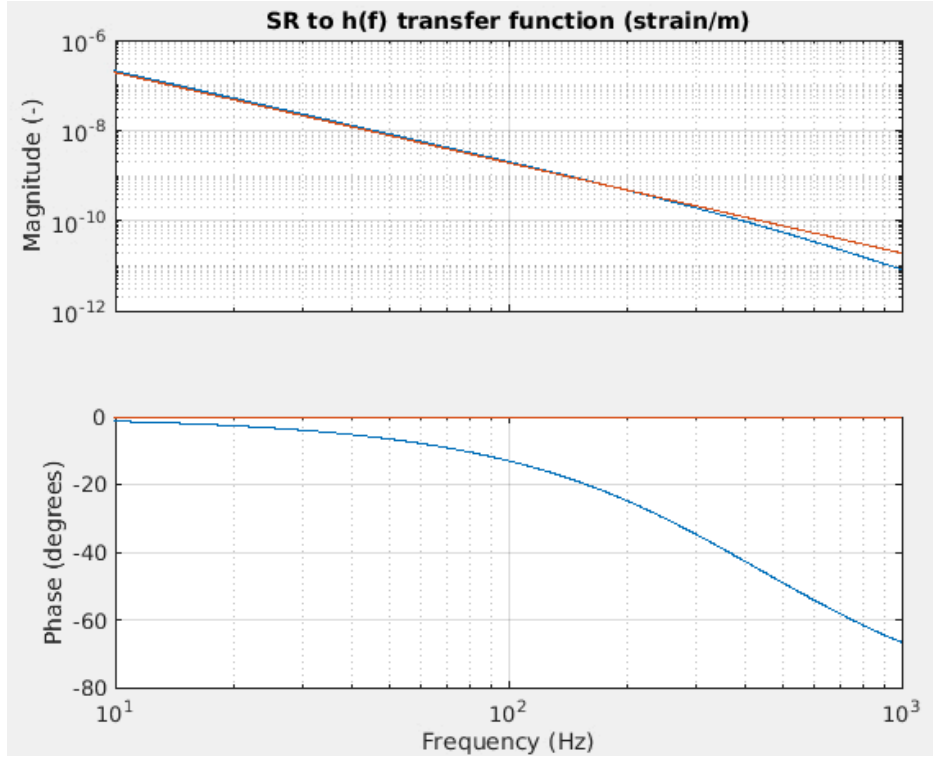


Figure 1 - Transfer function SRCL \rightarrow h (strain/m) using the parameters of AdV+ Phase II and assuming a DARM offset of 1 pm.

Since the signal recycling cavity is formed by three mirrors, two of which are folding the beam, the variation of the SRCL can be expressed as:

$$\delta l_{SRCL} = \sqrt{4 \cdot \delta z_{SRM3}^2 + 4 \cdot \delta z_{SRM2}^2 + \delta z_{SRM1}^2} \quad (2)$$

meaning that the signal recycling mirror SRM1 contributes to only 11% of the total energy of the signal recycling cavity length variation and the other two mirrors (SRM2 and SRM3) to about 45% each.

Knowing that for AdV+ Phase II the design value for P_{arm} is 400 kW and assuming DARM equal to 2 pm (this value have already been achieved during O2, O3 and during the commissioning of O4), one can

deduce the required $dl_{SRCL}(f)$ noise necessary to keep this noise source a **factor of ten below** the design sensitivity of AdV+ Phase II ([VIR-0501C-22](#)). The results is given in the table below:

	10 Hz	100 Hz
dl_{SRCL}	$3e-17$ m/sqrt(Hz)	$7e-17$ m/sqrt(Hz)

As expected, given that the coupling decreases with the frequency², the effect is more relevant at 10 Hz. At 10 Hz this requirement can be achieved if each mirror composing the signal recycling cavity has a displacement noise smaller than **$1e-17$ m/sqrt(Hz)**. Alternatively, if SRM2 and SRM3 are affected by a displacement noise of $5e-18$ m/sqrt(Hz) then the SR1 displacement noise at 10 Hz can be as large as $2e-17$ m/sqrt(Hz). Not surprisingly, these requirements are about three orders of magnitude less stringent than the equivalent requirements for the arm cavity mirrors. As a consequence, requirements on control noises, thermal noise and seismic noise of the suspensions used for these mirrors are considerably less stringent than the ones of the main mirrors.

1.4.3. Requirements for Virgo_nEXT i.e. postO5

The calculation above applies to the case of an interferometer operated in the DC readout configuration like AdV+. If the balanced homodyne technique is used, as it is planned for Virgo_nEXT, a different modeling is necessary. When balanced homodyne is used to extract the gravitational wave signal, the DARM offset is set to zero thus nulling the local oscillator created at the interferometer output. The remaining carrier at the output of the interferometer is then determined by the interferometer contrast defect. Note that what matters is the field transmitted by the output mode-cleaner so the TEM00 component of the output field. Compare to the previous case of DC readout, this residual TEM00 field at the interferometer output is on the opposite quadrature. As a consequence its reflection from the signal recycling mirror towards the interferometer does not produce radiation pressure noise anymore. The coupling into the gravitational wave signal takes place via the phase fluctuation of this residual field generated by the variation of the signal recycling cavity length. An Optickle simulation was done to evaluate the coupling in the case of Virgo_nEXT i.e. with a power in the arms equal to 1.5 MW (i.e. about ten times larger than the power stored in the arms nowadays with 23 W of input power). The simulation assumed 1 mW of power on the TEM00 mode i.e. ten times more than what was measured during the O4 commissioning with 23 W input power, simulated using a 15 ppm difference in round trip losses between the two arms. The SRCL to $h(f)$ coupling calculated with Optickle is shown in the Figure below. Figure 2 also shows the coupling of the displacement noise of the beam splitter that combines the local oscillator with the interferometer output.

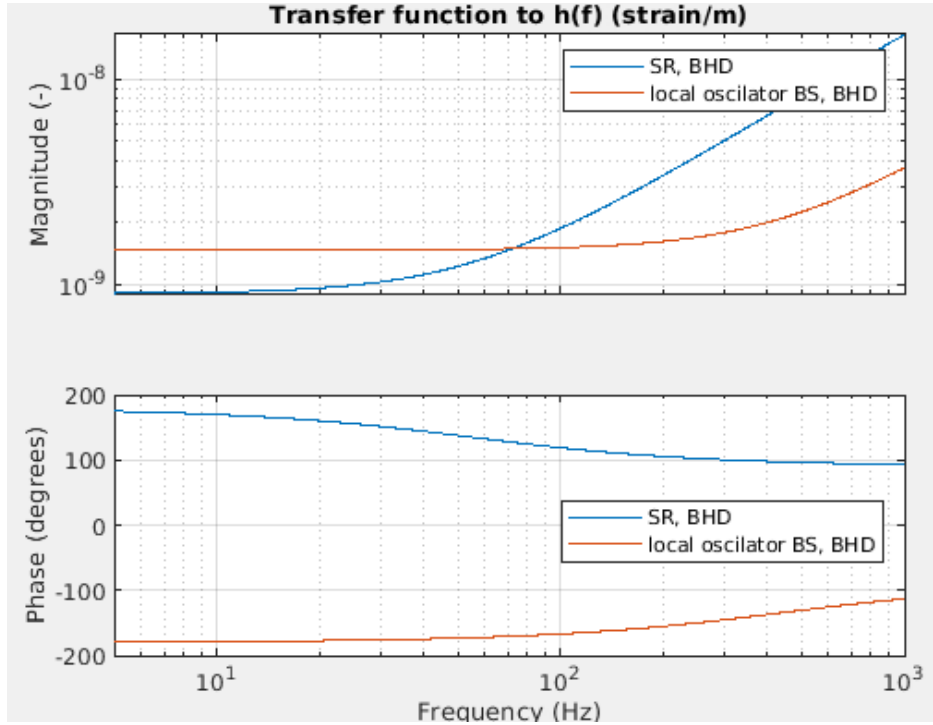


Figure 2 - Transfer function SRCL → h (in blue) and local oscillator beam splitter → h (in red) using the parameters of Virgo_nEXT and assuming strain detection with balanced homodyne .

The noise in h generated by the SRCL variation is about:

$$h = \frac{3 \cdot 10^{-6}}{L} \delta l_{SRCL} \text{ at } 10 \text{ Hz} \quad (3)$$

$$h = \frac{6 \cdot 10^{-6}}{L} \delta l_{SRCL} \text{ at } 100 \text{ Hz} \quad (4)$$

Given the best sensitivities expected for Virgo_nEXT ([VIR-0497D-22](#)) the requirements for δl_{SRCL} and δl_{LO} are:

	10 Hz	100 Hz
δl_{SRCL}	3e-15 m/sqrt(Hz)	7e-17 m/sqrt(Hz)
δl_{LO}	2e-15 m/sqrt(Hz)	9e-17 m/sqrt(Hz)

At 10 Hz this requirement can be achieved if each mirror composing the signal recycling cavity has a displacement noise smaller than **1e-15 m/sqrt(Hz)**. The requirements for the optical path of the local

	Short Stable Cavities Preliminary Design	Date 2024-05-22 VIR-0461A-24 Page 14 of 101
---	--	---

oscillator are very similar. It is worth noting that the noise coupling increases with the square root of the TEM00 power reaching the dark fringe. Thus, if this power increases to e.g. 10 mW the corresponding displacement noise requirements at 10 Hz will decrease to $3e-16$ m/sqrt(Hz). Thus the balanced homodyne technique relaxes considerably the coupling of SRCL to DARM and so the requirement on the signal recycling mirrors displacement noise at 10 Hz.

2. Short Stable Recycling Cavities

2.1. Layout

In the short recycling cavities scheme, each recycling cavity will consist of three mirrors that are implemented in the central building. As seen from the main beam splitter, the beam will travel to the concave SRM3/PRM3 mirrors which sit roughly in the same location as the present SIB/EIB benches. From there, the beam is focussed down towards convex SRM2/PRM2 mirrors, housed in new vacuum chambers that shall be located between the current recycling mirror towards and the beam-splitter tower. The beam is then further guided to the convex SRM1/PRM1 mirrors, located on new suspended benches. On the recycling mirrors, the beam will have a diameter of order 1mm, such that relatively small optics can be used. Most of the Gouy phase is accumulated in this last part of the cavity, and the waist lays just outside the recycling cavity. This geometry is also adopted by both LIGO and Kagra.

On the injection side, the present suspended input bench is split into two separate benches. The first (SIB1) hosts the flat mirrors of the input mode-cleaner and the reference cavity as it is the case now. The second one (PR bench) hosts the input Faraday isolator and the power recycling mirror suspended via a double pendulum on the top of this bench. The laser beam reaches SIB1 first and, after being filtered by the input mode-cleaner, is sent toward the PR bench.

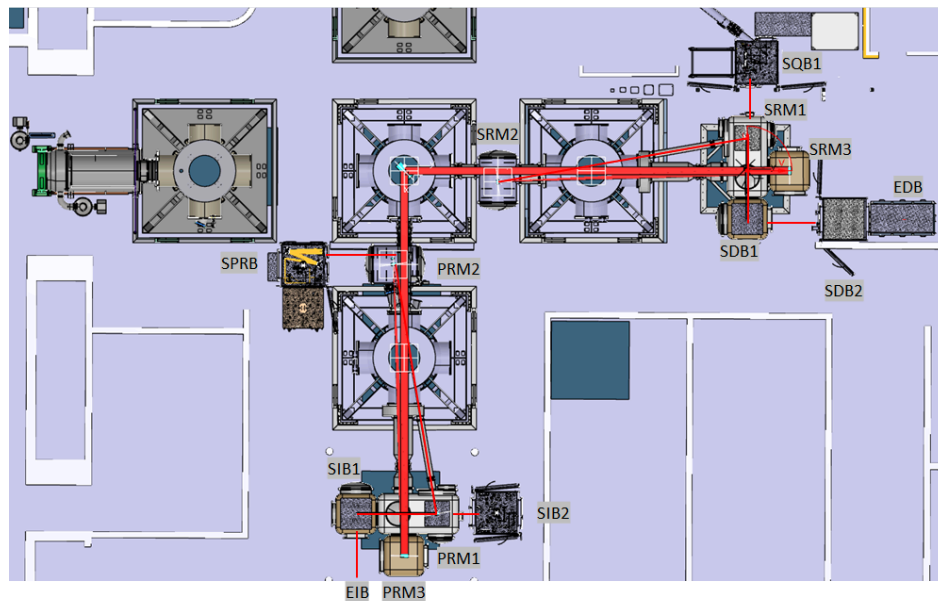


Figure 3 - Top view of the optical layout for the short recycling cavities option.

	Short Stable Cavities Preliminary Design	Date 2024-05-22 VIR-0461A-24 Page 16 of 101
---	--	---

The beam reflected by the interferometer is extracted by the Faraday Isolator on the PRM1 bench and sent toward the SIB2 bench at its current location. The pick-off beam providing access to the B3 (or B4) beam is extracted from the transmission of the PRM2 mirror and sent towards the SPRB bench. This has to be relocated to the west of its current position.

In order to fit the SIB1 bench, the PR bench and the PRM3 mirror in the building, the large injection vacuum tower is dismantled thus freeing a surface of 4mx4m. This space is used to place three vacuum chambers each containing a separate suspension. In this manner each critical mirror (PRM3, PRM1 and the input mode-cleaner dihedron) has its own suspension.

The signal recycling cavity follows a symmetrical scheme at the output of the interferometer (see figure 3). In this case the detection tower is dismantled to make the needed space available. The output Faraday Isolator is placed on the SRM1 bench and can be easily used to inject the squeezed vacuum beam from SQB1 at its current position.

2.2. Optical configuration

2.2.1. Principle

The short stable recycling cavity optical configuration is intended to be compatible with the present infrastructure and the total length between input masses and the PRM1/SRM1 mirrors needs to be between 35 m and 38.5 m depending on the sidebands modulation frequencies.

The optical configuration proposed is a folded recycling cavity as sketched in Figure 4.

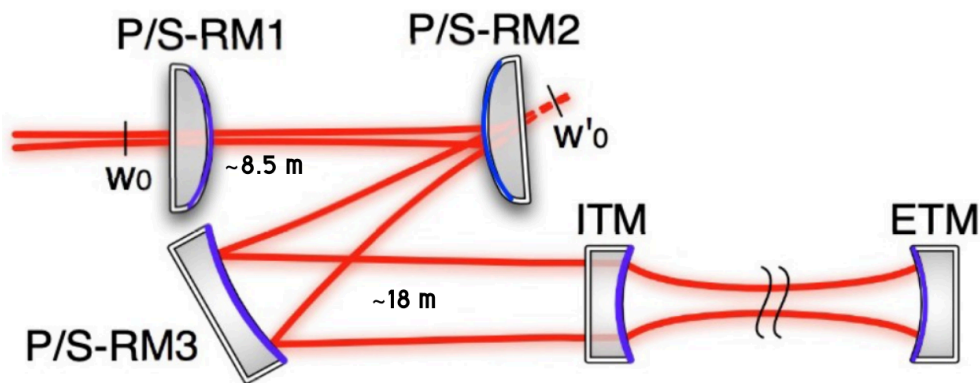


Figure 4 - Sketch of the principle of the short cavity layout. Here only one recycling cavity and one arm are represented, one should keep in mind that there is a beam-splitter between the P/S-RM3 mirrors and the ITM.

In order to have stable recycling cavities, the beam coming from the arm needs to acquire Gouy Phase in the recycling cavities. To do so the first mirror (P/SRM3) encountered by the beam coming the 3 km long arm cavities is a converging mirror, then the beam impinging a second mirror (P/SRM2) which is divergent and makes the beam less convergent, finally the last mirror (P/SRM1) is the actual recycling mirrors and has the same radius of curvature as the beam impinging on it. The beam is still converging when reaching P/SRM1, it has a convex shape and so is a diverging mirror. The Gouy phase is accumulated mostly between P/SRM2 and P/SRM1.

When one refers to the Gouy Phase in the recycling cavity one usually refers to the accumulation of Gouy phase during a one-way trip between the input masses and the P/SRM1 mirror or the other way around. Choosing properly the angle of incidence on the P/SRM3 and P/SRM2 mirrors allows to compensate for the astigmatism induced by the non zero angle of incidence on the P/SRM3 mirror. This technique has been described by Hello & Nary-Man in [VIR-NOT-LAS-1390-12](#) and has been used to avoid generating astigmatism inside the recycling cavity.

	Short Stable Cavities Preliminary Design	Date 2024-05-22 VIR-0461A-24 Page 18 of 101
---	--	---

Many optical configurations have been proposed and can be found in the wiki page of the [OSD stable recycling cavities](#).

In the next subsection only the last configuration called v3 will be presented, this version 3 of the configuration declines in 3 different versions that are presented in the next subsection.

2.2.2. Short cavity layout

In this section, 3 versions of the same configuration will be described, one intended for the power recycling cavity with a Gouy Phase of 25 degrees and a total length of 35m5274 and 2 with a Gouy Phase of 19 degree with a length of either 35m5724 or 38m2074.

All 3 configurations works with the following sets of sidebands modulation:

- Fmod1 = 6.320745 MHz (Adv+ Phase I modulation frequency + 1 arm FSR)
- Fmod2 = 9 x Fmod1 = 56.886705 MHz

With this set of sidebands the resonance conditions for the sidebands modulation are satisfied. The sideband 1 at 6.32 MHz is resonant in the recycling cavity and anti-resonant in the signal recycling cavity. The sideband 2 at 56.87 MHz is resonant inside the signal recycling cavity for both a length of 35m5274 and 38m2074 (the 56.89 MHz sideband being at resonance every 2.635 m). The sidebands chosen yield a reduction of the input mode cleaner (IMC) length by about 1.13 m.

The choice of Gouy Phase as 19 degree and 25 degree for signal recycling cavity and power recycling cavity has been driven by the LIGO experience, although it is quite easy to adapt the layout to another choice of Gouy phase by changing the radii of curvature of P/SRM2 and P/SRM1.

In the next subsections, the optical layout will be described in a single summary figure that can also be found in the [virgo wiki](#).

On figures 5 to 7 one can read on the bottom left the cavity parameters, i.e. the radius of curvature of the 3 mirrors, the distance between the mirrors, d_3 being the mean distance between the input masses (mean distance between West ITM and North ITM) and the P/SRM3 mirror, d_2 the distance between P/SRM3 and P/SRM2 and d_1 the distance between P/SRM2 and P/SRM1. Finally the angle of incidence on each mirror is given here.

On the bottom right side of the figures 5 to 7, one can find the beam parameters in the cavity : the beam size on each optics (for the resonating beam), the beam waist of the beam impinging on SRM1 and its location with respect to P/SRM1. The Gouy Phase is also reported here as well as the losses between the arm cavity beam and the recycling cavity beam computed by the mean of the overlap integral of the 2 beams, see section ABCD matrix simulation code for details.

The numbers are quoted for the tangential (x) and sagittal (y) planes of the beam.

The top plot shows the beam size changing in the cavity going from the input masses to the recycling mirror (P/SRM1); the vertical dash line represents the position of P/SRM3, P/SRM2 and P/SRM1 from left to right. The middle plot shows the accumulation of the Gouy phase along the beam path.

One can see that for the 3 configurations proposed, the beam circulating inside the cavity does not show astigmatism and that the Gouy Phase in both planes of the beam is very similar (0.2 degree difference at maximum). The 3 configuration shows very low losses, smaller than 5 ppm and so the losses due to astigmatism can be considered as negligible.

To be noted that the configuration described are for the nominal arm cavity, the one of Advanced Virgo + Phase I, which have been chosen to be the nominal solution for phase II. The design can be adapted for other configurations of the 3 km long arms such as the configuration with larger mirrors (large mirror on NE and WE), changing the P/SRM2 and P/SRM1 RoC by respectively ~3% and 13%, see the following presentation: [VIR-1003A-23](#).

PRC - 25 degree Gouy Phase - 35.5274 m length

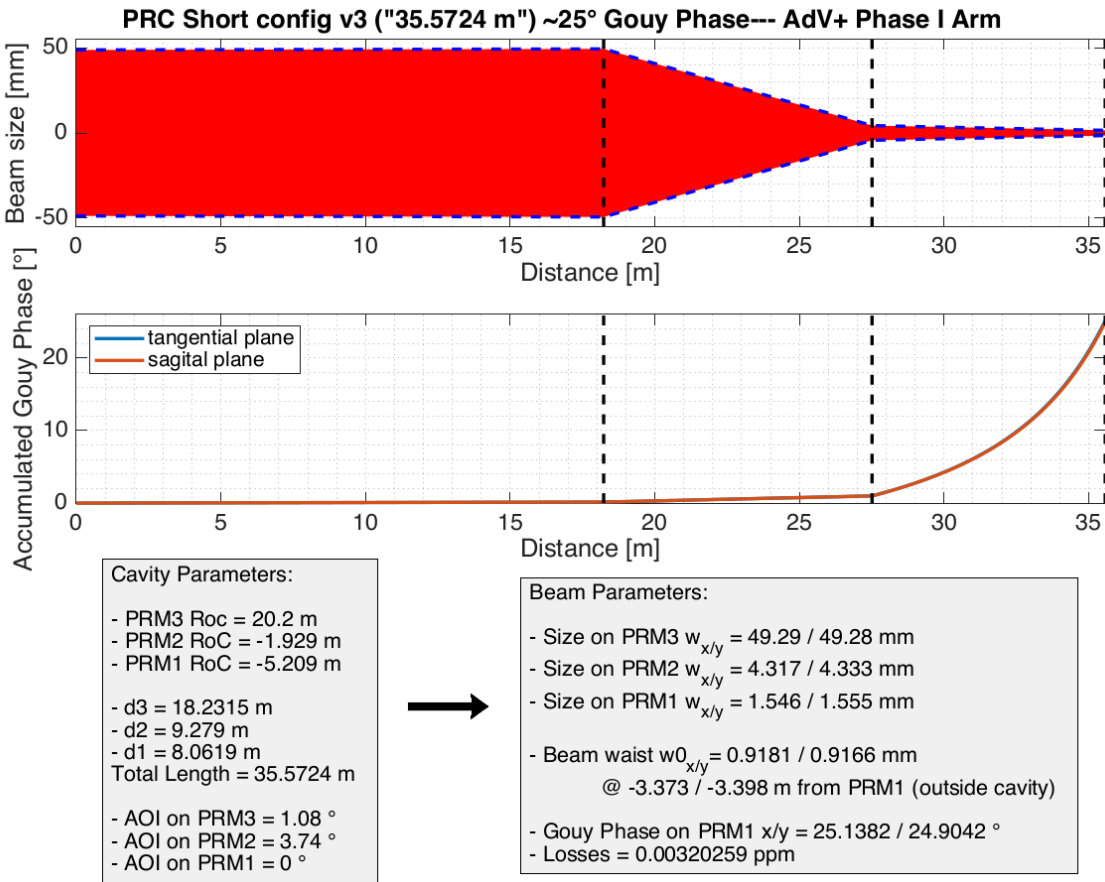


Figure 5 - Summary figure of the layout for the Power Recycling Short cavity with 25 deg Gouy Phase and length of 35.5274 m

SRC - 19 degree Gouy Phase - 35.5724 m length

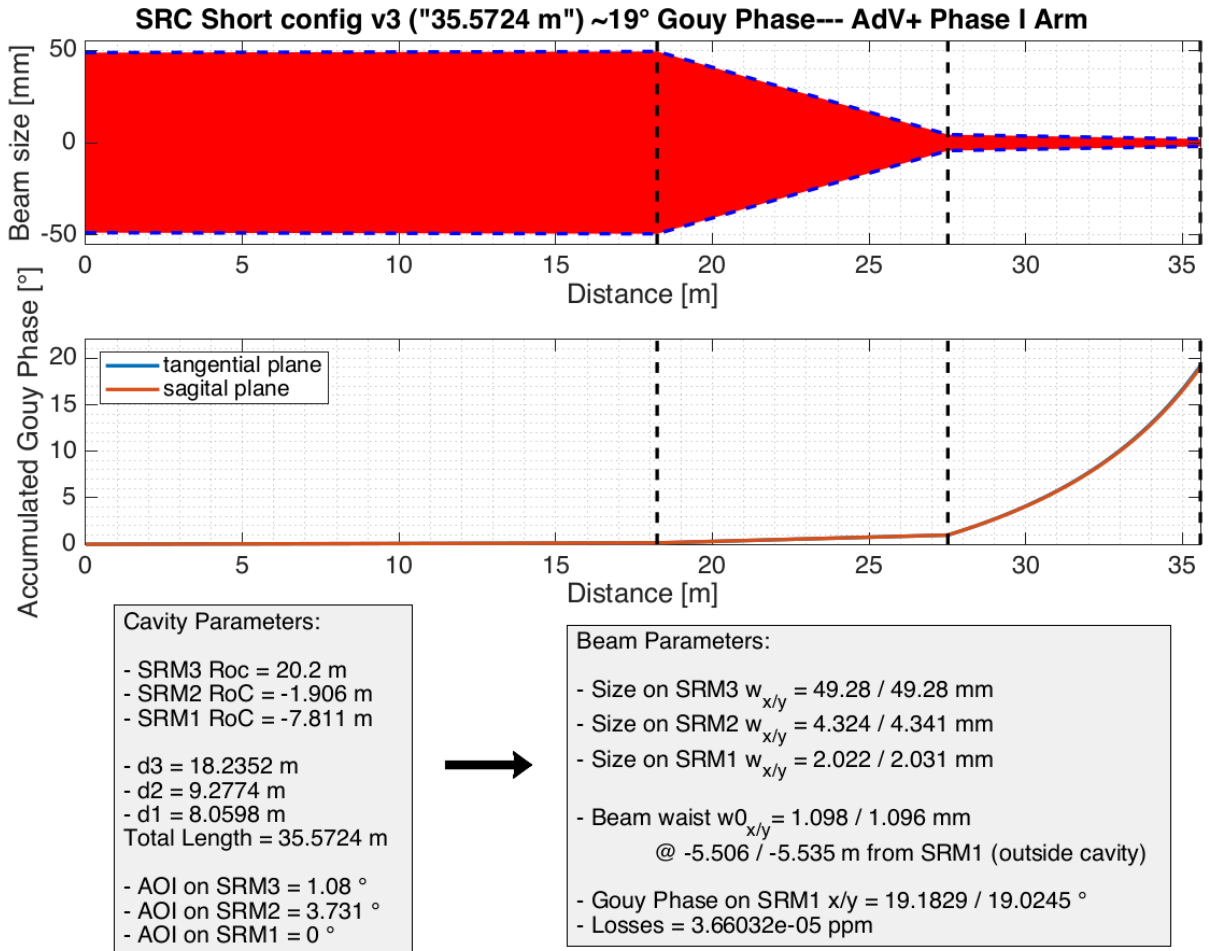


Figure 6 - Summary figure of the layout for the Signal Recycling Short cavity with 19 deg Gouy Phase and length of 35.5724 m

SRC - 19 degree Gouy Phase - 38.2074m length

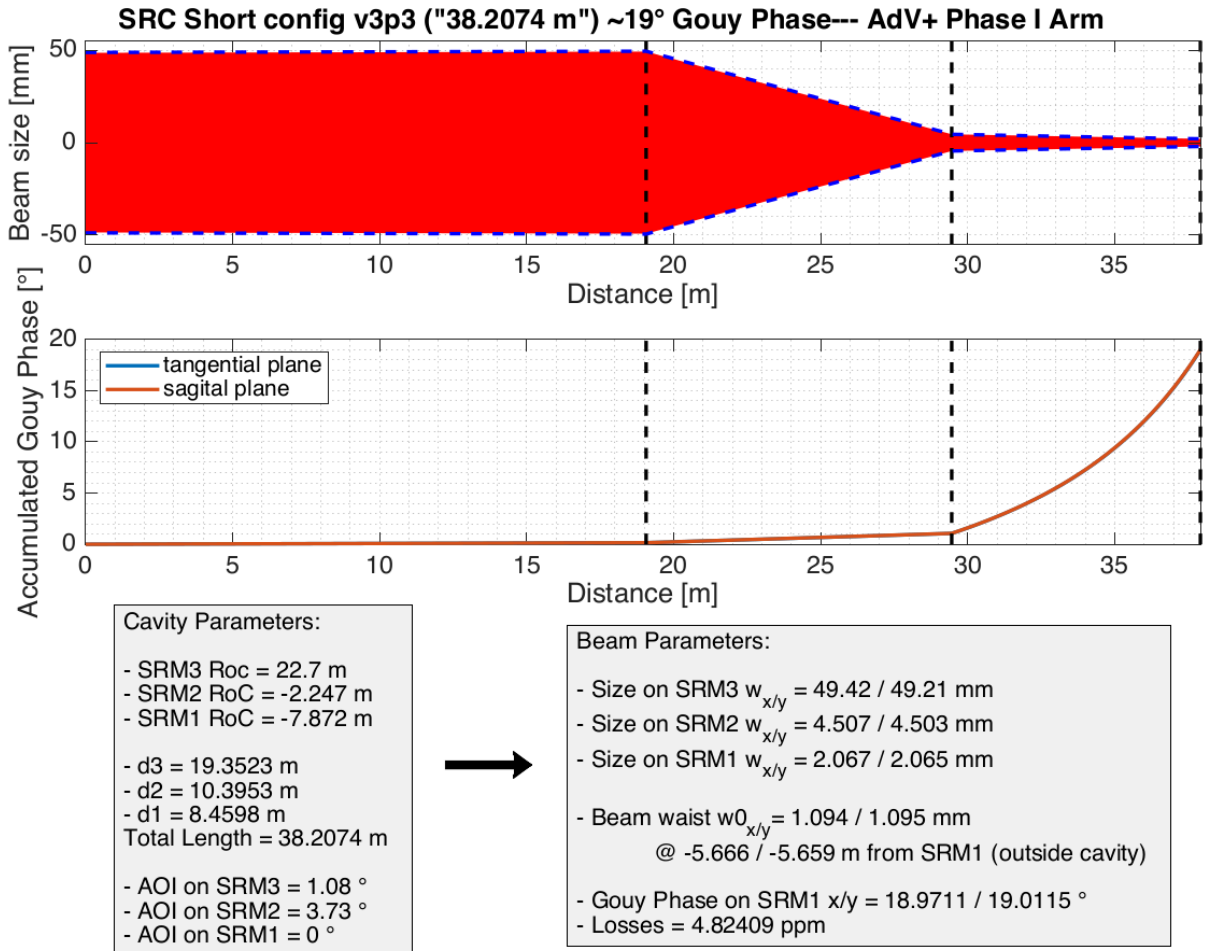


Figure 7 - Summary figure of the layout for the Signal Recycling Short cavity with 19 deg Gouy Phase and length of 38.2074 m

ABCD Matrix simulation code

A matlab-based ABCD simulation code has been written to study the propagation of the gaussian beam inside the signal recycling cavity (SRC). It can be found in the stable cavity folder of the [OSD git repository](#).

In the first commit of the code referred just above, we simulate the beam inside the nominal arm cavity and we propagate it through the signal recycling cavity mirrors. The eigenstate of the arm cavity as well as the eigenstate of the signal recycling cavity are computed. The eigenstate of the SRC is then propagated inside the arm cavity on the input mirror and the overlap integral between this beam and

the eigenstate of the arm cavity calculated at the same point is computed. The overlap integral between the signal recycling beam and the arm cavity beam is :

$$\langle \Psi_{RC} | \Psi_{FP} \rangle = \frac{2}{\sqrt{\omega_{RC}^t \omega_{FP}^t \omega_{RC}^s \omega_{FP}^s}} \times \sqrt{\frac{1}{\omega_{RC}^t{}^2 + \omega_{FP}^t{}^2 - i \frac{\pi}{\lambda} \left[\frac{1}{R_{RC}^t} + \frac{1}{R_{FP}^t} \right]}} \times \sqrt{\frac{1}{\omega_{RC}^s{}^2 + \omega_{FP}^s{}^2 - i \frac{\pi}{\lambda} \left[\frac{1}{R_{RC}^s} + \frac{1}{R_{FP}^s} \right]}}$$

with ω_{RC}^t and ω_{RC}^s being the beam size (radius) of the RC beam in tangential and sagittal plane respectively and R_{RC}^t and R_{RC}^s being the beam radius of the curvature of the RC beam in tangential and sagittal plane.

The coupling (γ) between the two beams is then the square value of the overlap integral:

$$\gamma = \langle \Psi_{RC} | \Psi_{FP} \rangle^2.$$

The code also computes the accumulated Gouy phase along the signal recycling cavity both in the tangential and the sagittal plane.

The code simulates only the case of the coupling between one arm of 3 km and one recycling cavity. It does not take into account that there are 2 arms in the interferometer and that the distance ITM-SRM3 is slightly different for the west and north arm because of the Schnupp asymmetry.

It has to be mentioned that losses due to other aberrations than astigmatism are not taken into account in this ABCD matrix simulation.

The simulation presented here are done with the nominal arm cavity of Advanced Virgo + in the O4 configuration, that is to say the following parameters :

- RoC ETM HR = 1683 m
- RoC ITM HR = 1420 m
- RoC ITM AR = 1420.2 m
- Cavity length = 2999.8 m

Tolerances Studies

Different tolerance studies have been carried out using the ABCD matrix code. For example the sensitivity to common thermal lensing inside the input mass has been carried out for different configurations, long and short and with different Gouy Phase have been presented in [VIR-1109A-23](#).

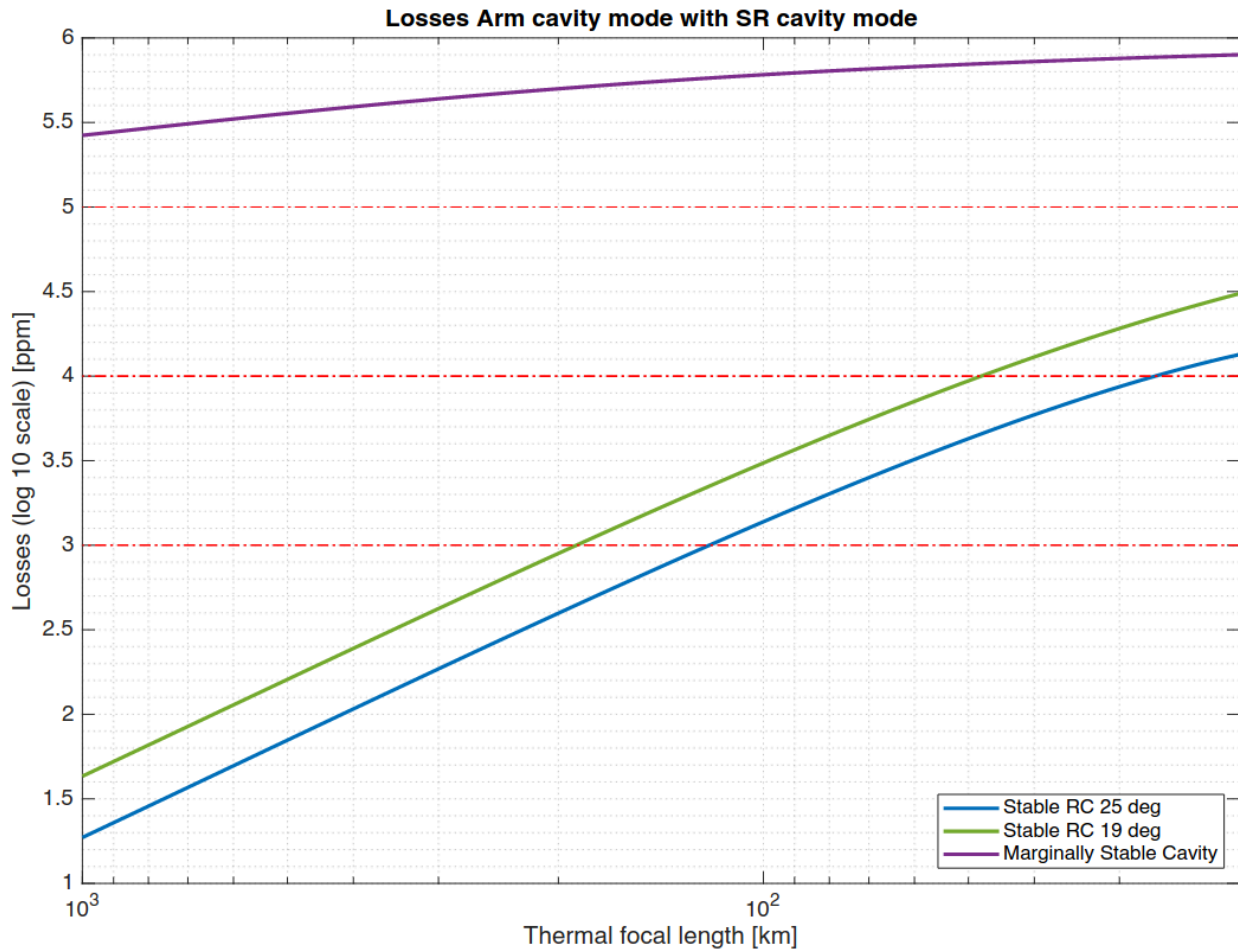


Figure 8 - Losses vs common thermal lensing in Input Masses for different configurations.

Figure 8 shows the losses expected for different configurations, it shows that the losses depend mostly on the chosen Gouy Phase, the larger the Gouy Phase the more resilient to losses the configuration is. Below, tolerance studies have been performed on the configuration of short cavity SRC - 19 degree - 35.5274 m length. They have been presented in [VIR-1003A-23](#). The choice of studying this configuration in particular has been driven by the fact that with a smaller Gouy phase, this configuration is more sensitive to losses. The results can be considered as higher limits for the other two configurations as their parameters are very similar.

Figure 9 shows that the thermal lensing in the input mass (ITM) can be compensated by changing the distance between P/SRM3 and P/SRM2 by a few millimeters. Shortening the distance between P/SRM3-P/SRM2 (d2 distance) by about 1.5 mm allows compensating for the losses due to a 100 km common thermal lens in the ITM. It has to be noted that the total length of the recycling cavity should

remain constant and thus the previous shortening has to be compensated by increasing the distance between P/SRM2 and P/SRM1 by twice the amount of the d2 distance, that is to say 3 mm.

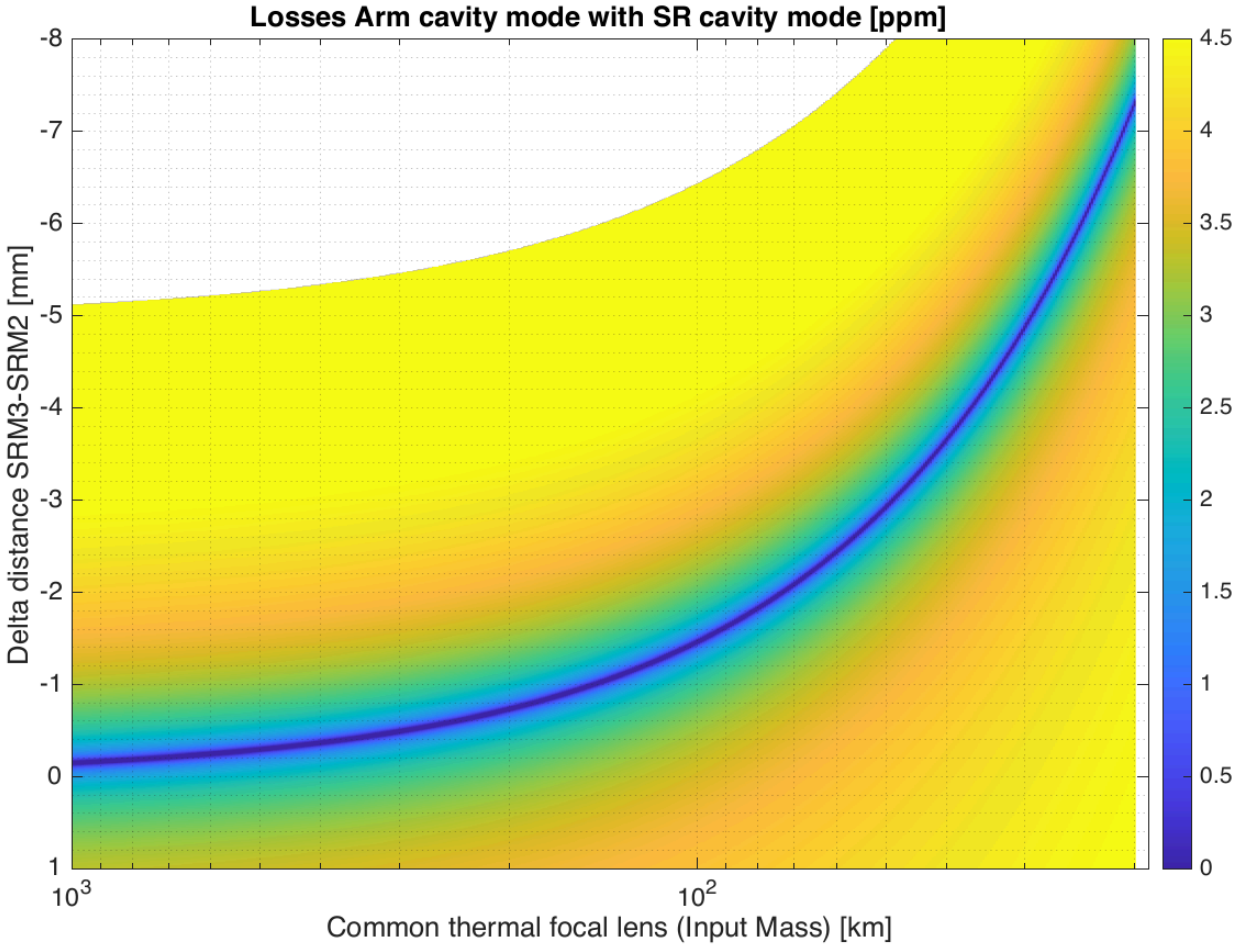


Figure 9 - Losses in log 10 scale (3 = 10000 ppm) vs common thermal lensing & variation of distance SRM3-SRM2.

To study the sensitivity to RoC errors (in the manufacturing process) we used the ABCD matrix code. The two figures of merit we look at are the Gouy phase and the losses (or the coupling between the recycling cavity and the 3km-long arm cavity).

Figure 10 shows that to compensate for a RoC error on SRM3 of 0.5% one needs to change the distance SRM3-SRM2 (d2) by about 50 mm. The white part of the figure is when the cavity is no longer stable. An error of 0.5% should be possible to obtain from the polisher given that LIGO got an error of less than 0.2 % on their P/SRM3 mirrors which have a RoC of about 36 m.

Figure 11 shows that we can retrieve the right Gouy phase for the same numbers (0.5% of errors on RoC of SRM3 and d2 changed by 50 mm).

The distance d2 is very critical to compensate for RoC errors and to correctly tune the cavity parameters.

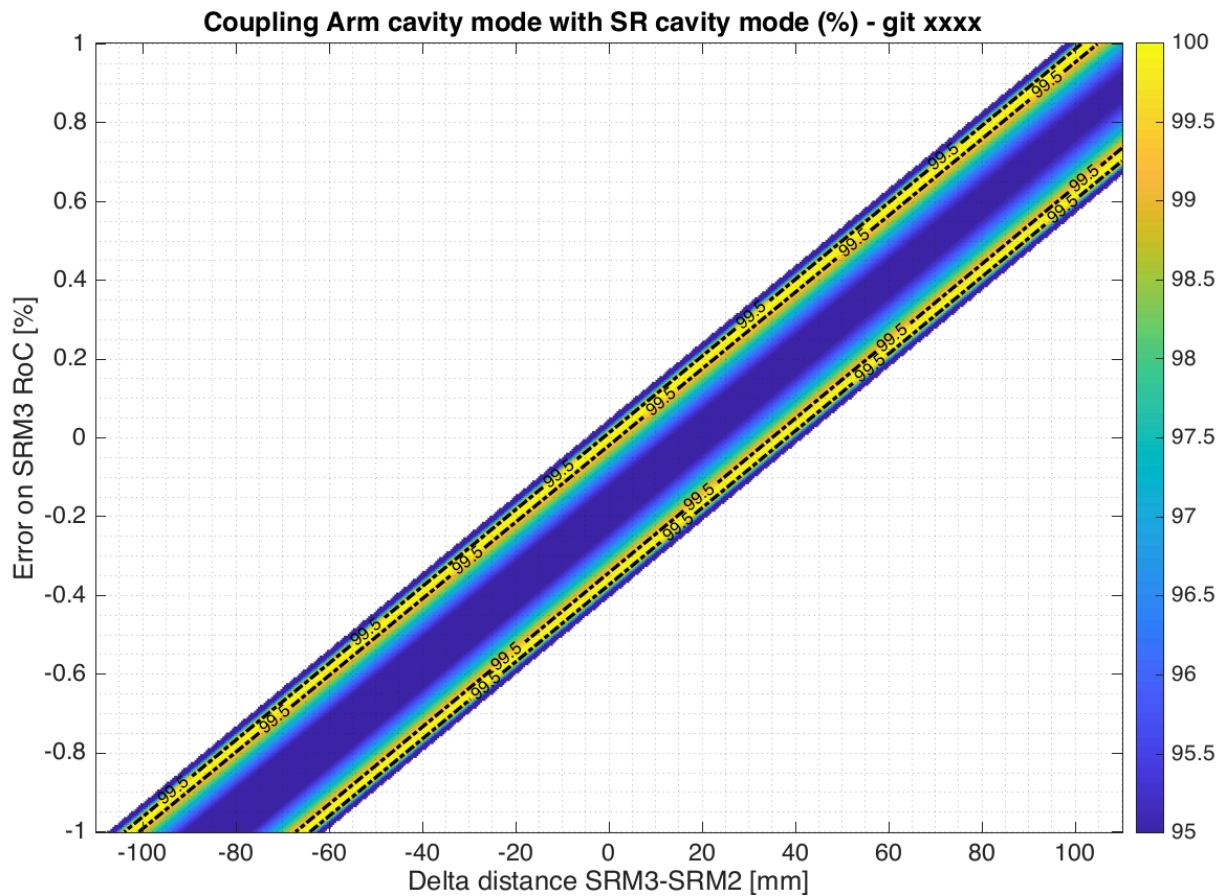


Figure 10 - Coupling vs Error on SRM3 RoC & variation of distance SRM3-SRM2 (d2).

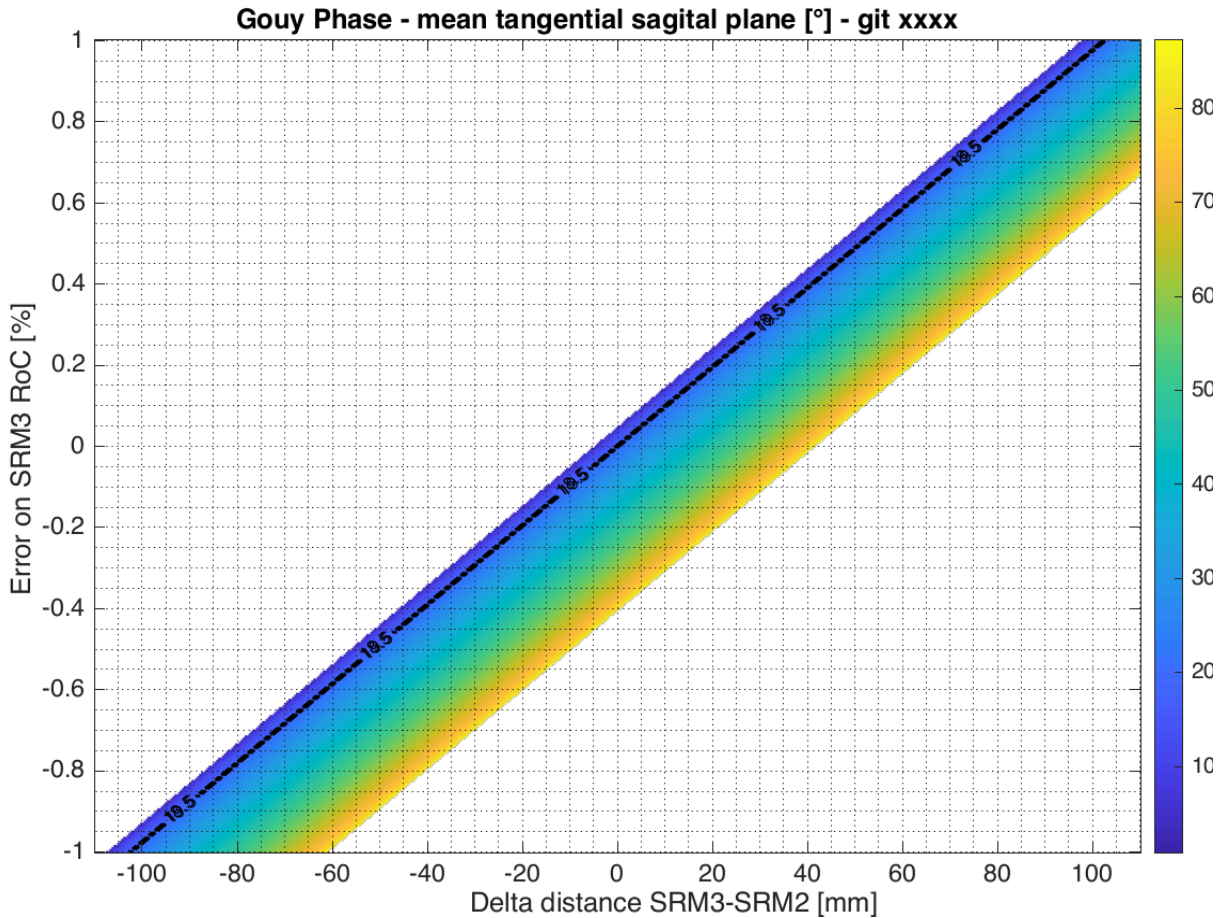


Figure 11 - Gouy phase vs Error on SRM3 RoC & variation of distance SRM3-SRM2 (d2).

The same kind of figure can be produced for the errors on SRM2 and SRM1. The table below shows how much the distance RM3-RM2 (d2) should be changed from the initial length for the 3 mirrors to retrieve the 19 degree Gouy phase and optimal coupling (or negligible losses < 50 pm).

	SRM3	SRM2	SRM1
Errors on RoC	0.5 %	1%	1%
d2 variation to compensate RoC errors	~ 50 mm	8 mm	< 0.28 mm

Figure 12 shows the variation of the Gouy phase as a function of RoC errors on SRM3 and SRM2 and figure 13 shows the same figure for the losses in log10 scale (3 = 1000 ppm, 2 = 100 ppm). One can see

that the region where the Gouy phase is nominal (19 degree) corresponds to the region where the losses are negligible.

We can say that RoC errors on SRM2 can be compensated also by tuning the RoC of SRM3 with thermal control. An error of 1% on SRM2 RoC can be compensated by a variation of 0.08% on SRM3 RoC (which is smaller than the possible RoC variation by thermal tuning of SRM3, 0.2% see Section Short Options: Thermal Control: PRM3/SRM3). One could imagine that such thermal tuning could be used also to compensate for some of the RoC errors of SRM2.

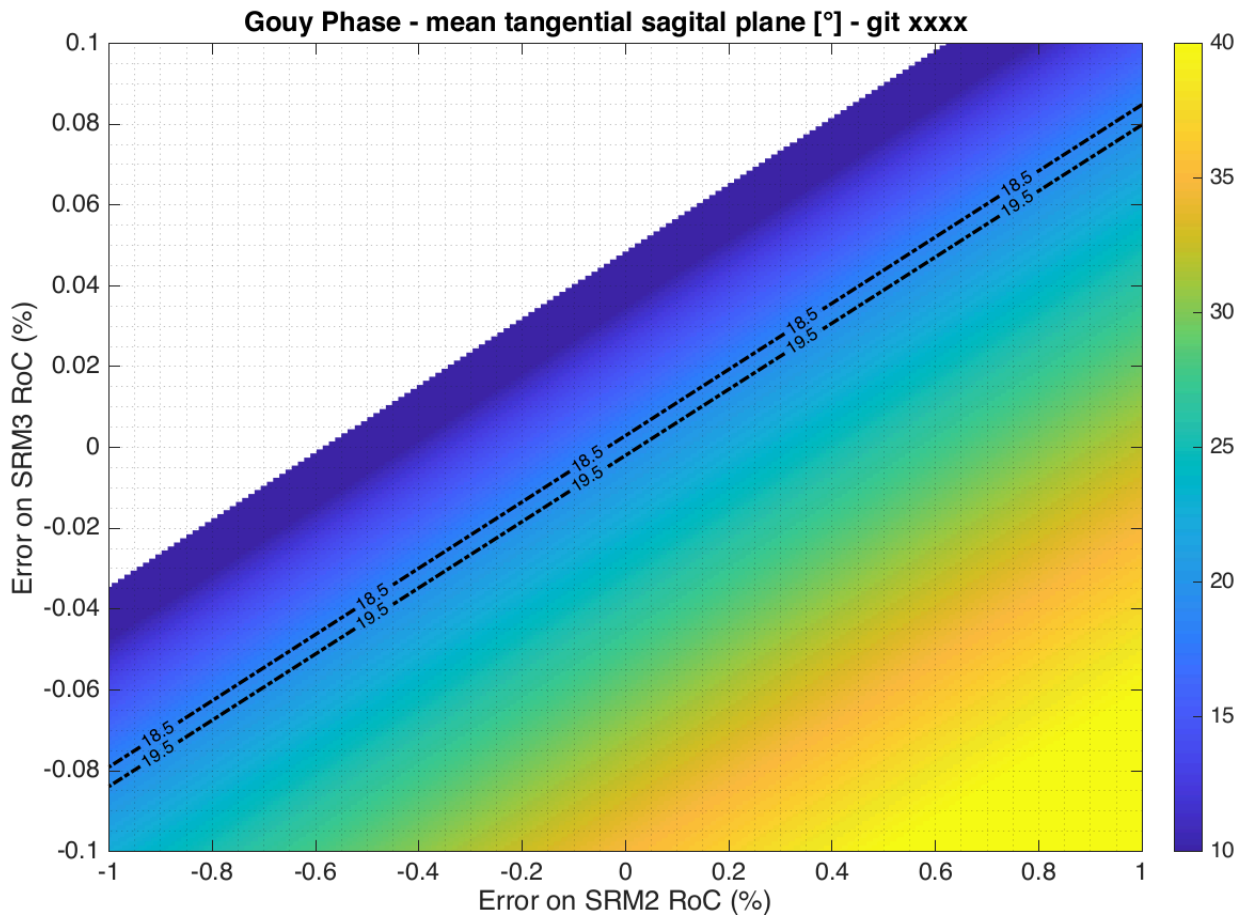


Figure 12 - Gouy phase vs Error on SRM3 RoC & Error on SRM2 RoC).

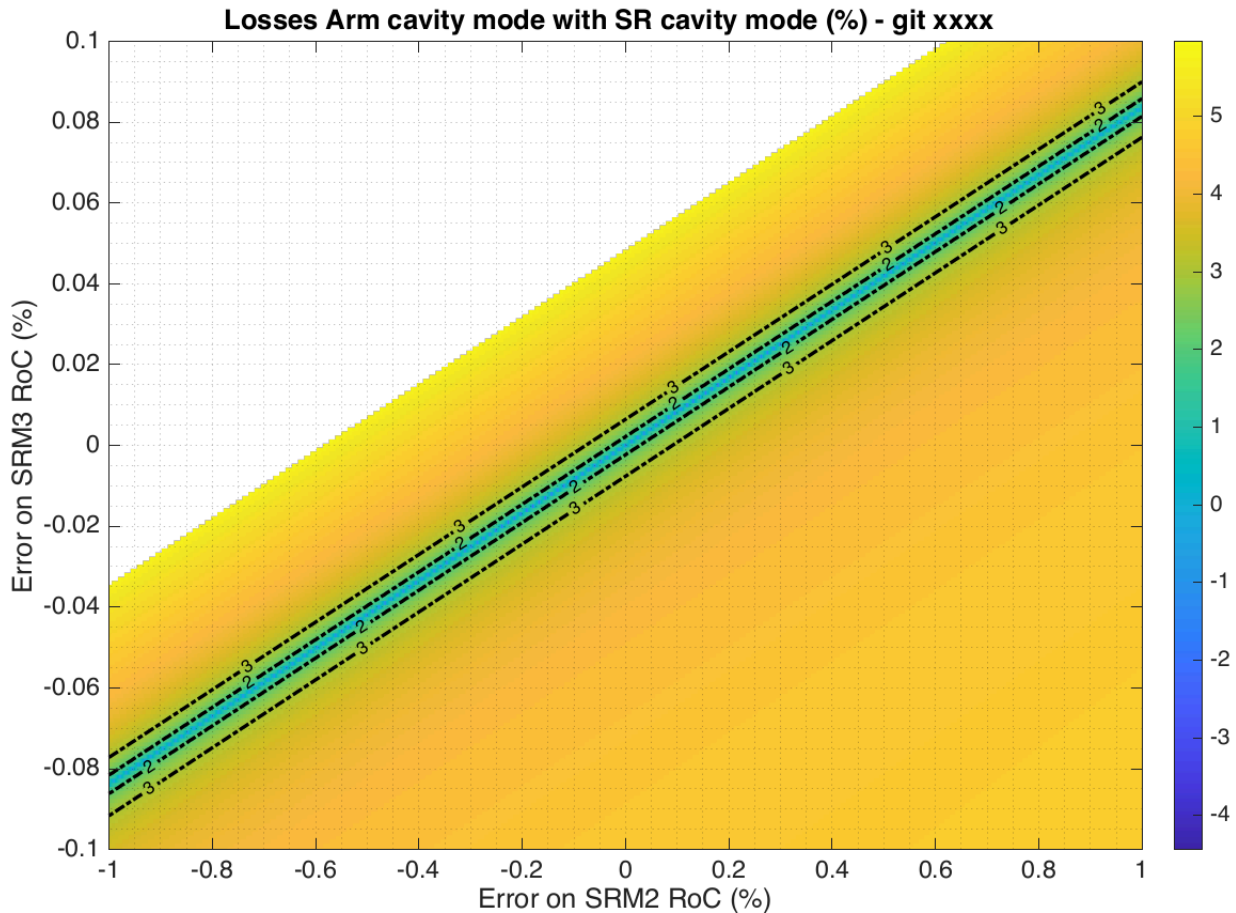


Figure 13 - Losses (log10 scale, 3 = 1000 ppm) vs Error on SRM3 RoC & Error on SRM2 RoC

Finally, the sensitivity to errors on the angle of incidence has been studied and it can be seen in slide 17 of [VIR-1003A-23](#). The design is not very sensitive to an error on the angle of incidence considering the mechanical constraints of the design. An error of 0.1 degree on the SRM2 AoI corresponds to a deviation of the beam on SRM1 of 280 mm (much greater than the SRM1 diameter) and would produce losses of about 20 ppm.

In conclusion, tolerance studies have been performed for the short cavity configuration. It shows that the errors on the RoC of the 3 mirrors of the cavity can be compensated by changing the distance (d_2) between P/SRM3 and P/SRM2. The same compensator (d_2 distance) can be used to compensate for common thermal lenses. Then, thermal tuning of SRM3 can be used to compensate for RoC errors of SRM2 and SRM1.

It has to be noted that the total length of the cavity should remain constant and thus any variation of the distance d_2 should be compensated by an opposite variation of the distance P/SRM2 - P/SRM1 by twice

	Short Stable Cavities Preliminary Design	Date 2024-05-22 VIR-0461A-24 Page 29 of 101
---	--	---

the amount because of the folded nature of the cavity. It should be foreseen to have the possibility to move the suspension of the mirrors inside the mini-tower by a few cm.

Thermal tuning and position of the mirrors can be used together to optimize the cavity parameters and minimize by which amount the mirrors have to be moved with respect to the initial condition.

It has to be noted that the configurations proposed can evolve depending on inputs from various subsystems.

	Short Stable Cavities Preliminary Design	Date 2024-05-22 VIR-0461A-24 Page 30 of 101
---	--	---

2.3. Auxiliary beams

2.3.1. Overview

Especially on the detection side, several beams co-propagate with the main B1 beam. These beams stem from the AR side of the beam splitter (B5, B5'), which are separated in the horizontal direction by about 5 cm from B1 and additionally propagate under a small angle of a few hundred microradians because of the beam splitter's wedge. In addition, we have the AR spots from the CP plates, both in the north and in the west arm. We have identified an additional beam, here labelled Bx, which is an AR reflex from the beam splitter that is then retro-reflected from the North ITM.

Tracing those beams is relevant for two reasons. Firstly, the stable recycling cavity will operate with SRM quite close to the beam waist, i.e. at the focal point of the SRM3/SRM2 telescope. Since parallel beams are focussed into a single point, a purely laterally displaced beam would end up overlapping with B1. However, since the relevant B5/B5' and CP beams carry a small vertical angle, they end up vertically displaced at the location of SRM. Secondly, the beams are still quite large on the SRM3 mirror, having the same radius as B1 has in the current AdVirgo+ configuration, i.e. about 5cm. This requires significant mirror sizes to not lead to clipping of beams, which would lead to problems with scattered light and also would prevent using e.g. B5 in a potential balanced homodyne configuration later on in V_nEXT as a local oscillator. Note that the relative alignment of the B5 beams with respect to B1 is fixed by the geometry of the beam splitter, while the CP beams can be moved with some considerable freedom by tilting the CPs.

Simulations were therefore undertaken in the ray tracing software Zemax, and also in the FFT simulation code DarkF. These two softwares have their own particular advantages and disadvantages:

- Zemax, inherent to its design as a ray tracing software, correctly takes into account the geometry of optics and gives visual feedback in the model of the beam paths. However, it cannot calculate interference of beams and the resulting beam shapes. In addition, the resolution is given by the amount of individual rays that are launched, thus calculation time sets a natural limit and beam shapes are approximated by the resulting point clouds.
- DarkF, as an FFT propagation software, accurately handles interference of beams and - within the resolution limits - results in accurate reproduction of beam shapes. However, the FFT code is agnostic about geometrical considerations, i.e. corrections such as angle of incidence, wedge angles etc. have to be manually added to the calculation.

Simulations about the situation in the power recycling cavity have not been performed yet.

2.3.2. Beam images

Figures 14 to 16 show the beam shapes as obtained with Zemax on SRM1, SRM2 and SRM3, respectively. Images obtained with DarkF show very comparable results, but are maybe less easy to interpret because of the interference effects. On SRM1, the beams are well separated. We have indicated substrate sizes of 100mm or 150mm diameter; both would by far cover the B1 beam and at this point the size is driven by suspension requirements rather than optical considerations. Looking at the SRM2 image, it is clear that the B5 beams are not yet sufficiently separated from B1 at this point, i.e. they will have to be caught just before the SRM1, with small mirrors located above/below B1, so that they will not interfere with the SRM1 suspension mechanics. Also for SRM2, a mirror size of 100mm or 150mm (not indicated) would suffice. The CP beams, being steerable, can likely be moved further outwards and can be caught there on baffles surrounding SRM2. The beam shape on SRM3 is very similar to the current situation on SR; the current size of SR of 330mm as indicated shall suffice.

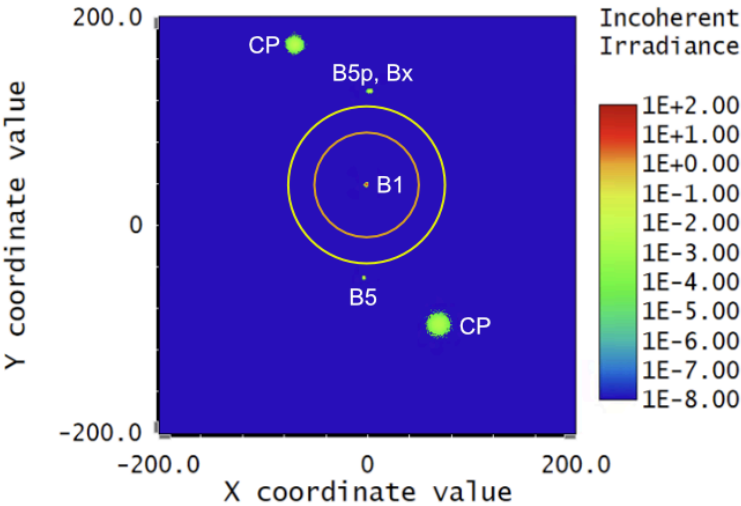


Figure 14 - Beam shapes on SRM1, annotated with beam names. Orange circle; 100mm tentative SRM1 diameter. Yellow circle; 150mm tentative SRM1 diameter.

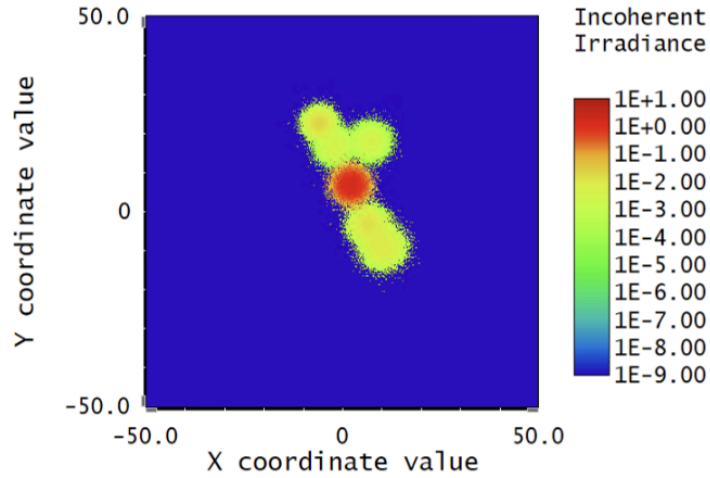


Figure 15 - Beam shapes on SRM2. The simulated area is 50mm x 50mm and completely encompasses all relevant beams.

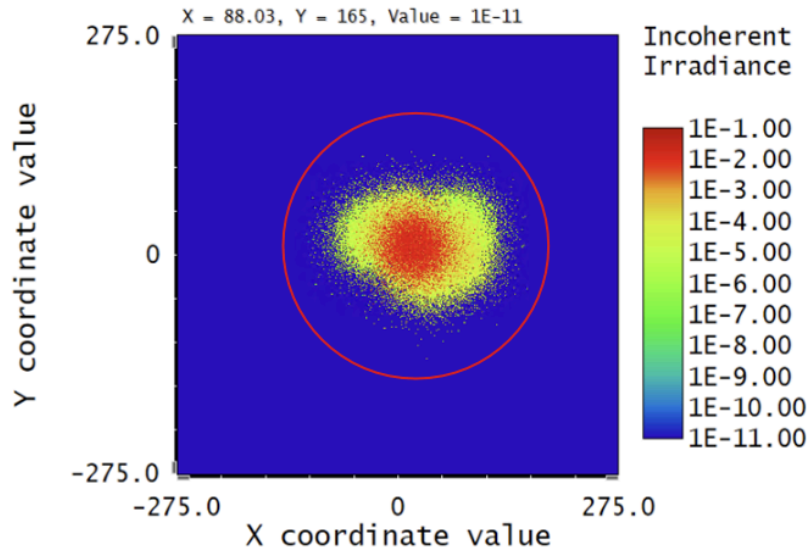


Figure 16 - Beam shapes on SRM3. Red circle; 330mm tentative SRM2 diameter.

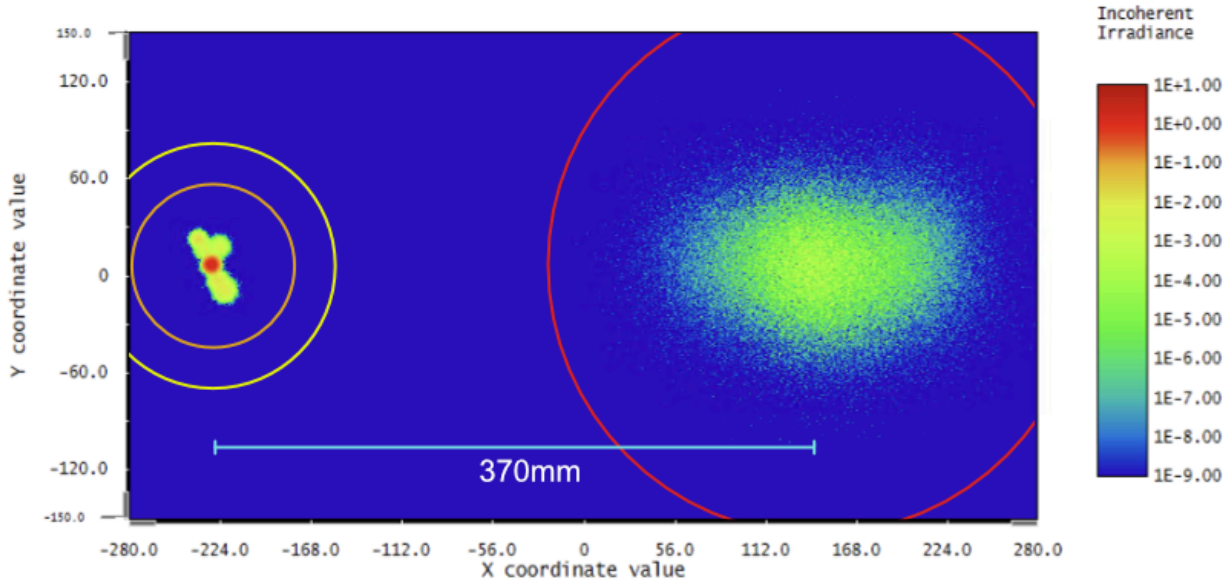


Figure 17 - Cross section of beams at location of SRM2 (left), showing separation from beams coming from BS (right). Red circle; 330mm diameter, Yellow circle; 150mm diameter, Orange circle; 100mm diameter.

Furthermore, in Figure 17 we have looked at the situation at SRM2, where the beams coming from the beam splitter pass by in close proximity. The distance between SRM2 and these quite large beams is relatively fixed, because to reduce astigmatism there is a certain relationship between focal lengths (therefore distances) and angles of incidence (therefore lateral beam separation). As indicated in the picture, there should be enough room to allow the large beams to pass by the suspension frame of SRM2; however suitable baffling at the rear of the SRM2 suspension should probably be foreseen to prevent any stray light issues.

	Short Stable Cavities Preliminary Design	Date 2024-05-22 VIR-0461A-24 Page 34 of 101
---	--	---

2.4. Modulation frequencies and Gouy phases

2.4.1. Introduction

In order to set requirements on the Gouy phases we have computed the recycling gains for HOMs (of carrier and sidebands). This computation is based on the field equations inside the dual recycled michelson interferometer reported in [VIR-0391A-24](#). Regions for which the gain of dangerous HOMs is too high have to be avoided. In the following the Gouy phase is defined as a one way phase. Only Gouy phases below ~ 50 degrees are considered. For reference, LIGO has chosen Gouy phases of 25 (PRC) and 19 (SRC) degrees and KAGRA of 16.4 and 13 degrees.

2.4.2. Modulation frequencies

The choice of the value of the modulation frequencies depends on the locking scheme (see Section 3.5) and it is also linked to the choice of Gouy phases as HOMs of sidebands must not be resonant inside PR and SR cavities.

All the modulation frequencies must be transmitted by the IMC and chosen to be far from resonance inside the Fabry-Perot cavities. The first modulation frequency (f_1) must be resonant inside PRC and weakly transmitted towards SRC (it will be used to sense PRC DOFs and the SSFS). The second modulation frequency (f_2) must also be resonant inside PRC and have a large transmission towards SRC (it will be used to sense SRC DOFs). It is planned to use a third modulation frequency for the alignment of the SR mirror, as it is done in LIGO. If a scheme similar to LIGO's ([LIGO-T1700215](#)) is used (still to be decided) this SB should also resonate inside PRC but it should not be at resonance inside SRC. This implies that SRC and PRC have different lengths. In order to avoid that SR alignment is sensitive to thermal transients the HOM2 of f_2 and f_3 should have low enough gain inside SRC. In this scheme the value of f_3 should be chosen together with the value of SRC Gouy phase such that the HOM1 of the lower or upper SB has a non-negligible gain inside SRC (see section 2.5).

The obvious choice for f_1 is to keep the 6 MHz. Other modulation frequencies must be even multiples of f_1 in order to resonate inside the PRC and remain close to anti-resonance inside the FP cavities.

The second modulation frequency, f_2 , could also be kept at 56MHz but alternatives could be explored in order to improve the decoupling of the sensing matrix (see Section 2.5). In particular, a modulation frequency of $f_2=31\text{MHz}$ ($5 \cdot f_1$) would provide a sideband which is well transmitted by SR and has a low power recycling gain (see [VIR-0393A-24](#) and [VIR-0391A-24](#)), on the contrary to the actual case. This would be similar to LIGO's scheme (see [LIGO-T1000298](#)). In the following, for the Gouy phase studies f_2 is set to 56MHz.

The third modulation frequency can be other even multiples of f_1 . If f_3 should not be at resonance inside the SR cavity (i.e. using LIGO's scheme, see Sec 2.5.3), its length should be different from PRC: the SR

cavity length can be chosen either longer or shorter than PRC by one FSR of f_2 (2.6m for $f_2=56$ MHz). The results shown below are the same for those 2 cases.

Given the chosen length for the PRC (35.57 m), the first modulation frequency (f_1) has to be changed by 50 kHz ($f_1=6.32$ MHz) and the second modulation (56.4 MHz) frequency by 9×50 kHz. This requires to shorten the input mode-cleaner length by 1.13 m. Given that in this solution the input mode-cleaner flat mirrors (so called dihedron) are moved in the west direction by 1.30 m, the input mode-cleaner end mirror will have to be moved in the east direction by 17 cm. These types of mode-cleaner tower displacement have already been done in the past. Note that 50 kHz corresponds to 1 FSR of the FP cavities meaning that the resonance conditions of all sidebands are unchanged.

2.4.3. Gouy phase inside PR cavity

Inside the PR cavity the distortions mainly arise from uncompensated cold and thermal defects and from ITF misalignments. In this study (see [VIR-1130B-23](#)) we therefore consider the HOMs of order 1 to 4 as these are the dominant ones that will be created by these defects. Indeed, thermal defects create large HOM2, which after the use of thermal compensation are mainly cancelled and the remaining HOMs are expected to be of order up to 4. This will have to be checked more quantitatively with simulation of the full ITF including these defects.

Figure 18 (right) Shows the carrier recycling gain computed for the HOMs of order 1 to 4 as a function of the PR Gouy phase. One should notice that in this case, a Gouy phase of zero does not lead to enhancement of HOMs: this can be understood as the HOMs are not resonant inside the FP (in contrary to the TEM00) they are also not resonant inside the PRC. This explains why the carrier is dominated by a TEM00 inside the PRC. A HOM of order $n+m$ will resonate for a Gouy phase equal to $f_G = p/2/(n+m)$. Regions around 22.5, 30, 45 degrees should be avoided.

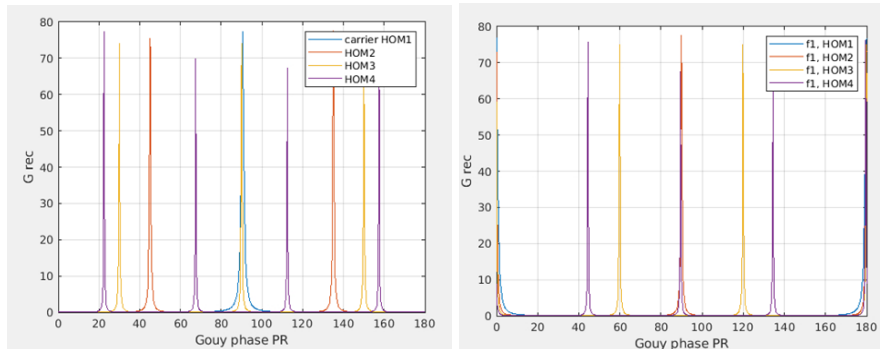


Figure 18 – HOMs recycling gain for (left) carrier and (right) sidebands (no losses are considered which explains why the gains are higher than one would expect)

	Short Stable Cavities Preliminary Design	Date 2024-05-22 VIR-0461A-24 Page 36 of 101
---	--	---

The conditions are different for the sidebands: as both the TEM00 and the HOMs are not resonant inside the arm cavities, they are all resonant for a zero Gouy phase. Figure 18 (left) shows the example of the 6MHz (but the picture is the same for other sidebands). A HOM of order $n+m$ will resonate for a Gouy phase equal to $f_g = 2\pi / (n+m)$. Regions around 0 and 45 degrees should be avoided. These results do not depend on the value of the SR Gouy phase. It should be underlined that some HOMs can become resonant inside FPs (this can be the case for the HOM4 of the 56 MHz depending on the FP Gouy phase) which will affect their resonance condition inside PRC. This should be avoided with a proper tuning of the FP Gouy phase (through the ETM RHs).

From these considerations, in order to avoid recycling gain of HOMs larger than 1 the following regions can be chosen for PR Gouy phase: $7 < f_g < 20$, $24 < f_g < 28$, $32 < f_g < 42$ degrees.

2.4.4. Gouy phase inside SR cavity

Inside the SR cavity the main constraint comes from the carrier. As stated above the resonance of HOMs must be avoided in order not to deteriorate the contrast defect. OSCAR simulations (see [VIR-0892A-23](#)) and OMC scan measurements (see logbook entry [61739](#) and [VIR-0892A-23](#)) have shown that modes up to order 9 are present with non-negligible power on the dark fringe. Modes of order 8 and 9 are of particular interest as these are close to the resonance of the FPs. Bad tuning of the FP Gouy phase can therefore enhance them. This has been observed during the O4 commissioning (and confirmed with OSCAR simulations, see [VIR-0892A-23](#)). Modes of higher order are not considered dangerous as these are clipped by the mirror's aperture and are therefore naturally reduced. We therefore consider modes up to order $n+m=9$ for this study.

Figure 19 Shows the SR cavity recycling gain for the HOMs created inside this cavity. In the O4 configuration ($f_g \sim 0$ degrees) all modes (except TEM00) have a gain close to 8. As the finesse of SR is small the modes are wider than in the case of PR. A Gouy phase between 15 and 18 degrees seems safe: all modes between order 2 and 8 have a gain lower than 0.5 (reduction by a factor 16 or more wrt now), modes of order 1 or 9 have a gain around 1. Note there is a handle to keep the mode of order 1 under control as it mainly originates from the ITF alignment. It has to be highlighted that the SR Gouy phase should not be too low as LIGO H1 encountered some problems due to this: the HOM1 of the carrier would become resonant inside SRC during the lock acquisition which caused the so-called "mode-hopping" (or jumps, see [T1500230](#)) from one state to another. The design Gouy phase in LIGO was 19 degrees but they suspect it was significantly lower in H1.

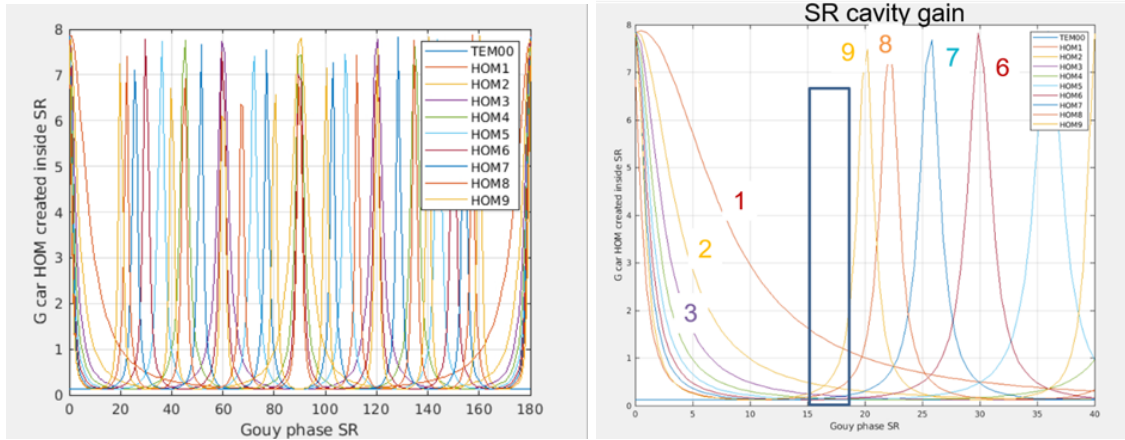


Figure 19 - SR cavity recycling gain for carrier TEM00 (constant blue line) and HOMs (other colored lines) as a function of the SR Gouy phase. Left plot shows a zoom for $0 < \phi_G < 40$ degrees, highlighting the recommended region and the modes resonances.

Concerning the sidebands, the constraints depend mainly on the alignment scheme chosen for the SR mirror (see [VIR-1076A-23](#)). Figure 20 shows the SR cavity gain for sidebands HOMs ($n+m=1$ and 2) created inside SRC for 2 different values of f_3 (82MHz and 94MHz) for SRC longer (or shorter) than PRC by 2.6 m (i.e. one FSR of f_2). Note that the resonance conditions of HOMs inside SRC depend only marginally on the value of PR Gouy phase as long as PR Gouy phase is above a few degrees, which simplifies the study. One can conclude that Gouy phases around 45 degrees should be avoided for f_2 HOM2 not to be resonant. The $f_3=94$ MHz would have the drawback that HOM2 of the upper SB would be resonant for Gouy phase around 20 degrees, while for $f_3=82$ MHz, for Gouy phase around 20 degrees the HOM1 would be resonant. The impact on alignment sensing has to be studied (see section 3.5). In the case where SRC has the same length as PRC then the resonant conditions of f_3 are exactly the same as f_2 (i.e. as shown on the left plot of Figure 66). Note that the picture would be different if a different value of f_2 is chosen (see [VIR-0391A-24](#)).

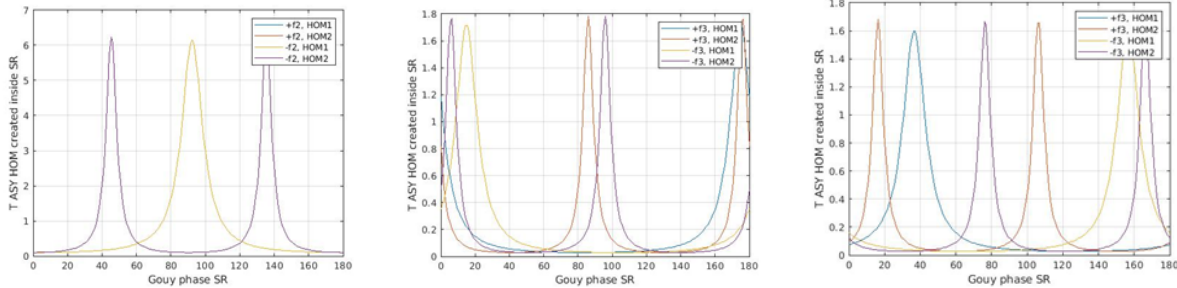


Figure 20 - SR cavity gain for HOM1 and HOM2 created inside the SR cavity for (left) $f_2=56\text{MHz}$, (middle) $f_3=13f_1=82\text{MHz}$ and (right) $f_3=15f_1=94\text{MHz}$. The upper (HOM1 in blue, HOM2 in red) and lower sidebands (HOM1 in yellow, HOM2 in purple) are shown.

Since the constraint coming from the carrier HOMs is quite stringent, the proposed strategy would be to fix the SR Gouy phase around 18 degrees (the highest value of the best region for the carrier, see above) and explore several values for f_3 within the possible ones.

2.4.5. Summary

There are several possible regions for the PR Gouy phase which avoid HOMs of the carrier and of the sidebands to be resonant: $7 < f_G^{\text{PR}} < 20$, $24 < f_G^{\text{PR}} < 28$, $32 < f_G^{\text{PR}} < 42$. The SR Gouy phase is more constrained because one needs to consider HOMs up to a large order on the dark fringe and also because its finesse being smaller the resonance peaks are wider. The safest region being: $15 \leq f_G^{\text{SR}} \leq 18$ degrees. It would be wise to choose the largest possible Gouy phase in this region in order to avoid the appearance of mode hopping during the transients.

In addition PR and SR Gouy phases might have to be chosen at different values in order to avoid degeneracy in the control matrices (see LIGO's design).

It has been checked that these results do not quantitatively change if the PR cavity length is changed by 4mm which is the current precision we have on this length. It should also be underlined that the sensitivity to SR cavity length is much lower due to the lower finesse of this cavity (see [VIR-1130B-23](#)).

2.5. Interferometer sensing and control

2.5.1. Microscopic length and control sidebands

Three modulation frequencies are used for the longitudinal control of Virgo, while only two are used in LIGO. The general considerations to choose them are:

- SB1 and SB2 have to be close to anti-resonance in the arm cavities (while the carrier is resonant) and resonant in the power recycling cavity, so they can be used for CARM and DARM control. This condition is particularly important for the sideband that is used to control CARM (and so the SSFS), since its bandwidth is very high (around 10 kHz). We have set an upper limit to this offset of 5 kHz.
- SB1 is almost not transmitted to the asymmetric port and anti-resonant inside the SRC.
- SB2 is significantly transmitted towards the asymmetric port and resonant inside the SRC. The different resonance condition of SB1 and SB2 in the recycling cavities aims to decrease the coupling of the fields inside the Central Interferometer (CITF).
- SB3 (Virgo-only) is anti-resonant in the arm cavities and anti-resonant in the power recycling cavity, in order to build a decoupled error signal for PRCL. Initially, we will try to find a sensing without the use of this extra sideband.

In order to facilitate the design as much as possible, we tried to respect one additional constraint:

- In order to minimize unnecessary changes, we have considered BS-North ITM and BS-West ITM as fixed lengths as well as the Schnupp asymmetry.

To keep the configuration as similar to the present one as possible, SB1 was chosen to have the same offset from anti-resonance in the long arm cavities as the present one 300 Hz (one FSR_{arms} away from the present SB1). Starting from this frequency, and considering infrastructure constraints (PRC length of around 35 m) the PRCL has been calculated. Since SB1 has been fixed, the FSR of the IMC has been modified to 1053457 Hz (SB1/6 rounded up to an integer number).

Regarding SB2, and being compliant with the aforementioned conditions, Romain B. came up with two proposals: one where the lengths of SRC and PRC are the same (Virgo-like configuration, where all the odd multiples of SB1 above 45 MHz resonate inside the SRC) and the other where the SRC is chosen so that SB2 is the only sideband resonant inside (LIGO-like).

	SB1 [MHz]	Offset [kHz]	Tasy	SB2 [MHz]	Offset [kHz]	Tasy	PRC [m]	SRC [m]
Virgo-like	6.320742	0.3	0.2	56.886678	2.7	0.98	35.5724	35.5724
LIGO-like	6.320742	0.3	0.2	56.886678	2.7	0.98	35.5724	38.2074

Table 1 - Sidebands' parameters and recycling lengths

	Short Stable Cavities Preliminary Design	Date 2024-05-22 VIR-0461A-24 Page 40 of 101
---	--	---

2.5.2. Simulation of the error signals

Starting from the parameters shown in Table 1 we have studied the longitudinal error signals. All the studies that we have performed have been done using Finesse 3. We have used the measured optical parameters of the main optics that are currently used in Advanced Virgo, but in order to simplify the simulations we have considered only the HR surfaces (no substrates or AR). Moreover, we have considered the distances between BS and the input test masses as fixed, meaning that we have also considered the Schnupp asymmetry as a fixed parameter. Also for simplicity, the telescope mirrors PRM2, PRM3, SRM2 and SRM3 are totally reflective and lossless. We have placed sensors in reflection of the PRC (B2), in transmission of the SRC (B1) and inside the recycling cavities (B4 and BSR). Since we are interested in the longitudinal DOFs only, we have worked with plane waves. Also for simplicity we will show the images of the LIGO-like configuration because the couplings and overall behavior of the error signals are very similar.

Working point

The first step in the simulation process is to find the longitudinal working point, which implies:

- the Michelson in Dark Fringe at the antisymmetric port and in Bright Fringe at the symmetric port for both the carrier and sidebands.
- the PRC in resonance for ALL the fields
- the SRC in resonance for the SB2 and NOT for the carrier and SB1
- the arm cavities in resonance for the carrier

Optical gain of the error signals

The first thing we did is to make the Transfer Function between each DOF and all the sensors at very low frequency (1e-3 Hz). This way we extracted the optical gain and optimal demodulation phase for each one of them. In order to be "input power independent", and so to ease the comparison, we have normalized the optical gains by the power impinging on the photodiode. For each DOF we then identified the best sensors in terms of Optical Gain.

- **DARM:** BSR SB2; **CARM:** B4 SB1; **PRCL:** B2 SB1; **MICH:** B4 SB2 I; **SRCL:** B4 SB2 Q

This is useful in order to reduce the number of sensors that we need to further study. Starting from the best candidates we then make two kind of plots:

- Compass plots: for each DOF it shows the optical gain of the sensor, and at which demodulation phase we obtain it.
- Coupling plots: once we decide for which DOF we want to use a given sensor, we project all the DOFs for the demodulation phase that maximizes the chosen one.

	Short Stable Cavities Preliminary Design	Date 2024-05-22 VIR-0461A-24 Page 41 of 101
---	--	---

This extra information is very useful because the optical gain alone does not give all the information about the quality of an error signal. The couplings are a key point in the selection process, and in order to evaluate the error signals we also need to know the coupling region and the presence of offsets if any. The coupling plots of the selected candidates are shown in Figure 21. CARM and DARM error signals are very strong and well decoupled from the rest of the error signals. However, the central error signals present a high coupling of the other DOFs. From the decoupling plots we can see that these couplings happen only within a narrow range and with peak-to-peak amplitudes that are small. For this reason we have chosen these error signals as candidates for building the sensing matrix and evaluating the decoupling angle and so their suitability to control the ITF longitudinal DOFs.

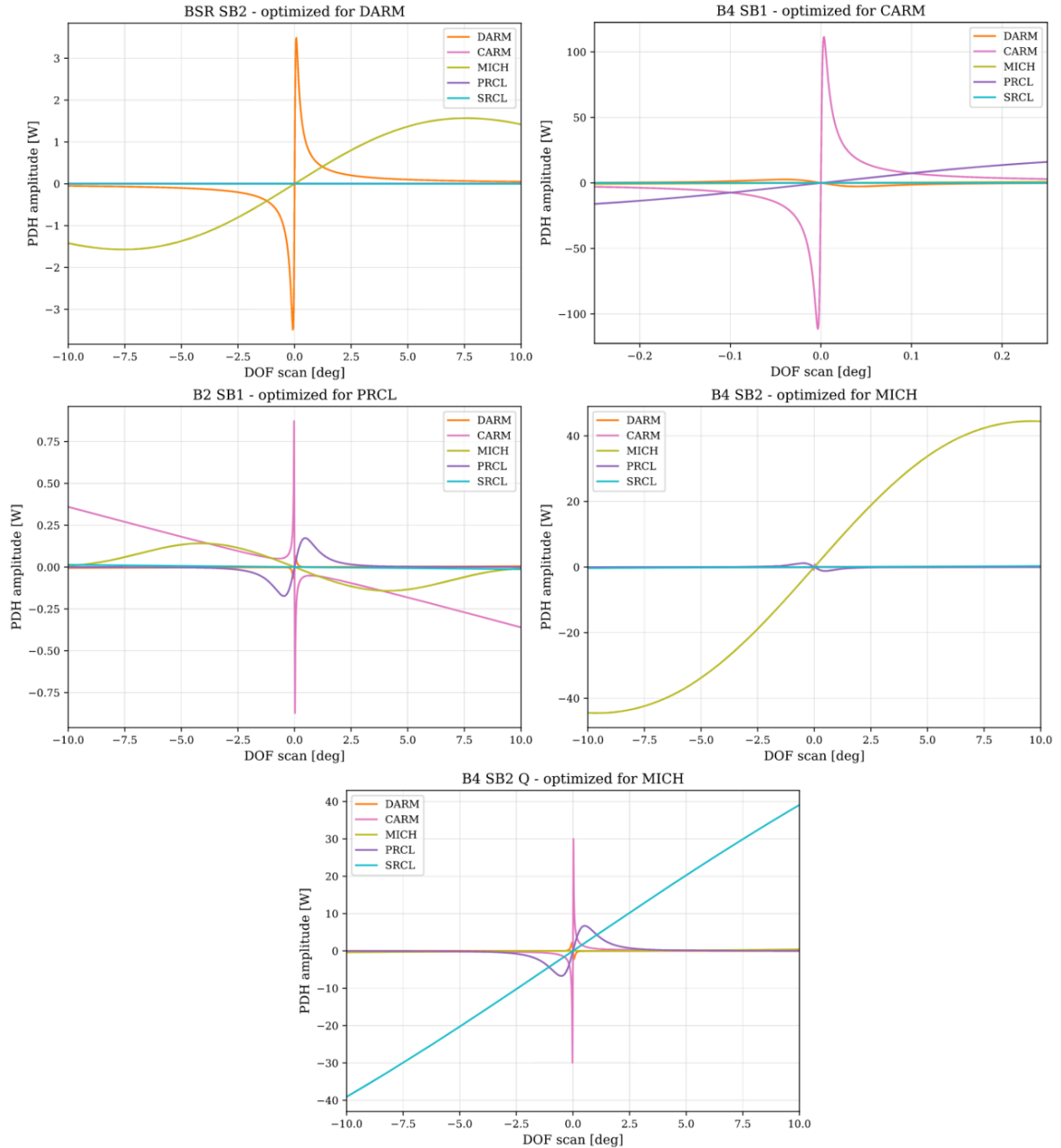


Figure 21 - Decoupling plots of the chosen error signals

Sensing matrix and decoupling angle

Starting from the error signals previously selected, we have built the so-called Sensing Matrix. For each one of the chosen error signals (demodulated for the DOF meant to be controlled by it) it shows the optical gain (normalized by the input power) of each DOF. The sensing matrix resulting from this study is shown in Table 2:

	DARM	CARM	MICH	PRCL	SRCL
BSR SB2	4.2e+10	0.4	2.5e+08	6.3e+04	1.1e+04
B4 SB1	1.7e+07	8.4e+09	5.3e+05	1.1e+07	1.2e+04
B4 SB2	1.4e+05	0.7	1.2e+06	6.4e+05	3.7e+04
B2 SB1	2.6e+07	1.3e+02	1.4e+06	1.7e+07	3.5e+04
B4 SB2	5.0e+06	25.5	0.6	3.4e+06	6.1e+05

Table 2 - Sensing Matrix

The sensing matrix summarizes what we had already observed from the Compass and Coupling plots: DARM and CARM error signals are very well decoupled, while the central DOFs are more coupled. As a side note, the sensing matrix reflects the slope of the coupling, but it doesn't show the peak-to-peak amplitude or the linear region of the coupling. This means that the sensing matrix represents the worst case scenario.

In order to compare different configurations, a useful parameter to calculate is the "decoupling angle" of the sensing matrix. It is defined as:

$$\alpha = \arcsin(\det(M_{norm}))$$

where M_{norm} is the sensing matrix, with each row normalized by its magnitude. The first row on Table 3 shows the decoupling angle of the sensing matrix. This number is quite small (0 corresponds to a completely degenerate matrix), so we tried to mimic the experimental approach we use for: hierarchical controls. This approach consists of using different bandwidths for each longitudinal dof, in order to minimize the cross coupling of the higher bandwidth to the lower bandwidth ones. We have used the bandwidths used in Advanced Virgo+ Phase I.

Using these values, we have normalized the matrix columns by the corresponding loop gain, and multiplied the rows by the gain of the loop that is to be controlled with the corresponding sensor. We left unchanged the diagonal cells and the column corresponding to CARM DOF. With this normalization, the decoupling angle improves significantly, as seen in the second row of Table 3.

	Short Virgo-like	Short LIGO-like	Long Virgo-like	Long LIGO-like	AdV+
α [deg]	2.7	2.6	2.6	2.5	0.39
α_{hier} [deg]	35.8	32.7	35.5	31.8	21.3

Table 3 - Decoupling Angle of the different configurations

The most important conclusion is that the performance of all the optical configurations is better than the one of AdV+ Phase I, which is the one presently used. Moreover, all the configurations studied show very similar behaviors. Since, from the longitudinal control point of view, there is no significant advantage in using a Virgo-like or LIGO-like configuration, our proposal is to drop the Virgo-like ones, which do not allow to control the SR alignment in an effective way. Thus, we will only study the alignment strategies for the LIGO-like configurations. More details on the simulations performed can be found in [VIR-1186B-23](#). The simulation's scripts can be found in the [Git repo](#).

2.5.3. Angular Control

The simulations on the angular control are yet in a very early stage, to extract any conclusion yet. However, based on ours (and LIGO) experience, the SR alignment is the most critical DOF. For this reason, the Gouy phase of the SRC needs to be chosen so that we can generate an error signal with a good SNR, low coupling and high robustness to defects. In particular, the choice is based on the ability to find a control sideband that has the HOM1 of only one component (upper or lower) resonant inside the SRC. Then, the one of the PRC will be chosen to provide a sensing matrix with a good decoupling, all while trying to keep the HOMs of the carrier far from resonance.

2.6. Thermal effects

2.6.1. Introduction

In Advanced Virgo, marginally stable cavity configuration imposed stringent demands on the thermal compensation system sensors and actuators (VIR-0128A-12). The implementation of stable recycling cavities makes the detector less prone to the development of HOMs, and consequently, less sensitive to thermal effects relaxing the TCS requirements.

This section presents the initial results aimed at evaluating the recycling gains in the short stable cavity configuration, especially in the scenario where the PRC has a Gouy phase equal to 25 degrees and the SRC 19 degrees.

2.6.2. Thermal effects evaluation

The main laser-induced optical path length increase has been evaluated assuming the same Fabry-Perot cavities configuration as in O4 (VIR-0128A-12). In this scenario, the cold RoC of the ITM is 1420 m and the beam size is 49 mm, while on the ETM, the cold RoC equals 1683 m with a beam size of 58 mm. The thermal effects due to the self-heating of the test masses with 40 W of input power have been computed using the parameters listed in Table 4.

Input power	40 W
ITM RoC	1420 m
Arm cavity Finesse	450
Carrier recycling gain	41
Coating absorption	0.5 ppm

Table 4 - Main parameters used for the estimation of thermal effects.

The temperature distribution within the mirror, considering the absorbed power of 118 mW in the Finite Element Analysis (FEA) model, is shown in Figure 22 (right). On the left side of the same figure, the resulting Optical Path Length (OPL) increase and the Gaussian weighted quadratic fit are displayed.

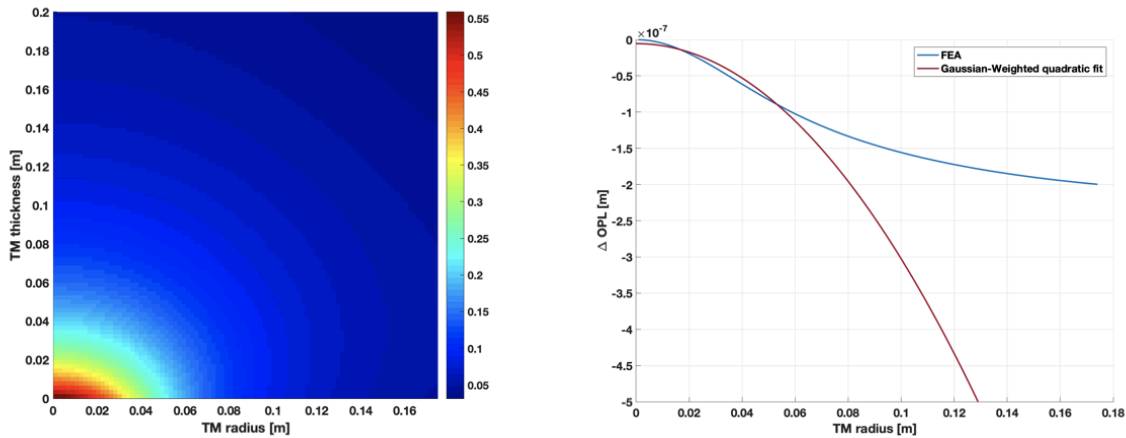


Figure 22 – Right: temperature distribution inside the TM for 118 mW absorbed power. Left: optical path length increase (blue) and Gaussian Weighted quadratic fit (red).

The obtained focal length is ~ 17 km, or equivalently $\sim 57 \mu\text{D}$, and the OPL map is shown in Figure 23.

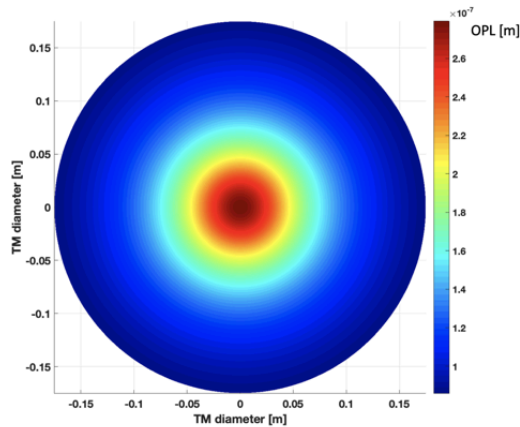


Figure 23 – OPL map considering 118 mW of absorbed power.

The impact of optical aberrations induced by thermal effects on the detector performance has been carried out using OSCAR. This tool has been previously employed in developing the Advanced Virgo optical layout and implementing the thermal compensation strategy during the observing run commissioning phases ([VIR-0128A-12](#)).

2.6.3. OSCAR simulations

The choice to use OSCAR ([Git repo](#)) is driven by the accuracy of the results also in presence of non-spherical deformations.

The OSCAR ‘short cavity’ simulation code

(Advanced_Virgo_stable_short_Gouy_25_deg_35m_review_document.m) has been developed by J. Degallaix and it is accessible at [this link](#).

The figures of merit identified to assess the impact of thermal effects include recycling gains, for both carrier (CAR) and sidebands (SB_1 and SB_2), as well as their percentage of TEM00 mode content. Relevant simulation parameters, such as the frequency and modulation depths of sidebands resonating in the recycling cavities, the RoCs of interferometer optics, the Angle of Incidence (AoI) of recycling mirrors, as well as their transmissivity (T) and losses (L), are summarized in Table 5.

SB_1	$f = 6.3208 \text{ MHz}$	Modulation depth = 0.22
SB_2	$f = 56.8872 \text{ MHz}$	Modulation depth = 0.25
$RoC_{PRM1/SRM1}$	-5.209 m	
$RoC_{PRM2/SRM2}$	-1.929 m	
$RoC_{PRM3/SRM3}$	20.2 m	
$AoI_{PRM2/SRM2}$	3.74°	
$AoI_{PRM3/SRM3}$	1.08°	
T_{PRM1}	0.05	
$T_{PRM2/SRM2}$	100e-6	
$T_{PRM3/SRM3}$	100e-6	
T_{SRM1}	0.4	
L_{PRM1}	1500e-6	
$L_{PRM2/SRM2}$	0	
$L_{PRM3/SRM3}$	0	
L_{SRM1}	0	
$T_{\text{North ITM}}$	0.01377	

$T_{\text{West ITM}}$	0.014
$T_{\text{NE TM/WE TM}}$	5e-6
$L_{\text{NE TM/WE TM}}$	55e-6

Table 5 - Main parameters settled in OSCAR code: RoCs (Radius of Curvature), AoI (Angle of Incidence), T (transmissivity) and L (losses) of the detector optics.

The results of simulations, with and without thermal effects, for both carriers and sidebands, are summarized and compared in Table 6 ([VIR-0031A-24](#)).

PRC carrier gain	All modes		TEM00	
Without thermal effects	41.8		99.9 %	
With thermal effects	41.8		99.8 %	
PRC 6 MHz gain	All modes		TEM00	
	Upper	Lower	Upper	Lower
Without thermal effects	71.9	71.9	99.9 %	99.9 %
With thermal effects	24.7	24.6	92.5 %	92.5 %
PRC 56 MHz gain	All modes		TEM00	
	Upper	Lower	Upper	Lower
Without thermal effects	52.1	52.1	99.9 %	99.9 %
With thermal effects	21.3	19.9	93.3%	93.4 %

Table 6 - OSCAR results in the perfect case compared with those obtained including thermal effects generated by 40 W of input power for the short cavity configuration.

The carrier gain remains unchanged compared to the perfect case, while the gains of the sidebands decrease by factors ~ 3 . Additionally, it is noteworthy that the percentage of TEM00 remains $> 90\%$ even in the presence of thermal effects.

2.6.4. Comparison with marginally stable configuration

For comparison, Table 7 summarizes the results from OSCAR, including the thermal effects expected at 40 W input power, in the double marginally stable cavities case ([VIR-0031A-24](#)).

PRC 6 MHz gain	All modes		TEM00	
	Upper	Lower	Upper	Lower
With thermal effects	6.0	6.1	10 %	9 %
PRC 56 MHz gain	All modes		TEM00	
	Upper	Lower	Upper	Lower
With thermal effects	5.0	4.2	9 %	7 %

Table 7 – OSCAR results including thermal effects generated by 40 W of input power in Advanced Virgo marginally stable optical configuration.

This comparative analysis is provided to highlight the differences in the interferometer figures of merit, particularly in describing the sideband behavior, between the stable and marginally stable configurations. Notably, in the latter case, there is a substantial reduction in the TEM00 percentage.

2.6.5. OSCAR results with 80 W of input power

To investigate the impact of thermal effects as the input power increases, simulations were re-run by doubling the previously considered input power, from 40 W to 80 W ([VIR-0049A-24](#)).

The carrier and sideband gains, as well as their TEM00 percentage, are summarized in Table 8 and compared to the ideal case (no thermal effects).

PRC carrier gain	All modes	TEM00
Without thermal effects	41.8	99.9 %
With thermal effects	30.3	93.7 %

PRC 6 MHz gain	All modes		TEM00	
	Upper	Lower	Upper	Lower
Without thermal effects	71.9	71.9	99.9 %	99.9 %
With thermal effects	2.7	2.6	85.7 %	85.7 %
PRC 56 MHz gain	All modes		TEM00	
	Upper	Lower	Upper	Lower
Without thermal effects	52.1	52.1	99.9 %	99.9 %
With thermal effects	2.6	2.5	85.3 %	85.5 %

Table 8 - OSCAR results in the perfect case compared with those obtained including thermal effects generated by 80 W of input power for the short cavity configuration.

In absence of thermal compensation, the gains decrease drastically at this input power, making the interferometer not workable. The positive aspect is that the TEM00 percentage remains > 80 %, highlighting once again the benefits of stable recycling cavities.

	Short Stable Cavities Preliminary Design	Date 2024-05-22 VIR-0461A-24 Page 51 of 101
---	--	---

2.7. Mirrors

2.7.1. Introduction

The main requirements for the three mirrors composing the recycling cavities are listed here below.

Diameter: this depends on the amount of beam clipping acceptable. The three power recycling mirrors should allow extracting B3/B4 without clipping too much of the secondary beams from the beam splitter and from compensation plates. Similarly the signal recycling mirrors should allow extracting B1 and B5 without clipping too much of the other secondary beams from the beam splitter and from the compensation plates.

Mass: in some cases, the beam impinging on the mirror is quite small and so a little mirror will be sufficient from an optical point of view. In the case of the recycling cavity the power impinging the mirror at the time of the Virgo_nEXT can reach up to 10 kW and so it is important to consider the effect of radiation pressure. This consideration may limit the minimum mass one could accept to have.

Thickness: small thickness could become a problem if the mirror becomes too soft and its deformation affects the radius of curvature. This is usually more important for mirrors having long RoC like the arm mirrors.

Wedge: for all the mirrors it is good to have a wedge so to avoid that the reflection from the second face of the mirror can recombine with the main beam. This is particularly important for PRM1 and SRM1 as their transmission is higher.

Coating characteristics: two of the three recycling mirrors composing the PRC are HR. Only a very small fraction of the light is transmitted to extract the B3/B4 beams. In the case of the SRC the mirrors are HR to minimize losses inside the signal recycling cavity. The reflectivity of PRM1 and SRM1 are determined by the desired recycling factor. The requirements in terms of scattering and absorption can be similar to the one of the cavity mirrors.

2.7.2. PRM1/SRM1

These mirrors have to be suspended on the top of the injection and detection bench respectively. For this reason it is interesting to minimize their mass. In the case of LIGO these mirrors are 150 mm in diameter and 100 mm thick for a total mass of 2.9 kg. In our case we propose to use 100 mm diameter and 75 mm thick mirrors for a mass of 1.3 kg. The effects of radiation pressure at the time of Virgo_nEXT have been studied, finding that they are manageable.

The mirrors RoC are given in section ‘Optical Configuration’. The accuracy of the RoC is assumed to be 1% (same specification as Advanced LIGO). Given the short RoC, it is possible to show that this level of error on the RoC can be compensated by changing the mirror position by one mm or less.

The required wedge needs to be defined. For sure a wedge is required to avoid that the reflection from the second face is reflected towards the interferometer and it can be separated from the main beam.

The mirror reflectivity can be decided at a later stage. At this stage we suppose that their transmissivity will be the same as for Adv+ Phase I i.e. 5% for PRM1 and 40% for SRM1.

	Diameter	Thickness	Mass	RoC	deltaRoC	Transmissivity
PRM1	100 mm	75 mm	1.3 kg	See Optical Configuration	1%	5%
SRM1	100 mm	75 mm	1.3 kg	See Optical Configuration	1%	40%

The substrates for these mirrors (one substrate plus one spare for each type) can be obtained from existing larger substrates from Advanced Virgo.

For each type of mirror PRM1/SRM1, one spare substrate will be needed (4 substrates in total).

We will use old Advanced Virgo substrates in Suprasil 3002 (low absorption), which are available, to produce these new substrates (no need to order new blanks).

The polishing specifications will be finalized when the final radius of curvature will be frozen in the optical configuration. Anyway, the flatness/microroughness requirement will be comparable to what was asked for Advanced Virgo+ ([VIR-0404A-22](#)) on the central part.

These mirrors will work at normal incidence.

2.7.3. PRM2/SRM2

PRM2 is the curved convex mirror that transforms the divergent coming from PRM1 into a further divergent one sent toward PRM3. SRM2 does exactly the opposite i.e. it converges the already converging beam coming SRM3 towards SRM1. These mirrors should also reflect the beams coming from the secondary faces of the beams splitter (B5 in the case of SRM2) and from the compensation plates. The beam size on these mirrors is already small (about 4 mm) so that these mirrors can be relatively

small. For convenience it is proposed to use 150 mm diameter mirrors i.e. the same diameter of the mirrors used for the filter cavity.

Both mirrors are HR. The transmissivity of PRM2 is to be determined according to the amount of light desired on SPRB given that the B3/B4 pickoff beam is extracted from the transmission of PRM2. In the case of SRM2 this should be smaller than 100 ppm to avoid contributing too much to the losses in the signal recycling cavity and to avoid potential issues with scattered light.

The mirrors RoC are given in section ‘Optical Configuration’. The accuracy of the RoC is assumed to be 1% (same specification as Advanced LIGO). Given the short RoC, it is possible to show that this level of error on the RoC can be compensated by changing the mirror position by one cm or less.

	Diameter	Thickness	Mass	RoC	deltaRoC	Transmissivity
PRM2	150 mm	100 mm	2.9 kg	See ‘Optical Configuration’	1%	100 ppm (TBC)
SRM2	150 mm	100 mm	2.9 kg	See ‘Optical Configuration’	1%	<100 ppm

For the PRM2/SRM2 substrates (one substrate plus one spare for each type - 4 substrates in total), old Virgo/Advanced Virgo substrates in Suprasil 312 or Suprasil 3002, which are available, will be re-used to produce these new substrates (no need to order new blanks).

The polishing specifications will be finalized when the final radius of curvature will be frozen in the optical configuration. Anyway, the flatness/microroughness requirement (TBC) will be comparable to what was asked for Advanced Virgo+ ([VIR-0404A-22](#)) on the central part.

2.7.4. PRM3/SRM3

PRM3 and SRM3 are curved concave mirrors working close to normal incidence (AOI=1.08 degrees). Their RoC is 20.2 m and it is mainly determined by their distance from PRM2/SRM2.

The precision on their RoC is important. Minimum specification is 0.5%, so PRM3/SRM3 needs good polishing. In the context of the LIGO project, polishers have already accepted this level of accuracy and were able to achieve accuracies of the order of 0.2% or better. The mirror focusing the beam into the filter cavity has a RoC similar to PRM3/SRM3. An accuracy of the order of 0.1% was achieved in that case. This is important because residual errors of 0.2% in the RoC of PRM3 can be compensated with a thermal actuator (Ring heater or CHRoCC). In case the PRM3/SRM3 mirror RoC’s were wrong by 0.5%,

the distance between PRM3/SRM3 and PRM2/SRM2 would have to be changed by about 5 cm and the one between PRM2/SRM2 and PRM1/SRM1 by 10 cm. If deemed necessary, these type of adjustments can be foreseen at the time of the construction of vacuum chambers and suspensions

Their size is determined by the need to properly reflect the beams coming from the second face of the beam splitter and from the compensation plates without too much clipping. Calculation shows that using a diameter of 265 mm (same as Advanced LIGO) the clipping of B1 is negligible and the clipping of B5 amounts to 900 ppm. Proposed thickness is 100 mm (same as Advanced LIGO), giving a mass of 12 kg. Alternatively the same mass can be achieved with a substrate 300 mm in diameter and 75 mm thick. Given the relatively short RoC of these mirrors, this aspect ratio (more favorable than e.g. the beam splitter) remains acceptable and allows having a larger aperture if required. Alternatively, the known issue with beam splitter vertical wedge can be solved and the new wedge chosen to be horizontal and appropriate to superpose B5 and B1 on the SRM3 mirror (as it was done in initial Virgo where the wedge was chosen so to have B1 and B5 superposed at the entrance of the detection bench).

Even if the coating will be HR, a wedge seems desirable (to be discussed).

The transmissivity of PRM3 is to be determined according to the amount of light desired on its transmission (if any). The transmission of SR3 instead has to be smaller than 100 ppm to avoid too much losses in the signal recycling cavity and potential issues with scattered light.

	Diameter	Thickness	Mass	RoC	deltaRoC	Transmissivity
PRM3	265 mm	100 mm	12 kg	20.2 m	0.5% min 0.2% goal	<100 ppm (TBC)
SRM3	265 mm	100 mm	12 kg	20.2 m	0.5% min 0.2% goal	<100 ppm

For the PRM3/SRM3 substrates (one substrate plus one spare for each type - 4 substrates in total), old Virgo/Advanced Virgo/Advanced Virgo+ substrates in Suprasil 312 or Suprasil 3002, which are available, will be re-used to produce these new substrates (no need to order new blanks).

The polishing specifications will be finalized when the optical configuration will be frozen. Anyway, the flatness/microroughness requirement will be comparable to what was asked for the Beam Splitter.

2.8. Thermal control: PRM3/SRM3

Control of the radius of curvature of these mirrors can be achieved with the known methods: Ring Heater or Central Heating Radius of Curvature Correction (CHRoCC). For the short cavities option, PRM3 and SRM3, have a very short radius of curvature, of the order of 20 m. In this case, the thermo-structural simulations show ([VIR-0911A-23](#) and [VIR-01034A-23](#)) that the absolute value of the dynamics of both the Ring Heater and the CHRoCC becomes very low, and a maximum polishing error of about 0.2% can be reasonably compensated with thermal actuators. The RH computed dynamics is about $6.3e-4$ m/W, thus about 40 W are needed to reduce the RoC by 0.15% (as shown in Figure 24).

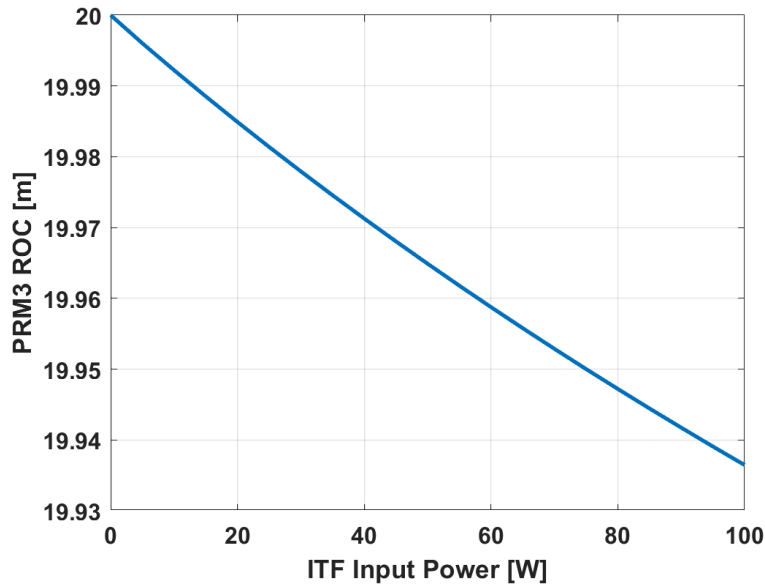


Figure 24 - RH dynamics as a function of the delivered power for a mirror with diameter 260 mm and thickness 100 mm.

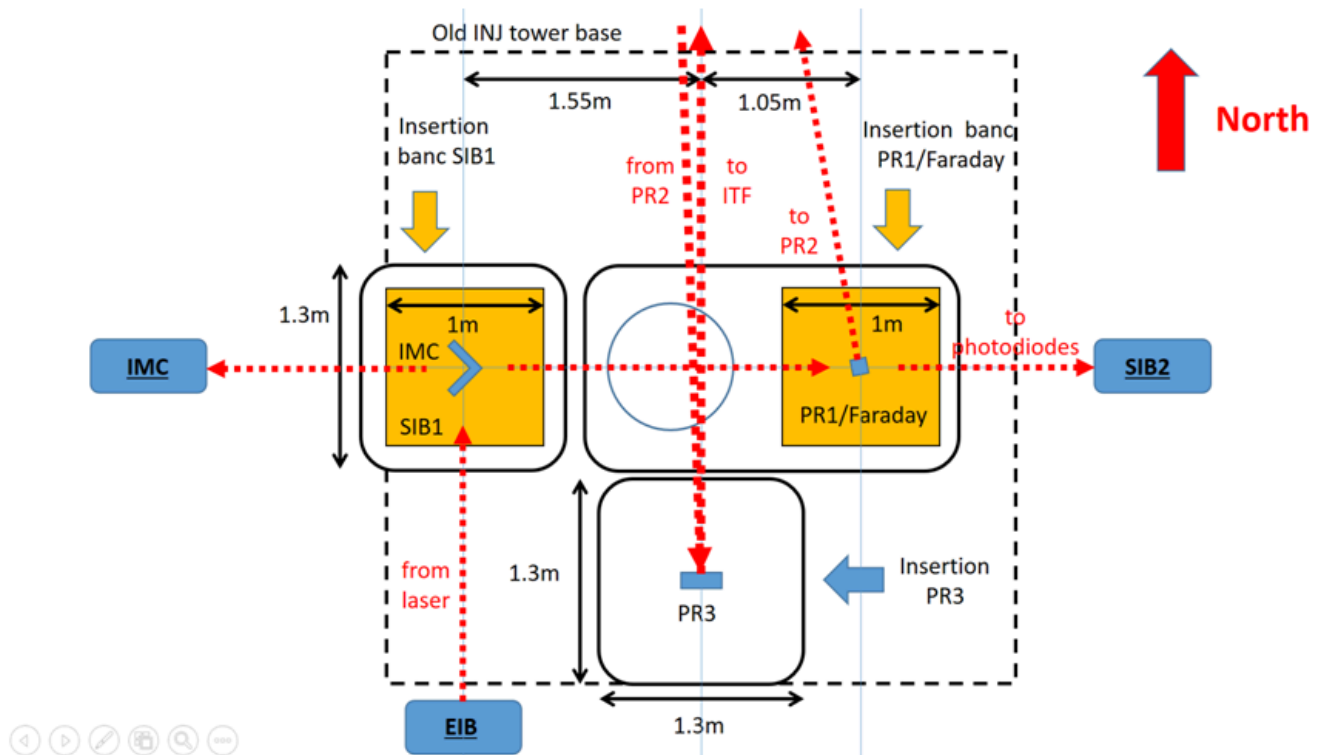
It must be noted that, within the LIGO project, polishers were able to achieve accuracies of the order of 0.2% or better ([VIR-1074A-23](#)). Thus, larger RoC errors need to be compensated by changing the distance between the recycling cavities mirrors. For instance, if the PRM3/SRM3 mirror RoC's error were about 0.5%, the distance between PRM3/SRM3 and PRM2/SRM2 would have to be changed by about 5 cm and that between PRM2/SRM2 and PRM1/SRM1 by 10 cm.

2.9. Injection: SIB1

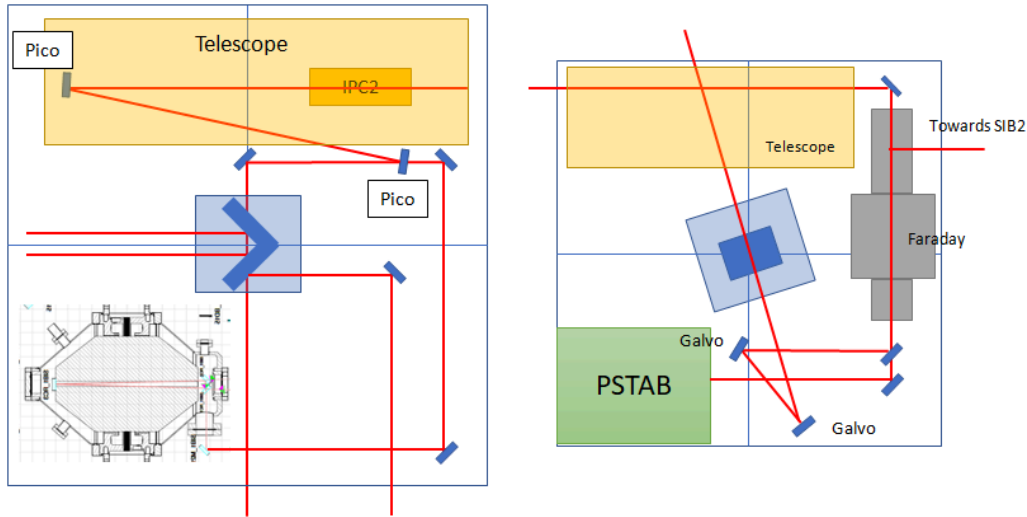
2.9.1. General considerations

In this arrangement, the current suspended input bench undergoes a division into two distinct benches. The initial one, SIB1, continues to accommodate the flat mirrors of the input mode-cleaner and the reference cavity, like in the current configuration. The second bench, referred to as the PR bench, accommodates the input Faraday isolator, the power recycling mirror suspended through a double pendulum at the bench's top, and the power stabilization box. The laser beam initially reaches SIB1 and, following filtration by the input mode-cleaner, is directed towards the PR bench. The corresponding overall layout is illustrated in the figure below.

A more detailed representation of the implementation of the hardware on the two benches is shown. The details of both benches are given in their respective subsection below. To be noted that there is space both on SIB1 and PR bench to accommodate the telescope needed to match the output beam of the IMC in the PRC. The two solutions have been studied but we are presenting only the one where the mode matching telescope is hosted on the SIB1 bench.



Conceptual scheme of the injection port with the short stable recycling cavities.



First draft of a possible optical scheme for the SIB1 and PRM1 benches

2.9.2. SIB1 considerations

SIB1 is planned to be a 1 m x 1 m bench, similar to what has been designed for SIB2. The final design is still pending and will depend on optical requirements but the first specifications are outlined in the dedicated section. The 1 m x 1 m dimensions provide ample space flexibility, and the maximum weight limit of 325 kg offers a substantial margin. The suspension system employs three wires, preserving the central space for potential dihedron accommodation. The plan is indeed to position the dihedron at the bench's center and suspend it with a double pendulum if necessary.

Considerations regarding the optics of the Input Mode-Cleaner (IMC) are addressed in the subsequent IMC length reduction subsection. Following this, the output beam from the IMC undergoes shaping through a mode-matching telescope, discussed in its dedicated subsection. To maintain alignment towards the PR bench, two actuators are employed.

The inclusion of IPC2 remains a topic of ongoing deliberation. Initially conceived to facilitate a gradual power increase during lock acquisition while maintaining injection locked, its current configuration proves ineffective. It causes the injection to unlock when used and also introduces unwanted stray light into the ITF. Should we decide to proceed with its installation, substantial efforts are required to mitigate noise issues and enhance the control of stray light resulting from discarded power.

	Short Stable Cavities Preliminary Design	Date 2024-05-22 VIR-0461A-24 Page 58 of 101
---	--	---

In the presented scheme, the pick-off beam is directed to the Reference Cavity (RFC) as is. However, it will require actuators to ensure precise alignment, along with a mode-matching telescope. Given the similar conditions, there is potential for reusing the optics currently in use.

2.9.3. PR bench considerations

The PRM1 bench was originally considered to be 0.8 x 0.8 m² and the draft of the optical scheme presented in this document has been done considering those 0.8 x 0.8 m² ; but in order to keep a uniformity between all the new benches it has been decided to increase its dimension to 1 x 1 m². This increase of space will be taken into account in the next upgrades of the optical scheme.

The main feature of this bench is the placement of PRM1 at its center suspended by a double pendulum. Again specific suspension specifications are provided in the dedicated section.

The beam from SIB1 traverses the Faraday Isolator, whose considerations regarding magnetic screening are still under discussion. Such a measure would aim at preventing external magnetic disturbances to couple to the permanent magnet, which in turns induce some additional motion of the bench. The details of the noise coupling are explained in <https://tds.virgo-gw.eu/ql/?c=18990>, paragraphs 1.2 and 1.3. This adjustment is also intended to enhance a safety operation of the galvo actuators, which operate through magnetic means. The initial stages of this study have commenced, and an initial version of a magnetic shield has been simulated. While the specific details of the magnetic shield for SIB1 are not provided in this document (see VIR-0061A-24 for more details), it is important to note that implementing this magnetic shield will slightly increase the overall footprint of the Faraday system and introduce an additional weight of approximately 10 kg.

Following the Faraday Isolator, a pick-off beam is directed towards the PSTAB box. The decision on whether to utilize the quadrant photodiodes of the PSTAB or employ dedicated ones, coupled with the position actuators of SIB1, is yet to be defined.

The main beam is then actuated towards the PRM1 using some beam pointing actuators. Specifically we want to install some galvo actuators already successfully employed for beam pointing on SIB2 and for the SQZ,. We're in the process of refining the specifications, but the goal is for the galvo actuators to accommodate 1 inch mirror, having a resonant frequency up to 100 Hz to allow an actuation up to 20-30 Hz. The actuation range is still being worked out and will depend on the final optical design.

	Short Stable Cavities Preliminary Design	Date 2024-05-22 VIR-0461A-24 Page 59 of 101
---	--	---

2.9.4. IMC length reduction

To be noticed that for this configuration a slight modification of the fundamental frequency (F_{mod}) of the sidebands is necessary. So this requires an adaptation of the FSR and the IMC needs to be shortened by approximately 1.15 m, reducing its length from 143.44 m to 142.29 m.

Because of the configuration SIB1 is already shifted by 1.55 m towards the west. We also mentioned before that the dihedron will be placed at the center of SIB1, around 25 cm towards the east.

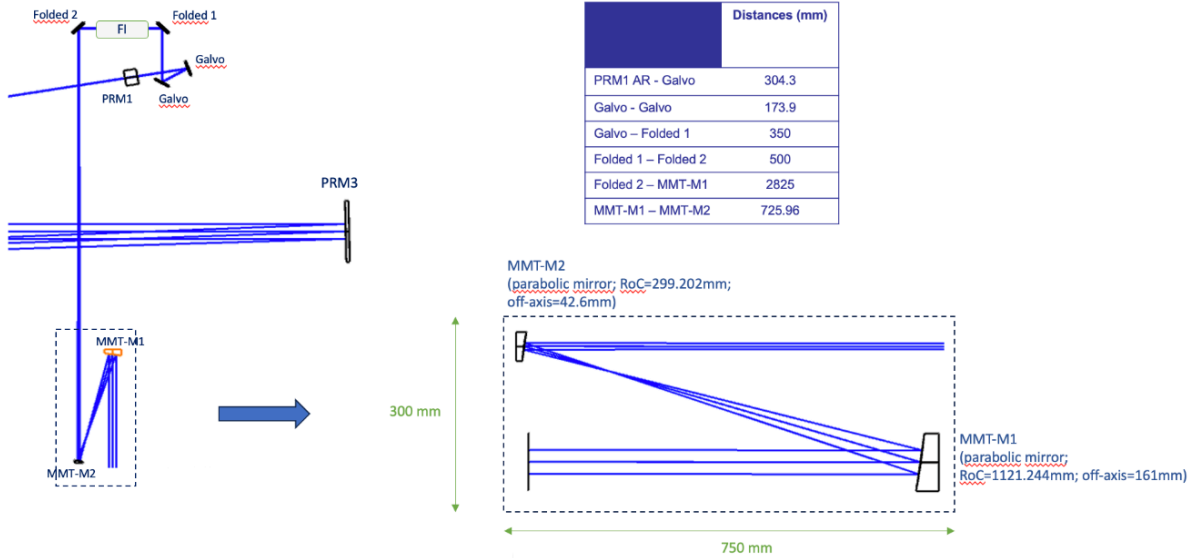
So at the end of the day, we will need to lengthen the cavity by about 15 cm. This could be done by relocating the IMC tower westward. Fortunately, similar displacements of IMC towers have been successfully executed in the past. Another solution potentially less invasive but not studied yet would be to slightly adjust the current proposed design to have SIB1 15 cm eastward.

Such a change in the cavity length will change the size of the intracavity waist of about 5.1 mm by about 20 μm . Regarding the current optics, the existing dihedron can be retained, it will only slightly modify the impact point. Simulation work is in progress to assess the compatibility of the current Mode Cleaner mirror.

2.9.5. Mode-Matching Telescope

The telescope should decrease the size of the beam in the IMC (~ 5.1 mm) to the size of the beam at the input of the cavity (~ 1.5 mm on PRM1) and be able to reach a matching of the laser beam to the ITF beam higher than 99%. Moreover, it should fit the space constraints on SIB1 and stay inside a rectangle of $\sim 800 \times 300$ mm². The amount of back-scattered light or back-reflected light from the telescope optics should be compliant with the sensitivity requirements, i.e AdV+ Phase II sensitivity/10.

A preliminary design has been considered, using an afocal parabolic telescope that decreases the beam size from 5.1 mm to 1.3 mm (magnification 3.9). Then, a curvature on the PRM1 AR side is used to match the beam to the short cavity beam. The big interest of this configuration is the compactness of the telescope (as currently for AdV+ Phase I), and the very good matching (higher than 99.88%).



Optical parameters for a possible mode matching telescope made of two parabolic mirrors and using a curved surface for the AR side of PRM1.

Note that this design is preliminary. Some improvements will be done to increase the matching, and a tolerancing analysis has to be performed to evaluate the sensitivity to the RoCs, the surface imperfections and the motion of the optics. We will especially study the lateral motion of the curved surface of PRM1 that would couple into a tilt of the input beam. Moreover, the impact of the FI thermal lens has to be considered and the straylight will be analyzed. This layout and optical parameters have been simulated considering the current test masses (AdV+ Phase I), and have to be considered with the large test masses (AdV+ Phase II) with as few modifications as possible.

	Short Stable Cavities Preliminary Design	Date 2024-05-22 VIR-0461A-24 Page 61 of 101
---	--	---

2.10. Detection: SDB1

2.10.1. Introduction

This section briefly describes how the detection port can be adapted to the short signal recycling cavity configuration. An overview of how the detection port will be reshuffled is shown on Figure 25. It is foreseen to dismount the current detection tower (floor imprint of 16 m²) and to replace it with three new vacuum chamber modules, all sharing the same vacuum. One of these modules will host the SRM3 mirror. A second module will host a suspended optical bench, called SRB for Signal Recycling Bench, and a third module will host the suspended bench called SDB1. Therefore, in this new configuration, the present SDB1 bench is replaced by two new suspended optical benches. The SRB bench will host the SRM1 mirror and its suspension, as well as the output Faraday Isolator. The new SDB1 bench will host the mode matching telescope and the Output Mode Cleaner cavity.

The main reason for having a shared vacuum between the three chamber modules is to avoid permanent windows in between the chambers (to avoid extra optical losses and scattered light) and this solution allows having access to the payloads and benches from a larger number of sides. At the time this document is being written we are discussing whatever we need to have a separation in the case of SDB1 for commissioning purposes, which could result in a compromise between vacuum separation (with a valve) and bench accessibility.

The beams exiting the SDB1 bench will be sent towards the SDB2 bench. For this purpose the SDB2 minitower will be displaced towards the south edge of the detection lab. An extension of the detection clean area will have to be performed in order to leave sufficient spare around the SDB2 minitower, and also to include the new vacuum chamber modules in the clean area.

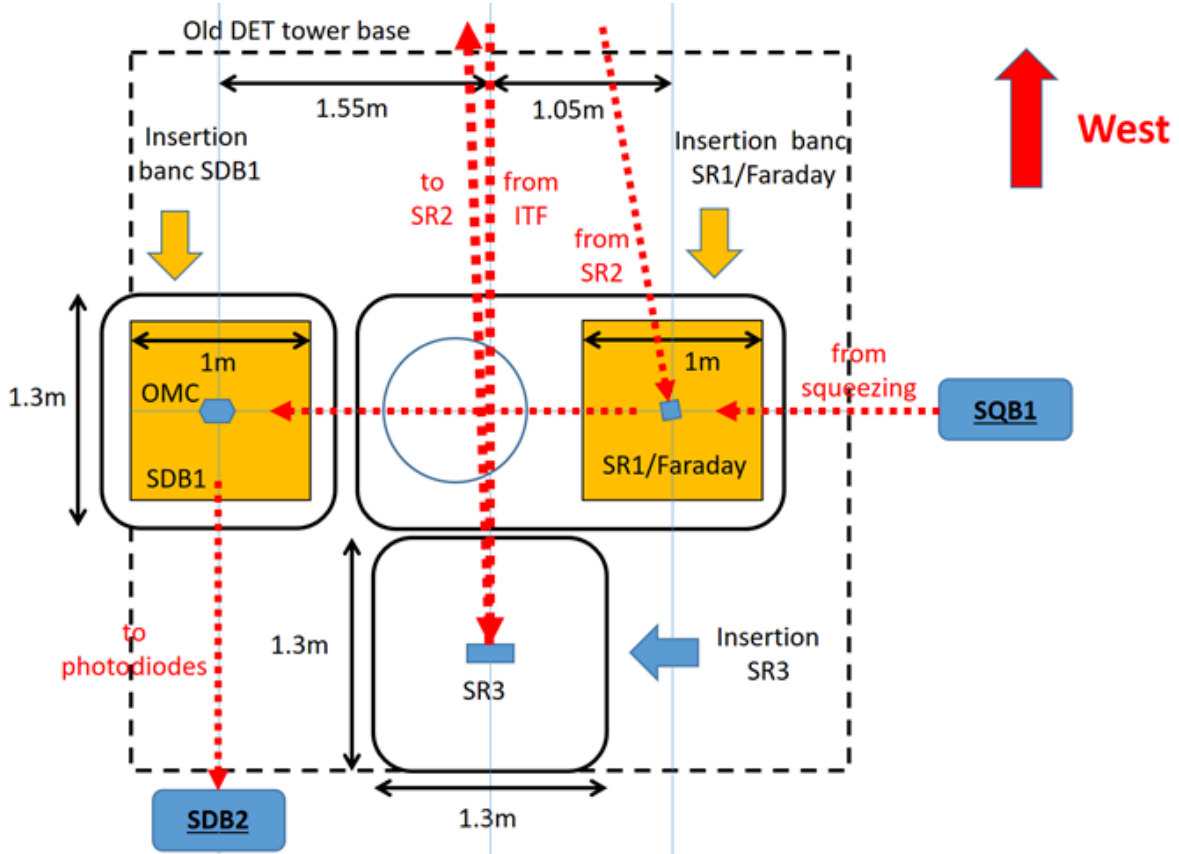


Figure 25 - Conceptual scheme of the detection port with the short stable recycling cavities.

2.10.2. Possible optical scheme for the SRB and SDB1 benches

An example of an optical scheme for the SRB bench is shown on Figure 26. This optical scheme is driven by the following requirements:

- The SRB bench surface has been considered to be a square of 0.8 m side. Very recently, after better checking the constraints for the new vacuum chamber modules and the bench suspension, it has been decided to increase this bench size to 1 m² to provide more space margin for future upgrades. However this has not yet been taken into account in the optical scheme shown in this document.
- The SRB bench is suspended with 3 wires to the marionetta as SDB1 today, which has the advantage to make it possible to control the angular position of the bench by acting on the

marionetta, without any need for magnets on the bench itself, thus reducing the coupling of external magnetic fields.

- The bench must host the SRM1 mirror and its suspension. The suspension legs of SRM1 will be set down on the bench. Their imprint on the bench is materialized by the grey rectangle of 220 x 205 mm² that is placed at the center of the optical scheme (this is an arbitrary choice that may be reviewed in the technical design). The dark fringe beam is coming from the SRM2 mirror located towards the west side of the bench, with an angle of 9.6 deg with respect to the west arm axis, as shown on Figure 26.
- The B5 beam must be extracted before reaching the SRM1 mirror to avoid clipping on the SRM1 mirror edge and to avoid having any light from the B5 beam interfering inside the signal recycling cavity. For the time being optical simulations have assumed a vertical wedge for the beam splitter. Under this assumption the B5 beam is separated vertically from the dark fringe beam at the entrance of the bench by about 90 mm and the two beams have a size w of about 2 mm. Considering that the height of the dark fringe beam is 100 mm with respect to the bench floor this implies that the B5 beam would be at about 10 mm above the bench floor and could be extracted with a small mirror and then brought to the nominal height of 100 mm with a periscope. However, in view of the possible future upgrades such as the Balanced Homodyne Detection, for which the mirror used to extract the B5 beam needs to be suspended, it would be simpler to change the orientation of the beam splitter wedge to have an horizontal separation between the dark fringe beam and the B5 beam.
- The SRB bench layout must be compliant with the injection of the squeezed vacuum field coming from the north side of the bench. The squeezed vacuum field is injected at the level of the rear polarizer plate of the output Faraday Isolator.
- The dark fringe beam must pass through the Faraday Isolator to attenuate the back scatter light that may recouple with the interferometer beam. Optical components at low incidence angle (for instance lenses) must be avoided between the SRM1 mirror and the Faraday Isolator.
- The bench should be compatible with the Hartmann wavefront sensing. However the TCS team is studying the possibility of injecting the Hartmann beam through the SRM2 mirror, which in this case would relax this requirement.
- A couple of DC quadrants are foreseen along the B5 beam path to provide error signals for the bench alignment drift control.
- A fast shutter is placed before the Faraday Isolator and is used to protect the detection components from the powerful flashes triggered by the interferometer unlock.

An example of an optical scheme for the SDB1 bench is shown on Figure 27. This optical scheme is driven by the following requirements:

- The SDB1 bench surface is a square of 1 m².
- As for the SRB bench, the SDB1 bench is suspended with 3 wires to the marionetta.
- The bench hosts the output mode cleaner cavity, as well as a mode matching telescope (see next section). The output mode cleaner cavity (OMC) is assumed to have the same beam waist (~320 um) as the one currently installed in Virgo.
- The bench should allow the extraction of the B1, B1p, B1s and B5 beams. All these beams will be sent to the SDB2 bench through mini-links.
- The bench remains compatible with the Hartmann wavefront sensing.
- A shutter is placed on the path to the OMC and will be closed during the lock acquisition up to the dark fringe state to protect the OMC.
- A couple of DC quadrants is foreseen along the B5 beam path, which will provide error signals for the bench alignment.

Additionally a pair of mirrors mounted on controllable mounts in rotation (based on galvanometer systems or PZT actuators) is foreseen along the path of the dark fringe beam towards the OMC in order to have dedicated actuators for the OMC alignment. Thanks to these actuated mirrors, the bandwidth of the OMC alignment control will be independent from the bandwidth of the bench angular control. Error signals for the OMC alignment will be obtained from RF quadrants placed along the B1s beam on the SDB2 bench.

The position of the B1, B1p, B1s, B5, Hartmann beams traveling from SDB1 to SDB2 is different from the current one. This means that the position of the mini-links will have to be adapted to the new layout, with a modification of the west flange of the SDB2 minitower. The SDB2 bench optical layout will need some reshuffling to accommodate the new positions of the beams but this is not considered to be critical.

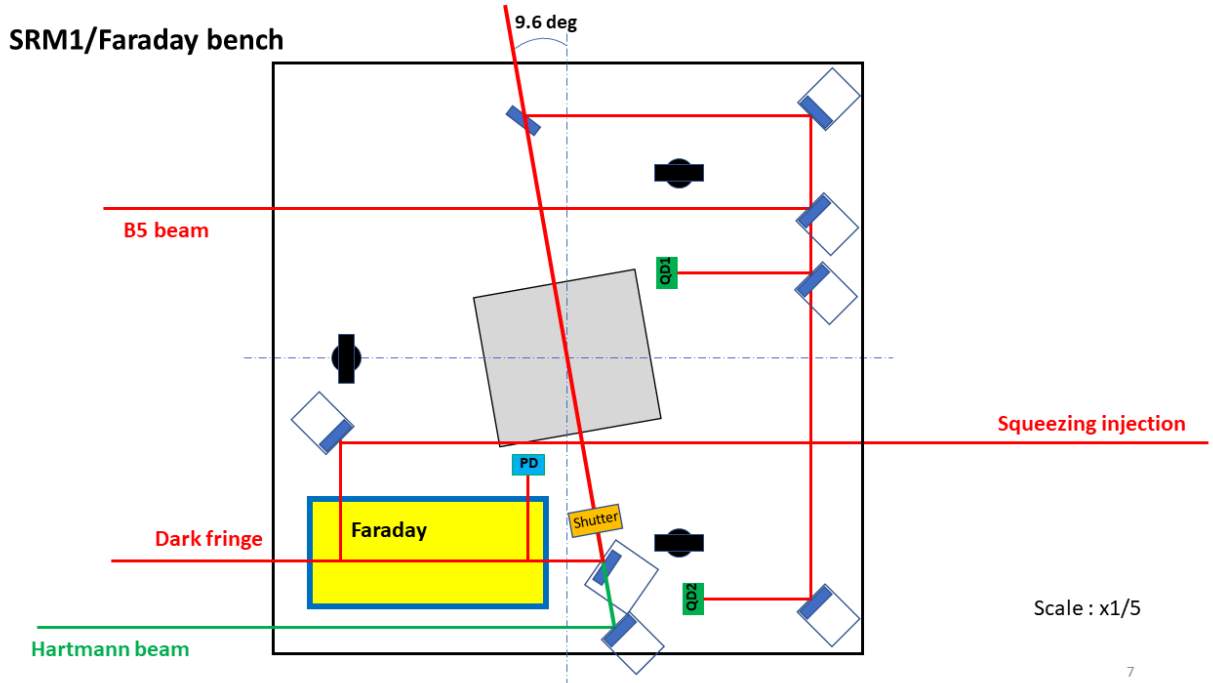


Figure 26 - Example of optical scheme for the SRB bench, hosting the SRM1 mirror and the Faraday Isolator. The bench surface was considered to be $0.8 \times 0.8 \text{ m}^2$, but this is going to be updated to $1 \times 1 \text{ m}^2$.

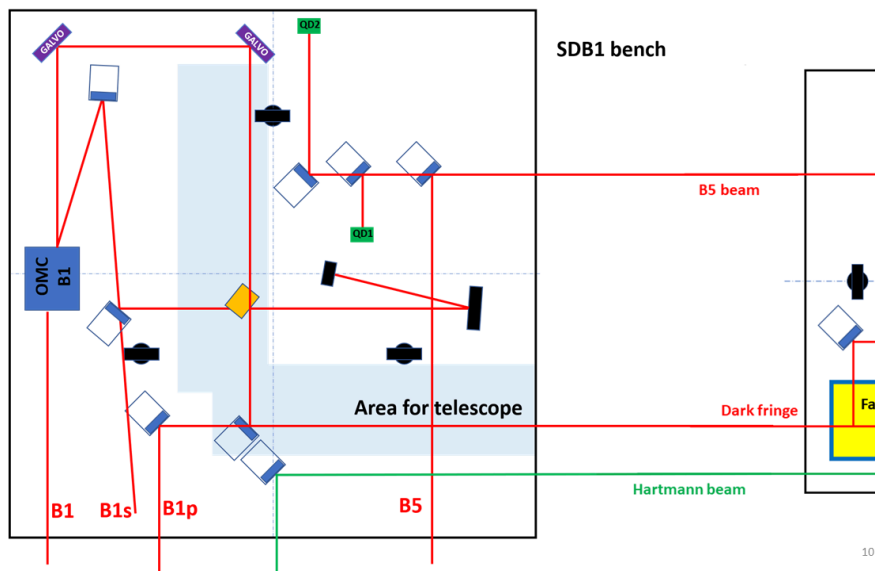


Figure 27 - Example of optical scheme for the SDB1 bench, hosting the Output Mode Cleaner cavity. The SDB1 bench surface is considered to be 1 m^2 .

	Short Stable Cavities Preliminary Design	Date 2024-05-22 VIR-0461A-24 Page 66 of 101
---	--	---

One of the technical risks associated to stable cavities comes from the fact that the SRM1 mirror longitudinal noise must be kept below $1e-17$ m/rtHz @ 10Hz, which translates into a residual motion of $1e-13$ m/rtHz at the SRM1 suspension point. The SRM1 suspension point is about 0.8 m above the bench surface, therefore the bench tilt should not exceed $1e-13$ rad/rtHz @ 10 Hz. Presently the estimated angular motion of SDB1 at 10 Hz is about $3e-13$ rad/rtHz in TX/TY and about $6e-11$ rad/rtHz in TZ and seems to be dominated by the corrections applied. It should be possible to reduce further the residual bench angular motion by improving the control filters. If that is not sufficient, it will also be possible to reduce the control bandwidth of the bench. Unlike the case of the long recycling cavities, the fact that the OMC cavity is not hosted on the same bench as the SRM1 mirror will make it simpler to optimize the bench angular control focusing only on the SRM1 mirror requirements. A fall-back solution consisting in attaching the bench to the Filter 7 of the suspension, and leaving the marionette to suspend SRM1 only could even be envisioned if it is simpler.

2.10.3. Mode-Matching Telescope

The telescope should decrease the size of the beam on SRM1 (~ 2 mm) to the size of the beam at the OMC (~ 0.32 mm) and be able to reach a matching of the laser beam from the ITF to the OMC higher than 99%. Moreover, it should fit the space constraints on SDB1 and stay inside a rectangle of $\sim 400 \times 200$ mm². The amount of back-scattered light or back-reflected light from the telescope optics should be compliant with the sensitivity requirements, i.e AdV+ Phase II sensitivity/10.

A preliminary design has been considered, using a two lens' telescope that decreases the beam size from 2 mm to 0.328 mm. The interest of this configuration is the compactness of the telescope ($\sim 200 \times 100$ mm²), and the very good matching (higher than 99.89%).

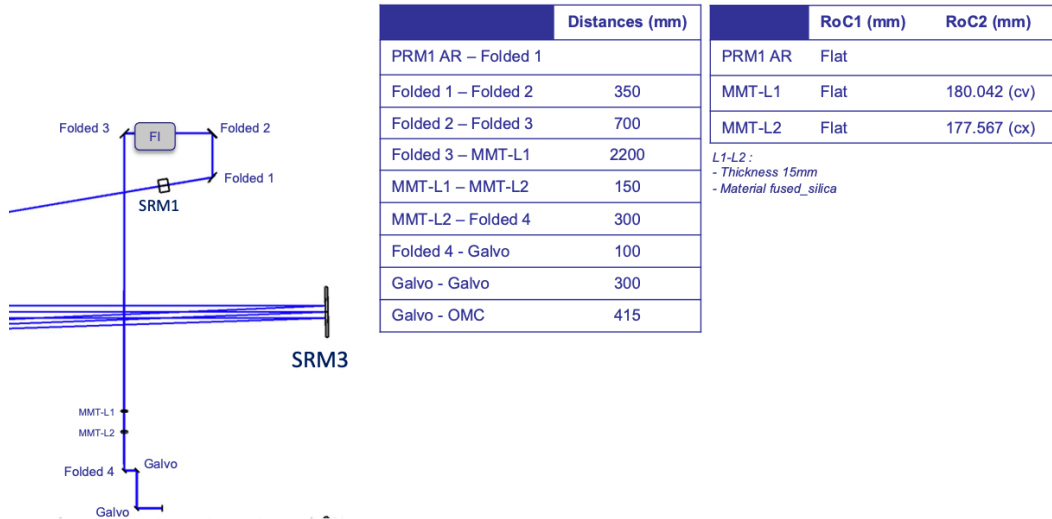


Figure 28 - Optical parameters for a possible mode matching telescope made of two spherical lenses.

Note that this design is preliminary. Some improvements will be done to increase the matching, and a tolerancing analysis has to be performed to evaluate the sensitivity to the RoCs, the surface imperfections and the motion of the optics. Moreover, a reflective configuration is under study in order to compare lens/mirror telescopes. This layout and optical parameters have been simulated considering the current test masses (AdV+ Phase I), and have to be considered with the large test masses (AdV+ Phase II) with as few modifications as possible.

2.10.4. Compatibility with future upgrades

The two new suspended benches needed for the implementation of short stable cavities offer significant space margin that can be used for the implementation of future upgrades such as the Balanced Homodyne Detection.

The bench optical design will be made compatible with the space constraints imposed by the future Balanced Homodyne Detection, in particular on the SRB bench where the final position of the SRM1 mirror will be driven by these constraints.

2.11. Detection: Pick-off

2.11.1. Path for the extraction of the power recycling cavity pick-off

A possible path for the extraction of the power recycling cavity pick-off (B3 or B4 beam) is shown on Figure 29. The beam will be extracted in transmission of the PRM2 mirror. To this purpose a folding mirror plate should be attached to the filter 7 of the suspension (as currently done for the Pick-Off-Plate). This folding mirror will then be used to direct the B3 or B4 beam towards the SPOB bench (Suspended Pick-Off Bench, formerly called SPRB). The second beam transmitted by the PRM2 mirror will be simply dumped on a diaphragm or beam dump. The beam coming from the PRM3 mirror and the beam coming from the PRM1 mirror are separated by an angle of 7.46 deg, which leads to a separation of ~ 40 mm after 30 cm of propagation. Thus the beam dump could be installed inside the PRM2 vacuum chamber, and maybe even attached to the filter 7 of the suspension together with the pick-off plate.

The minitower hosting the SPOB bench will be displaced by a few meters towards west in order to make room for the new vacuum chamber hosting the PRM2 mirror, as shown on Figure 29.

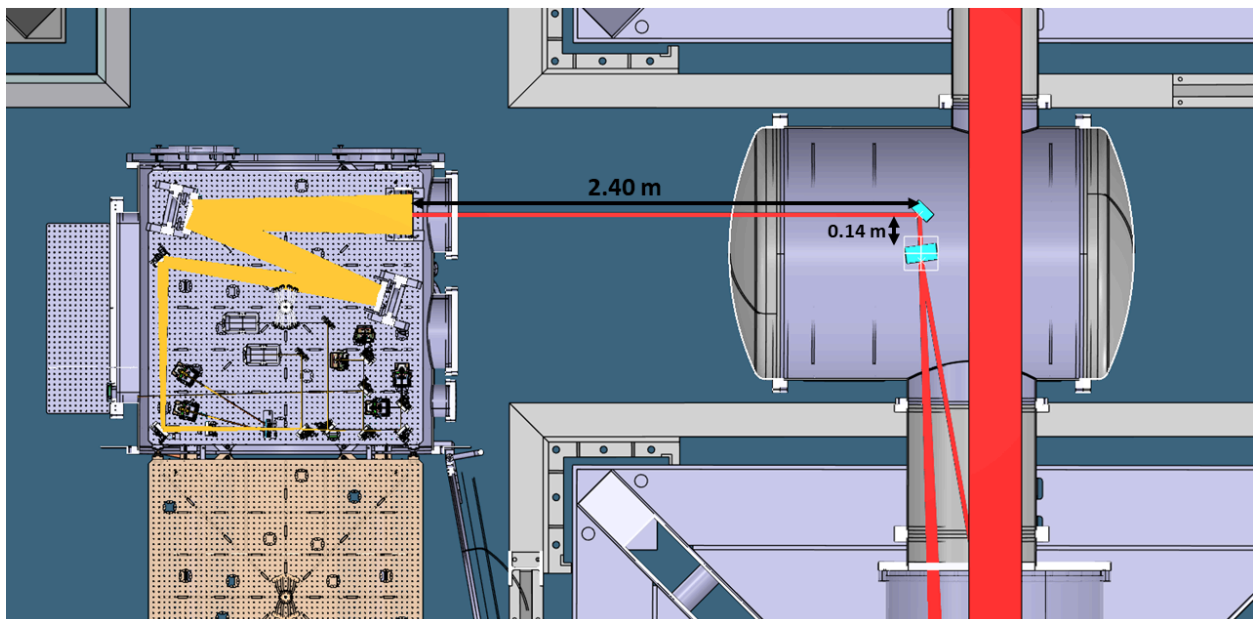


Figure 29 - Extraction of the B4 beam in transmission of PRM2.

2.11.2. Mode-Matching Telescope

	Short Stable Cavities Preliminary Design	Date 2024-05-22 VIR-0461A-24 Page 69 of 101
---	--	---

The telescope should decrease the size of the B4 (or B3) beam on PRM2 (~ 4.3 mm) to the size of the sensors (~ 400 μm). It should be able to reach a matching higher than 99%, even this constraint is less sensitive than for the ITF/OMC mode-matching telescopes. The amount of back-scattered light or back-reflected light from the telescope optics should be compliant with the sensitivity requirements, i.e. Adv+ Phase II sensitivity/10.

This telescope has not been studied yet, however the current telescope used for O4 decreases the beam size from 49 mm to 400 μm , using a doublet associated with a single lens. In the short cavity configuration, the magnification will be much lower, leading to a simplest telescope design. In this case, no showstopper and difficulty for the design and production of this telescope are highlighted.

2.12. Suspensions

2.12.1. Introduction

A total of eight new vibration isolation systems is needed for the implementation of the Short Cavities solution: four attenuators for single suspended optics (SRM2, SRM3, PRM2, PRM3) and four attenuators for suspended optical benches (SIB1, SDB1, SRM1, PRM1). For both SRM1 and PRM1 recycling mirrors, the payload consists of a table-top double pendulum suspension; a similar configuration might also be adopted for the IMC dihedron, which is currently rigidly mounted on SIB1. The design of all seismic isolators is new in Virgo, despite it is based on building blocks already implemented elsewhere ([VIR-0653C-18](#), [VIR-0213A-22](#), [ET-011A-20](#), [LIGO-P2200135-v2](#)), and it will require considerable engineering work. Only conceptual schemes and rigid body simulations (using the Mathematica™ based code developed by Mark Barton for LIGO, in combination with the SUMCON GUI from Takatori Sekiguchi [JGW-T1503729-v2](#)) are presented here.

2.12.2. Technology

Mechanics

The attenuators consist of a MultiSAS-like seismic isolation stage and a payload with the standard Virgo configuration. MultiSAS units (see Figure 30) fit a short (0.5 m long) inverted pendulum and two geometric anti-spring (GAS) vertical filters in a small volume, 1 m-diameter X 1 m-height, and feature a maximum load capacity of 400 kg. The top stage (Filter-0) is instrumented with sensors and actuators for static positioning and dynamic control (inertial damping) of the suspension chain; both GAS filters are equipped with fishing-rod type DC actuators for long term drift (temperature induced) compensation.

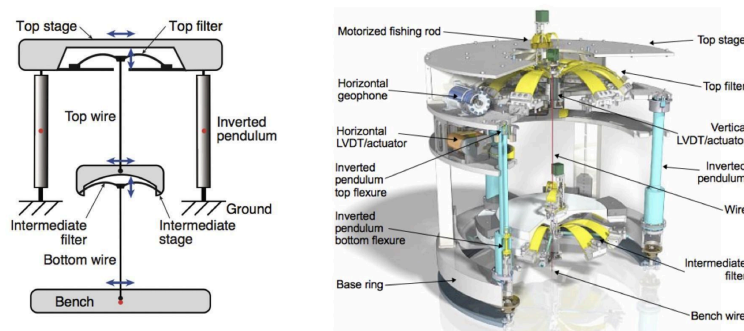
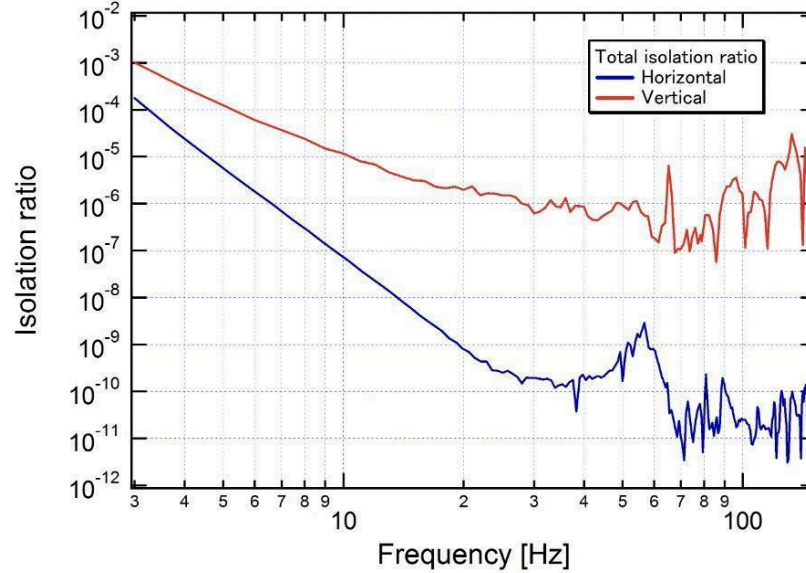


Figure 30 - Left panel: MultiSAS block scheme. Right panel: CAD overview of a MultiSAS attenuator



Projected SDB2 bench horizontal motion

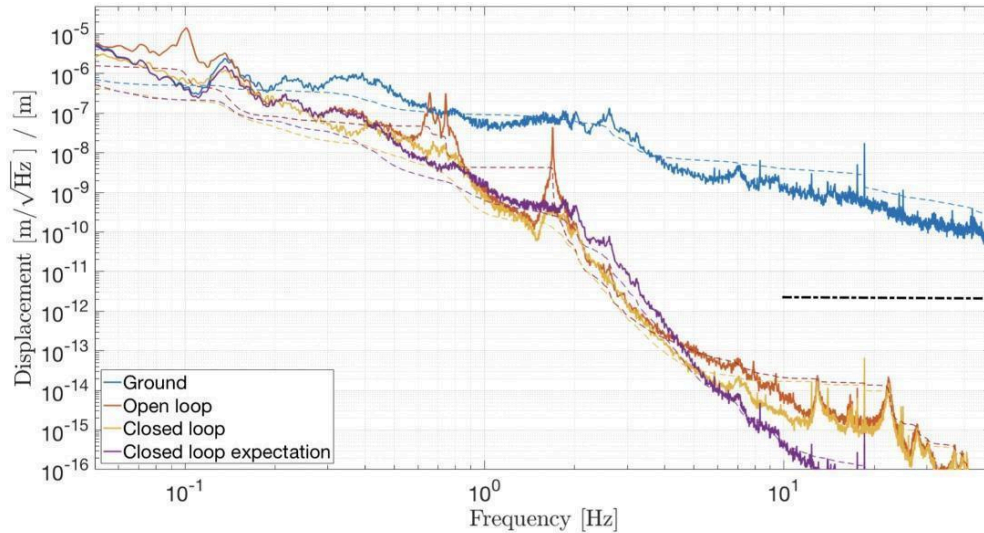


Figure 31 - Top panel: MultiSAS vertical and horizontal displacement transfer function measured stage-by-stage from the inverted pendulum base ring to the suspended bench. Bottom panel: estimated residual motion of the SDB2 bench. The noise projection was obtained by multiplying the signal from an out-of-loop inertial sensor, installed on the Top Filter, by the measured transfer function from Top Filter to bench. The result (red and orange lines) exceeds theoretical expectations (purple line) from naively multiplying the ground motion spectrum by the transfer function shown in the top panel. The difference is due to the dynamics of the vacuum chamber on top of which the MultiSAS is installed; the structures between 10 and 30 Hz were identified as rocking modes of the Minitower.

Seven MultiSAS isolators are currently operational in Virgo to suspend in-vacuum optical benches of DET and SIN subsystems and limit their residual motion to 10^{-14} m/ $\sqrt{\text{Hz}}$ above 10 Hz (see Figure 31).

The payload design (see Figure 32) reproduces the scheme successfully implemented in Advanced Virgo for the core optics of the detector, featuring:

- The mirror (bench) suspended from a large moment of inertia marionette to allow pitch and roll common mode tuning below the microseismic peak, thus reducing angular dynamics and local control bandwidth and noise;
- The marionette suspended with a single wire from a vertical filter (hereafter Filter-7), that provides additional vibration isolation and the body of which serves as reaction mass for the actuators of marionette and, in the case of single optic suspension, mirror.

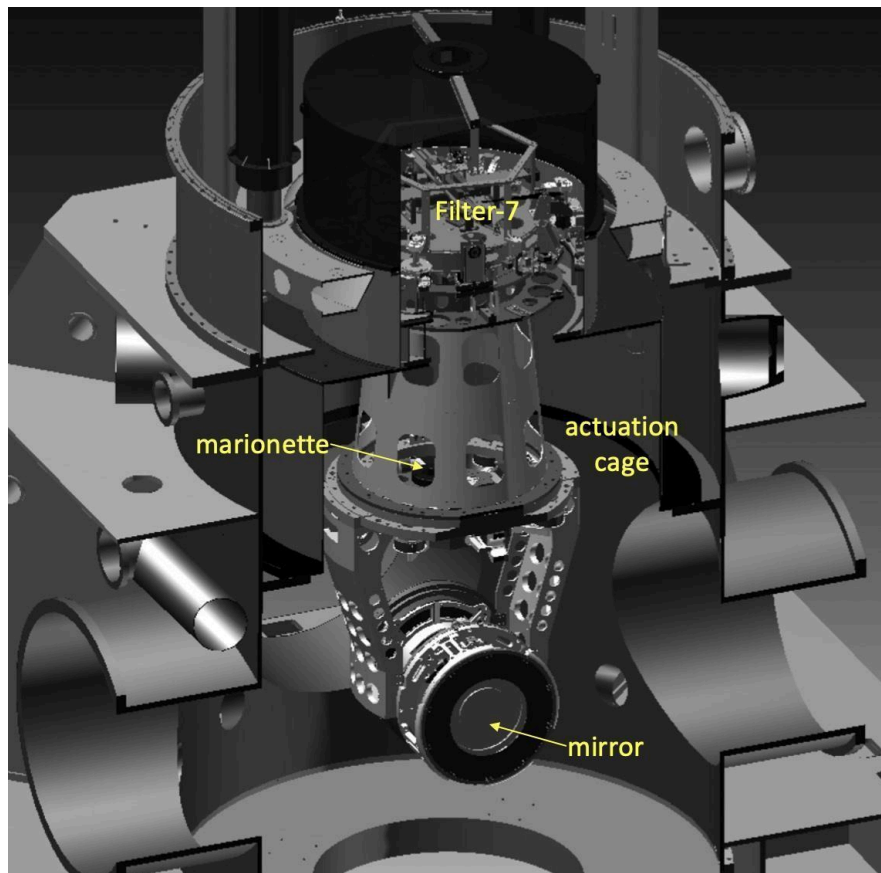


Figure 32 - CAD view of an Advanced Virgo payload. The actuation cage is rigidly connected to the body of Filter-7.

Sensors and actuators

Position controls at Filter-0 and Filter-7 level rely on combined LVDT/actuators similar to those currently used on Adv+ in-vacuum optical benches. The exception is the vertical degree of freedom of Filter-0 where LVDT and actuator are separated in order to use a more powerful voice-coil type actuator. Each GAS filter of the suspension chain includes an LVDT for monitoring the set point.

Inertial control of inverted pendulum is done by means of two commercial triaxial seismometers Nanometrics TC-120-SV1; each sensor is enclosed inside an air-tight vacuum pod, in the manner of LIGO HAM-ISI and BSC-ISI. The same type of sensor is already in use in Virgo in SBE systems and in Filter Cavity mirror suspensions. Vertical inertial damping makes use of only the LVDT of Filter-0; optionally, the microseismic peak can be subtracted from the LVDT signal by exploiting the vertical channels of the two seismometers.

Optical levers are used for the local controls of the payload. In the case of the bench-top double pendulum, additional local damping of translational degrees of freedom might be necessary. In that case, low noise requirements can be met by introducing interferometric displacement sensors [\[VIR-0417A-24\]](#) measuring the position of the marionette with respect to the suspended bench. All payloads are controlled with standard coil-magnet actuators. Dynamic range and typical noise level of the sensors are summarized in Table 9.

Sensor	Dynamic range	Noise level @ 1Hz	Reference
LVDT	$\pm 5\text{-mm}$	$3 \text{ nm}/\sqrt{\text{Hz}}$	
Seismometer	$\pm 800\text{-}\mu\text{m/s}$ with pre-amp	$< 50 \text{ pm}/\sqrt{\text{Hz}}, 1 \text{ pm}/\sqrt{\text{Hz}} @10\text{Hz}$	VIR-0596A-19
Optical lever	$> \pm 5\text{-mrad}, \pm 5\text{-mm}$	$< 1 \text{ nrad}/\sqrt{\text{Hz}}, 3 \text{ nm}/\sqrt{\text{Hz}}$	VIR-1197A-22, VIR-0070A-16
HoQI interferometer	$\pm 5\text{-mm}, \pm 10\text{-mrad}$	$1 \text{ pm}/\sqrt{\text{Hz}}$	

Table 9 - Dynamic range and noise level of sensors

DAQ

The baseline design foresees the suspensions to be controlled with RTPCs and ACL (acronym of Algorithms for Control and Locking [VIR-0938A-19](#)) software. ADC and DAC channels are provided by DAQ-Boxes, while integration/communication to global interferometer controls is done via a TOLM interface. Typical noise figures of ADC and DAC are shown in Figure 33. However, the mechatronics of the systems is fully compatible with the DSP-based SAT electronics, an upgrade (and new production run) of which is being planned ([VIR-0406A-24](#)).

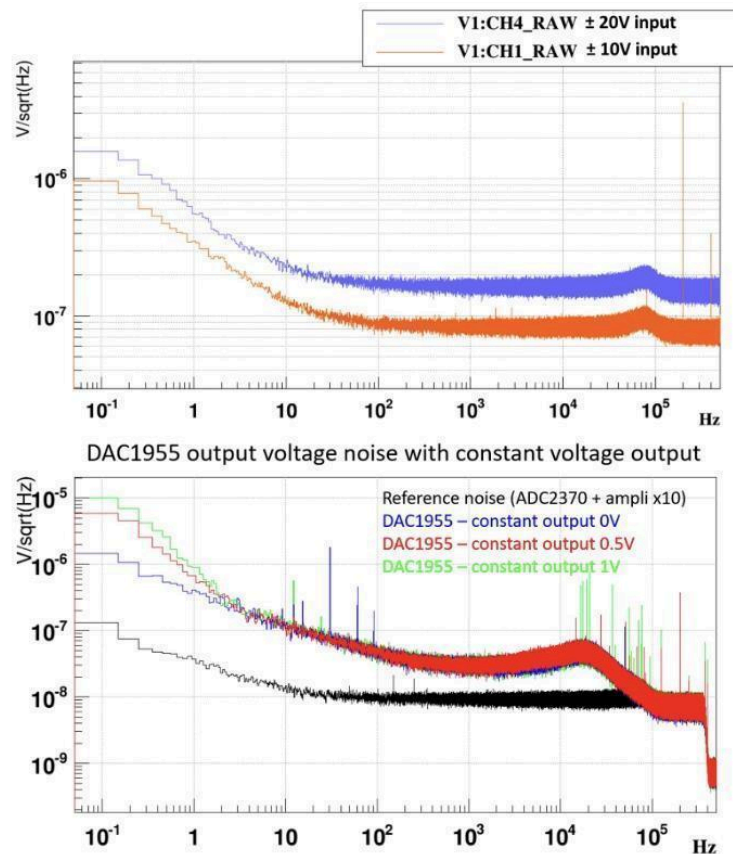


Figure 33 - Measured DAQ-Box ADC (top panel), for different input ranges, and DAC (bottom panel), for different DC offsets, noise. The DAC output range is $\pm 10\text{V}$.

Materials selection and UHV compatibility

All suspensions must be compatible with the main vacuum environment of Virgo.

2.12.3. Suspensions for SRM3/PRM3 and SRM2/PRM2

Conceptual design

The sketch in Figure 34 shows a possible implementation of single optic suspensions. In both cases, payload components design is inspired by the existing one devised within the ETPathfinder project for 3 kg mass silicon optics. In this preliminary study, a standard MultiSAS has been considered as seismic isolator for the 12 kg mirror payload, while for the 3 kg optics a downscaled (in terms of masses and moment of inertia) version of it has been preferred for better mechanical impedance matching and inertial damping effectiveness.

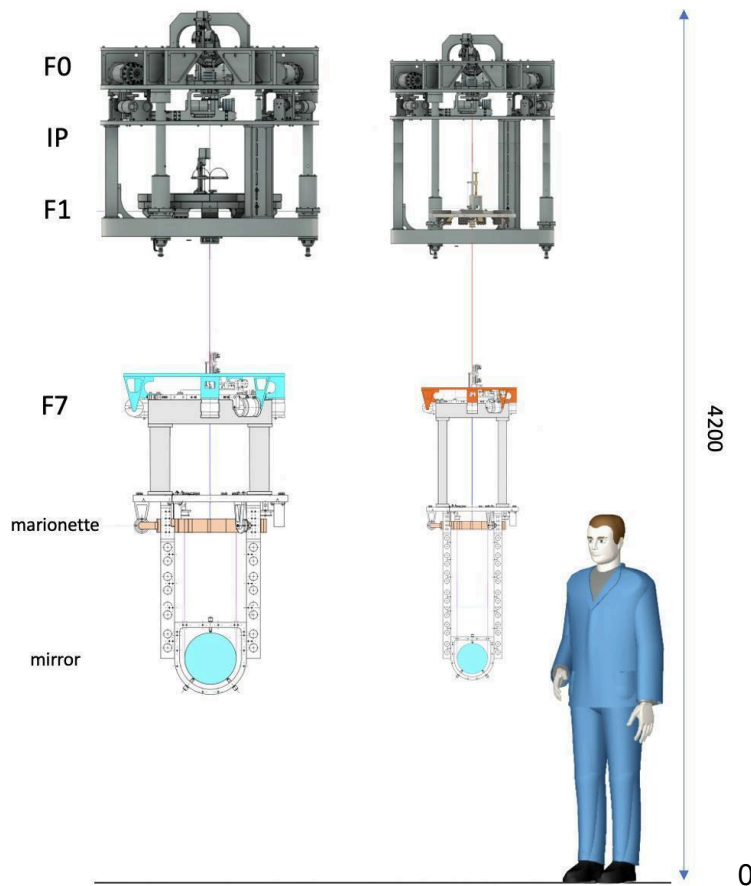


Figure 34 - Impression of the suspensions for S(P)RM3 (left) and S(P)RM2 (right) mirrors. The frame connecting the inverted pendulum base ring to Filter-7 sensing/actuation coils support is not shown. The sketch reproduces the situation in the CEB, where the beam height from the floor is about 1100-mm.

	Short Stable Cavities Preliminary Design	Date 2024-05-22 VIR-0461A-24 Page 76 of 101
---	--	---

Adopting the same seismic isolator for all single optic payloads would pay in terms of development time (no major technical issue can be expected with that solution, as proven by the current IMC mirror (3-kg) payload which is isolated with a standard Short SAT attenuation chain). However, it is more beneficial to tailor each isolator to its own payload to optimize the footprint of the vacuum chambers; this is very important to ensure maximum flexibility in terms of future space occupancy in the CEB. Another advantage to consider is that it may be useful to move each XR2 suspension to optimize the matching between the recycling cavity and the cavities in the arms, once the RoCs are known. Given a vacuum chamber, we expect this to be easier to do this with a less bulky suspension.

Expected performance

A noise budget for each of the two systems is presented in Figure 35. In both cases, the five (including the pre-isolation from the inverted pendulum) horizontal and three vertical passive isolation stages provide plenty of seismic attenuation, overkilling the 10^{-17} m/ $\sqrt{\text{Hz}}$ requirement at 10 Hz by more than two orders of magnitude. The suspensions are actually expected to be Brownian noise limited above 4 Hz; the thermal noise spectrum has been extracted directly from the rigid body model and takes into account the mechanical impedance of the complete system. C-85 steel wires, 600 mm long and loaded to 1 GPa stress level, have been considered for the mirror suspension stage. The simulation shows that specifications are exceeded around the mirror bounce mode. If necessary, this feature can be corrected by suspending the mirror with fused silica fibers, thanks to the much lower loss angle; as an additional benefit of monolithic suspensions, the bounce mode frequency would be shifted below 10 Hz .

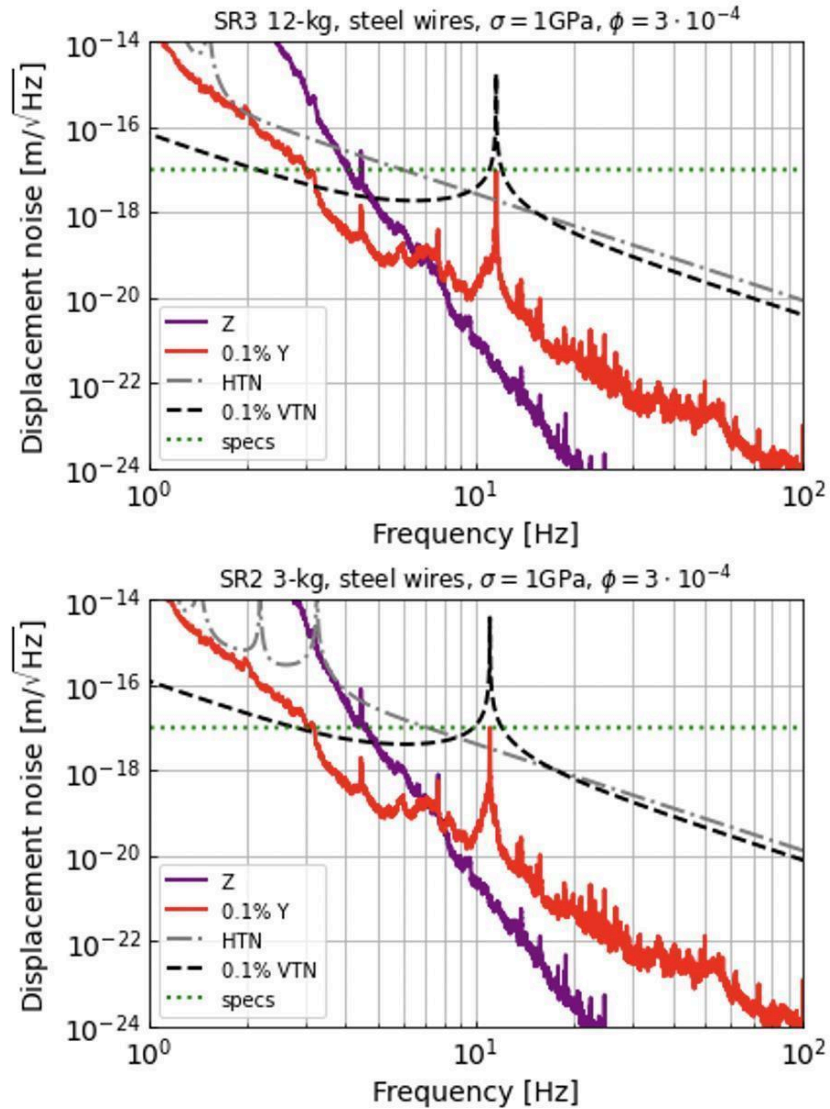


Figure 35 - Estimated residual motion for SRM3 and SRM2 mirrors. In both cases, the system expected to be thermal noise limited above 4 Hz. The peak at 11 Hz corresponds to the bounce mode of the last suspension stage.

The models assume a 0.1% vertical-to-horizontal coupling; this figure was experimentally validated on the test masses payloads during the O3 commissioning (see [VIR-0379A-18](#) for details). Eventually, it should be noted that the rigid body model used in this preliminary analysis is not able to capture the details of the dynamics at high frequencies, and a more detailed study should be carried out.

2.12.4. Suspensions for SIB1, PRM1, SDB1, SRM1 optical benches

Conceptual design: vibration isolated optical benches

A single design common to all benches (see Figure 36) has been considered. The bench size is 1000x1000-mm and its mass is 175 kg, 85 kg of which is a useful load; the benches are suspended from a marionette by means of three wires over a 440 mm diameter to accommodate at the center, in the case of PRM1 and SRM1, the table-top double pendulum payload for the 1.3 kg recycling mirror.

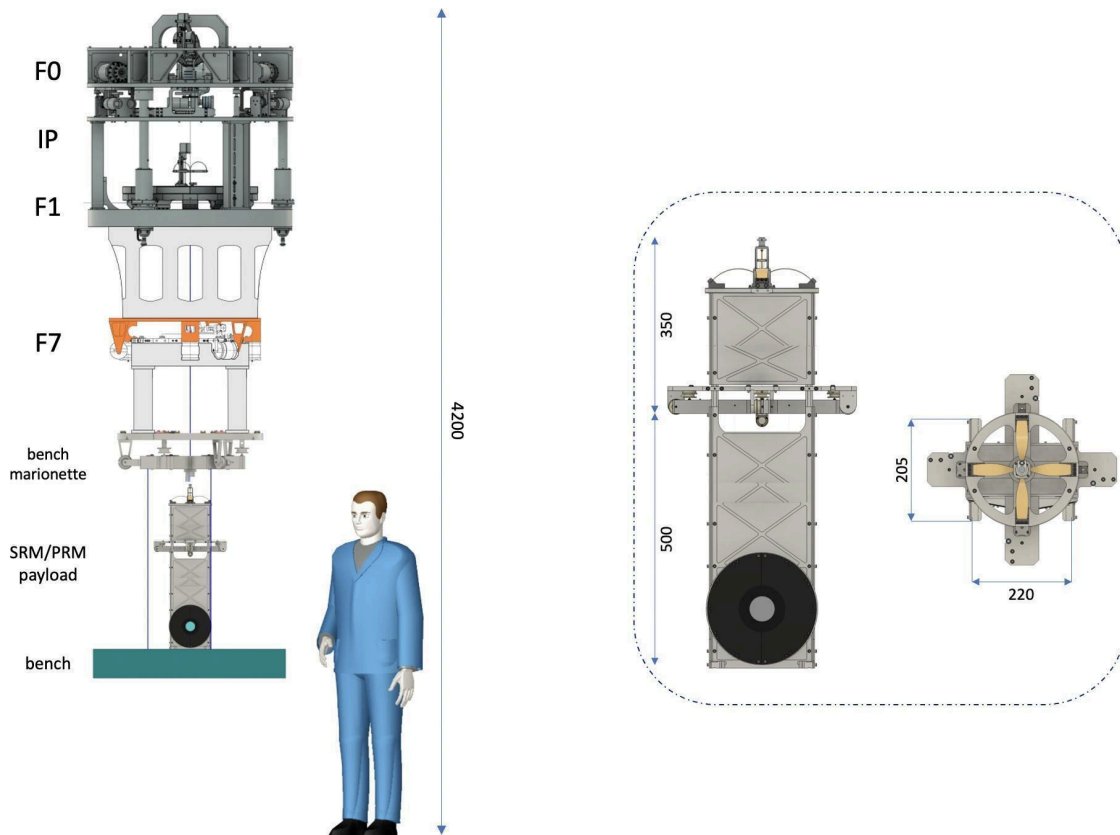


Figure 36 - Impression of the suspension for SRM1, PRM1, SDB1, SIB1. Relevant dimensions for a benchtop payload (SRM1, PRM1) are shown in the enlargement on the right.

Conceptual design: bench-top payload

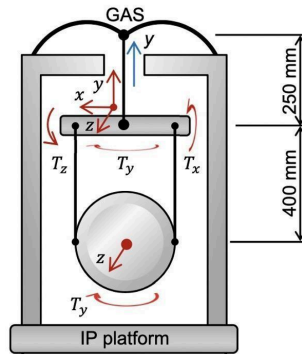


Figure 37 - Block scheme and picture of the Adv+ Filter Cavity payload from which the benchtop double pendulum suspensions are derived.

The design of the benchtop payload for SRM1 and PRM1 is a modified version of the one currently used for the mirror of the Adv+ Filter Cavity (see Figure 37); the length of the pendulum stages was preserved while the size of GAS filter, marionette and support cage were downscaled to match the smaller and lighter optic. The system is instrumented with a vertical LVDT, for monitoring the position of the small GAS filter, and with actuators both at the level of the marionette and the mirror; for the angular local controls, a dedicated set of optical levers from the ground is the preferred solution, though alternatives can be evaluated.

Control aspects

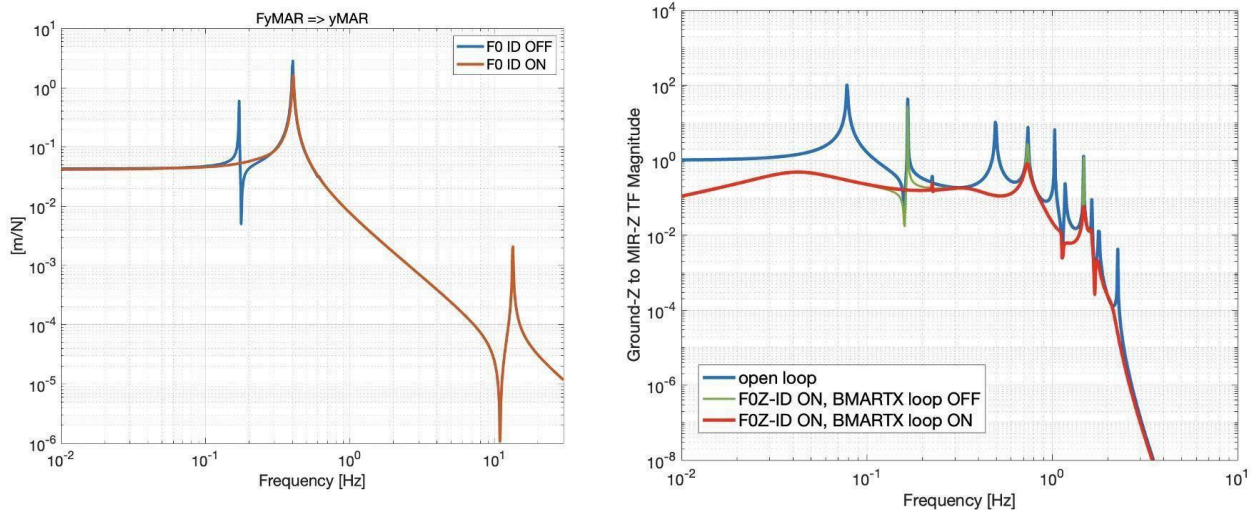


Figure 38 - Left panel: payload vertical plant, with Filter-0 inertial damping OFF and ON, showing little impact of ID on the fundamental mode at 0.4 Hz. Right panel: horizontal ground-to-mirror transfer function in different control conditions. Also in this case, the Filter-0 inertial damping is not very effective in smoothing down the resonances of the payload's common (0.74 Hz) and differential (1.48 Hz) modes. A significant improvement is achieved closing the loop on the TX (pitch) control of the bench marionette.

The small mass ratio between mirror and the bodies of the seismic isolation chain makes the standard Virgo inertial damping, engaged at the level of Filter-0, poorly efficient. This aspect is very clear in the results of the suspension control simulations presented in Figure 38: both in vertical and in horizontal, the resonances of the payload modes, in particular the horizontal differential one at 1.48 Hz, are scarcely affected by the status of the F0 control loop. On the other hand, it can be observed that engaging the pitch (TX) control loop of the bench marionette substantially improves the situation for the two pendulum modes (Z). This is due to the strong geometric coupling between these degrees of freedom (the same is happening for bench marionette roll (TZ) and payload X), as clearly shown in Figure 39-top panel. This peculiarity of the system, that fundamentally distinguish it from the LIGO's benchtop suspensions mounted on stiff active isolators (HAM-ISI), can be exploited to avoid increasing the complexity of the SRM1/PRM1 payloads by adding sensors for local damping of Z and X modes. However, further investigation is needed to evaluate the impact of such a mechanical coupling on the optics installed on the benches when global control loops, involving forces applied to the payload, are engaged.

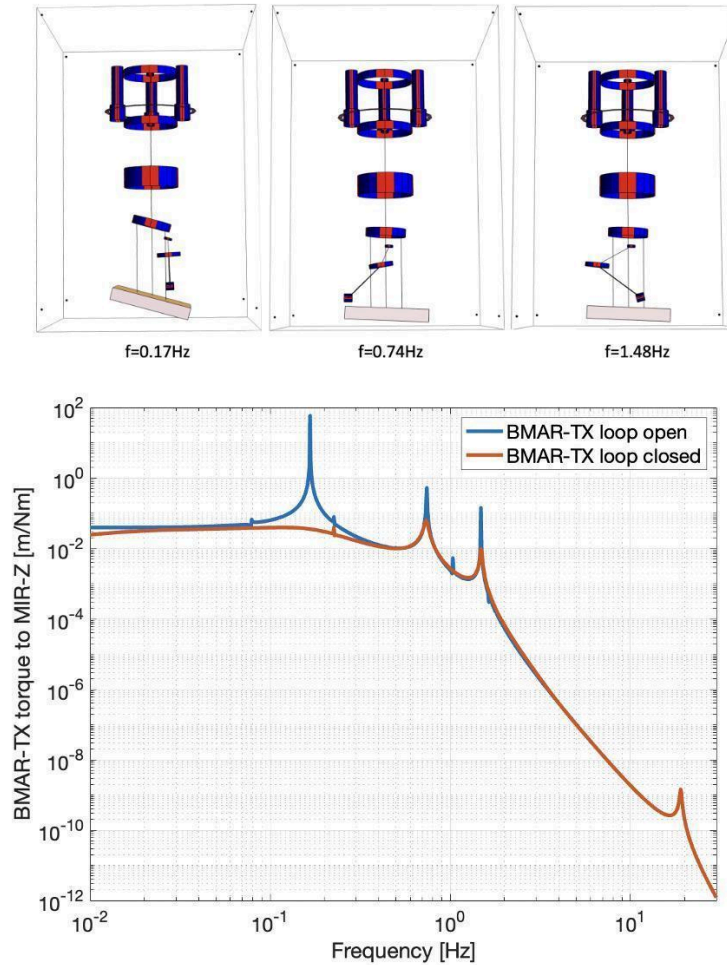


Figure 39 - Top panel: visualization of the three bench marionette - TX/payload - Z coupled modes. Bottom panel: modeled transfer function from bench marionette TX actuator to mirror displacement in open and closed-loop conditions. The coupling of the payload horizontal modes to the bench marionette rotation allows damping them without the need of additional local controls (at least in locked cavity conditions).

Expected performance

A noise budget for SRM1 (PRM1) mirror is presented in Figure 40. Thanks to the additional double pendulum attenuation stage, impact of transmitted seismic noise is even less relevant than in SRM2 and SRM3; thermal noise figures are comparatively worse, due to the smaller mirror mass and shorter final pendulum length, but still compliant with the requirements. On the other hand, a significant noise

contribution, that can be addressed by optimizing the loop filter, is expected from the local angular control of the bench marionette (gray and rose lines in Figure 40).

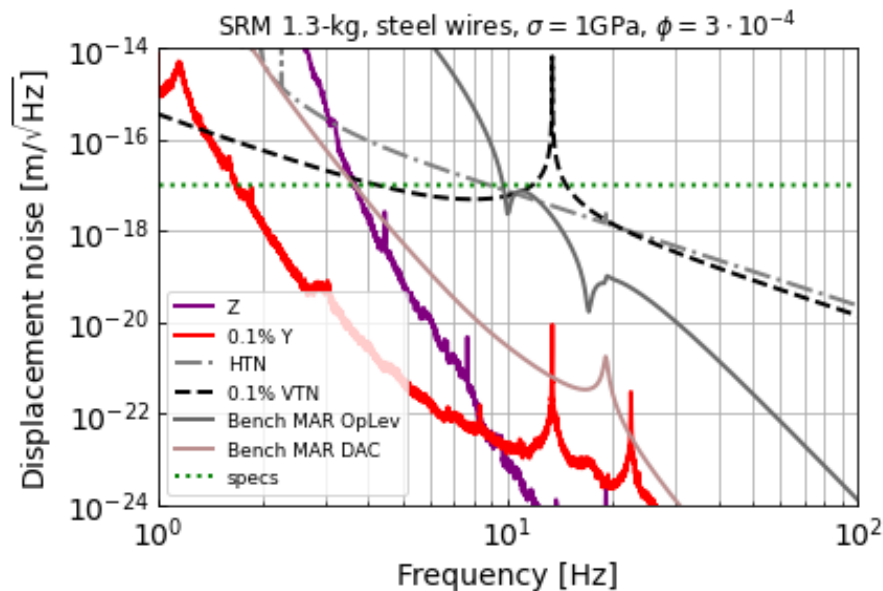


Figure 40 - Noise budget for the benchtop payload showing that the requirements above 10 Hz can be met. In principle, the system would be limited by thermal noise above 4 Hz; however, bench marionette control noise (sensing) is expected to provide a major additional contribution. The DAC noise model includes a whitening filter with double pole at 0.16 Hz and double zero at 8 Hz.

The modeled thermal noise is based on the mechanical impedance of the complete suspension, including the seismic isolation part. Therefore it takes into account the mechanical losses from all stages in the system. However, the assumption made for the losses in the bench marionette+bench stage could have been optimistic; for this reason, an additional simulation has been made by introducing large dissipation (for example from massive electrical cabling, which is typical for benches in Virgo) both in the bench marionette and bench suspension stages. The result (Figure 41) shows the expected substantial increase in Brownian motion at low frequencies and the filtering effect from the payload making such that the thermal noise from the last suspension stage remains the dominant one above 4-5 Hz.

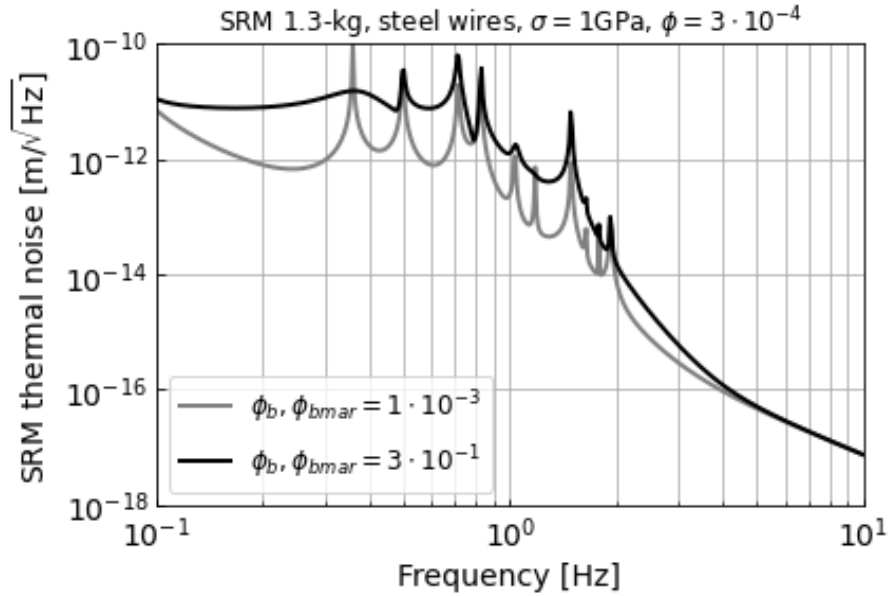


Figure 41 - Mirror thermal noise spectrum for different values of loss angle for the bench marionette suspension stage.

Open issues

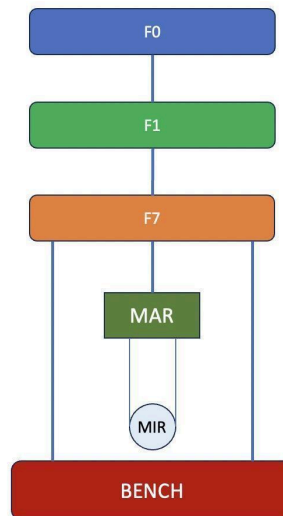


Figure 42 - Alternative SRM1/PRM1 suspension configuration for decoupling of mirror and bench dynamics.

	Short Stable Cavities Preliminary Design	Date 2024-05-22 VIR-0461A-24 Page 84 of 101
---	--	---

The configuration with the benchtop payload, though promising, requires further investigations on some aspects such as the handling of the vertical degree of freedom and the impact of the bench/mirror coupling on the global controls of the recycling cavities. For the first issue, one could evaluate whether it would be beneficial to stiffen the vertical mode to move the corresponding resonance to higher frequencies, where the excitation from the environment is largely suppressed by the seismic isolator, and leave the degree of freedom undamped. In case the bench/mirror coupling proves to be critical, one could consider to change the configuration to the one illustrated in Figure 42, in which the bench and the payload marionette are suspended, respectively, from the body and from the keystone of Filter-7. In this way the dynamics of the payload would be much more decoupled from the bench one, but there would be the drawback of having two instead of three vertical isolation filters for the optics mounted on the table.

	Short Stable Cavities Preliminary Design	Date 2024-05-22 VIR-0461A-24 Page 85 of 101
---	--	---

2.13. Vacuum

2.13.1. General Overview

The solution for stable recycling cavities requires adding more suspended mirrors and benches in the central building, both on PR/INJ and SR/DET sides. The mirrors and benches will be suspended independently, with one suspension for each. Vacuum tanks are designed to host the various suspensions and payloads. As this configuration is not compatible with the existing INJ and DET towers in the central building (CEB), these two towers will be dismantled and removed, as shown in Figure 43. It is also envisaged to remove the PR and SR towers to gain even more space in the CEB experimental hall (16 m² for each tower).

In order to remove the two, or the four tower bases, two solutions are under study: (i) Enclose the towers in a structure to cut with plasma one tower base into 8 pieces (of masses less than 3 tons), then remove the structure and remove the pieces using the two trolleys of the main building crane. This is the baseline solution; (ii) Open the roof of the building to remove the entire tower bases. In this case, removing the four towers will be faster than in the first solution. Possibly, this option could allow tanks of similar size and weight to be inserted in the same way. Confirmation of this option is pending.

Concerning the cutting of the towers (thickness ≥ 10 mm) with a plasma tool, the idea is to install a waterproof box properly sealed to avoid any pollution. The box could be then maintained at a lower pressure with respect to the main building. A fresh air inlet will be provided from outside the central building (for the operators) and another flexible pipe will extract the fumes resulting from cutting operations. A fan will expel this air to the outside. The confinement performances of the box shall be tested as an initial step by using a set of particle counters placed outside the containment, and improving the containment features where necessary. A continuous dust monitoring system will be always active during cutting operations.

The following drawings show the CEB with the new vacuum chambers. In these drawings, the towers PR and SR are still present and not removed from CEB (worst case scenario for the available space in CEB). If the PR and SR towers are removed, it must be ensured that the vacuum effect is retained on BS/NI/WI: some pieces and different anchorages will be done or redone.

The new chambers will operate at a residual pressure in the low 10^{-8} mbar range, e.g. at the same level as the present DET and INJ towers .

	Short Stable Cavities Preliminary Design	Date 2024-05-22 VIR-0461A-24 Page 86 of 101
---	--	---

2.13.2. Tanks

The designs for the INJ and DET sides are the same, with a rotation by 90° around the vertical BS axis (see Figure 44), hence all the vacuum tanks are needed by pairs:

- 2x1 tank for PRM2/SRM2 mirrors: this can be similar to a Virgo minitower, but with smaller size.
- 2x1 tank for PRM1/SRM1 mirrors, the payload being a bench (with suspension for the mirrors, and the Faradays).
- 2x1 tank for PRM3/SRM3 mirrors.
- 2x1 tanks for SIB1/SDB1 benches.

As shown in the drawings, the three PRM1/PRM3/SIB1 or SRM1/SRM3/SDB1 tanks will be rigidly connected together. Three constraints guide the design: (1) Each part of the INJ/DET system must be less than 4.8 tons due to the trolleys of the main building crane (presently rated for 1.8 T and 3.2 T for trolley, to be changed to 2.5 T each, possibly used in pair); (2) Because of the optical design, the tanks must be very close to each other, which defines the design of the connection flanges; (3) The required residual pressure for the tanks is in the range of 10^{-8} mbar (H_2 and H_2O as main species) with strict control of 'hydrocarbon' contaminants, consistent with O5 and with future upgrades ([VIR-0578A-21](#)).

The new tanks will have UHV features to keep under control the outgassing rate effectively: internal surfaces with low roughness and free of contaminants, possibly incorporating electropolishing and a one-time prebaking process. Flanged joints will be of metal-sealed type, except for the "access lids" and "custom viewports" where double o-ring seals will be used.

As visible in Figures 45 to 47, an access is planned from the bottom gallery in the PRM1/SRM1 tanks, with access to the three payloads for a person (without ITF beam). Lateral accesses are planned in the vacuum tanks to introduce the payloads and to access them from different sides, possibly with the ITF beam still reaching the chambers optics. Through the side accesses it will be possible to intervene on the whole area of the benches for simple adjustments or to introduce small parts while remaining outside (this possibly helping with respect to the risk of contamination). Final design will depend on the design of the payloads.

The drawings show the current hole in the concrete floor used to access the INJ/DET towers from the gallery. They must be closed since the set of three tanks will be installed around this position, but keeping the access to the PRM1/SRM1 tanks. Different solutions are under study: (i) reduce the hole aperture by a concrete structure, generally preferred for the stable dynamic behavior but this is a potentially dirty and relatively long intervention (ref. to INF chapter), or (ii) fit the hole with a welded

	Short Stable Cavities Preliminary Design	Date 2024-05-22 VIR-0461A-24 Page 87 of 101
---	--	---

metallic structure. This will be realized as a welded metallic frame screwed on the ground on the central building plus a symmetric part fixed on the top of the gallery floor. These 2 pieces will be screwed together. A metallic plate will be fixed on these both frames and sealed. Possibly, we could inject resin or special concrete inside the space between the 2 frames in order to enhance damping characteristics.

Another design option could be considered if openings are made in the roof of the CEB building: we could then install the new INJ and DET towers through the roof, maintaining a weight similar to the existing ones. In this case the new tanks could therefore be larger and cover the 2.5x2.5 meters hole in the floor. They would include towers PRM3-PRM1 for IINJ and SRM3-SRM1 for DET. They will be anchored to the floor independently from the solution for closing these square holes. Larger tanks will also allow easier access to payloads. The SIB1 and SDB1 tanks would be partially attached to this same structure and partially anchored to the ground. They will be separable by vacuum valves with integrated viewport for independent venting/evacuation.

In conclusion, the baseline option still considers the 'plasma' cutting of the towers . Opening the roof of the CEB building is a critical option in the design of the new tanks and the choice is a priority in the upcoming design phase.

The SPRB minitower will be displaced towards West, in a position close to the one shown on the drawings, and connected to the PRM2 tank. In addition, the SDB2 minitower and EDB bench will be installed at new positions still to be tuned. In preparation of the installation of the new tanks, it will be possible to move the SIB2, SBPR, SDB2 minitowers and EDB bench to gain space if needed for other activities, for example for clean room modifications.

Connecting tubes will be installed between the towers (links). They will host pumping ports and gate valves, positioned there for space efficiency, easy access, and minimized environmental noise. Gate valves will possibly integrate viewports embedded on the gate. Bellows will also be included. Finally, the links will accommodate optical baffles for scattered light, to be considered in collaboration with SLC.

Note that the narrowest aperture in the link pipes corresponds to the vacuum valve: the valve has a diameter of 400 mm, which is identical to the current diameter between the SR and DET towers, as well as between the PR and BS towers. In this conceptual design, we plan to use the same existing valve to save on costs and space, assuming that this is acceptable given the short length of the narrow section. It shall be enlarged if this will not be the case.

In case the option of removing the PR and SR towers is chosen, a new "long link" will replace each of them. This will provide enhanced flexibility for positioning accessory pumps.

	Short Stable Cavities Preliminary Design	Date 2024-05-22 VIR-0461A-24 Page 88 of 101
---	--	---

2.13.3. Pumps & Materials

A two-stage pumping system is envisaged for each independent volume: evacuation will start with rough pumping from atmospheric pressure to 0.1 mbar, achieved with a multi-root type pump, and then high vacuum pumping down to reach the 10^{-7} mbar range, achieved with turbo-molecular pumps installed on each tank. These pumps will then be switched off. Normally there will be 4 independent volumes: DET tanks assembly; INJ tanks assembly; SR2 tank; PR2 tank.

Cryogenic pumps ('Smalltraps' already present and adaptable to the new setup) and other UHV pumps like NEG's (as earlier already planned for O5) will be then used during the 'ITF running phase' (10^{-8} mbar range) offering increased pumping speed with minimal acoustic and seismic disturbances. Additional turbo-molecular pumps shall be present too, kept permanently running in case of large gas loads. For environmental noise considerations, these pumps will not be installed directly on the tank chambers and distant from viewports and optical benches: they will be integrated into the existing (becoming unused) PR and SR towers, or within the pipe link that in their place if PR and SR towers will be removed. Also, the pumps will be equipped with bellows and floor anchorages to limit the transmission of seismic emissions.

All pumps have to be lubricant-free to avoid risks of accidental contamination.

The materials designated for in-vacuum use will be chosen in accordance to outgassing budgets. The gas load will be estimated from the components inventory and will typically consist mainly of H_2O and H_2 , with a smaller proportion of N_2 and other gasses (figure 48).

Rigorous control of low-volatile molecules ('hydrocarbons') is essential to prevent contamination. Following the standard UHV practice, cables, motors, coils, polymers, and all non-metallic materials will undergo individual pre-baking procedures in the on-site facilities prior to installation.

2.13.4. Dust Control

The tolerance to dust contamination is expected to become even more critical for O5 and post-O5 than it is today, when problems (e.g. point absorbers) are already emerging. Accessing the 'top' part of the tanks through the CEB hall via the bridge-crane, would expose the optics to the main hall environment, risking uncontrolled contamination. To mitigate this risk, we may consider the presence of a 'separating roof' inside the chamber (IVC), similarly to what is already installed in the existing towers, figure 49. At this time the IVC can be conceived for 'dust shielding' purposes only rather than for isolating different

	Short Stable Cavities Preliminary Design	Date 2024-05-22 VIR-0461A-24 Page 89 of 101
---	--	---

vacuum levels (concept shown in figure 48). This picture is a concept with a payload with one suspension wire: the IVC for S-SRC should fit with a payload like a “marionetta + 3 wires”.

It can be considered also that, because of the relatively small size of the foreseen towers, a permanent clean room encompassing the new towers can be installed. The operations on suspensions / benches would then be easier while maintaining a high level of cleanliness. In conclusion, the upgrade presents the opportunity to improve the CB cleanroom facilities. These shall be enlarged and the entrance process of personnel and equipment shall be upgraded to include air showers and dust control systems (figure 92).

2.13.5. Tanks structure

A concern often raised during project meetings is the potential need for an upgrade of the foreseen 'short' suspension in the long term. To address this concern on the VAC side, we could design the relevant tanks with a size and structure capable of accommodating an enhanced suspension, considering a modest increase in height and mass of the suspension structure.

FEA of the new vacuum tanks will be produced during the finalization of the design in order to:

- keep the frequencies of vibrational modes of the whole system tanks + base above the needed threshold.
- estimate and optimize the transfer function between the ground and the flange where the inverted pendulum is attached.

The exact specifications will have to be determined in collaboration with SAT .

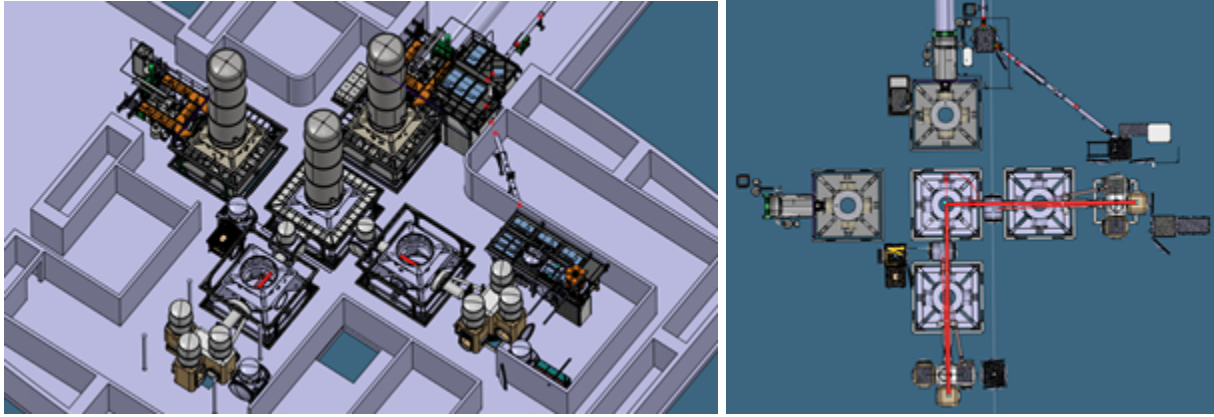


Figure 43 - general view of the central building with the new tanks, and the INJ/DET towers removed. The PR/SR tower bases are still present on this drawing.

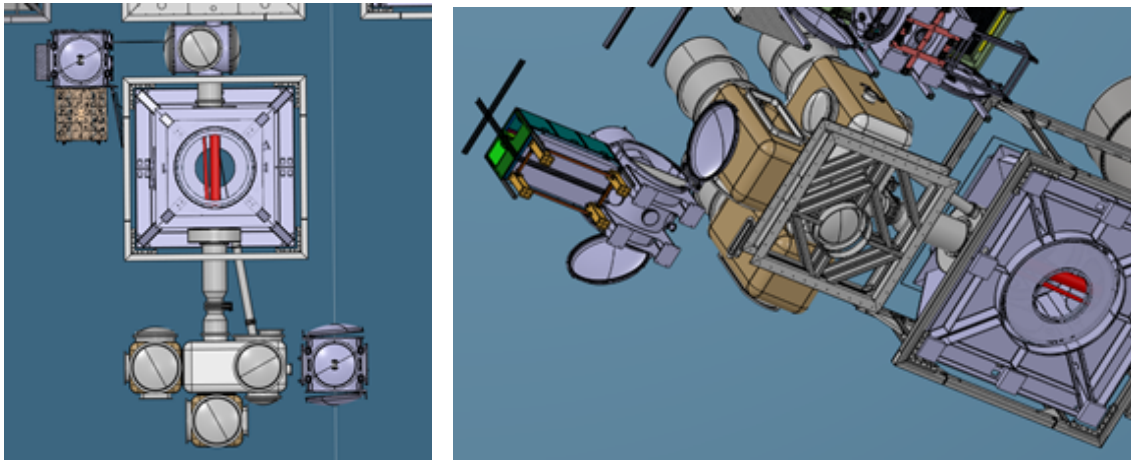


Figure 44 - top views of the INJ area (left) and DET area (right) with the four new tanks. In the INJ area, SPRB is visible at the top-left and SIB2 at the bottom right. In the DET area, SQB1 can be kept at its current position, while SDB2 and EDB are to be moved. The PR and SR towers are still present on these drawings.

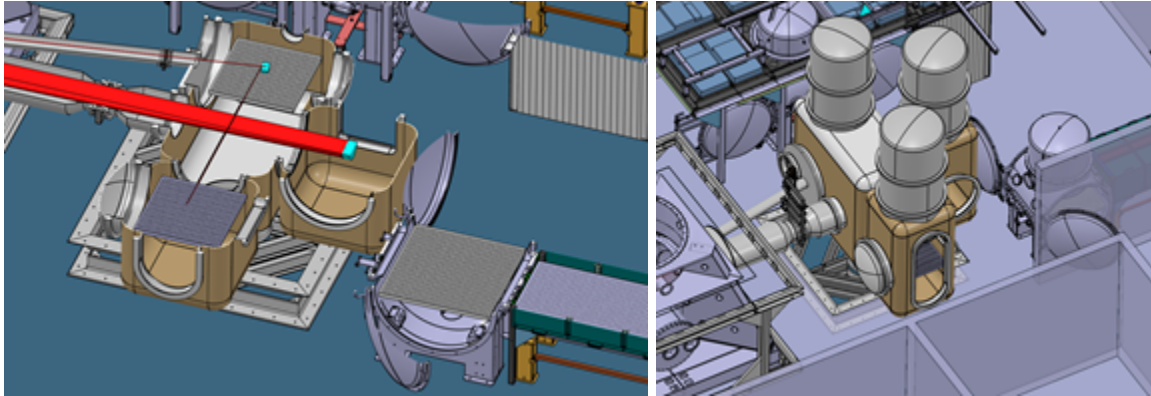


Figure 45 - views of the DET area (SRM1, SRM3, SDB1) with preliminary designs for the access from the gallery and from the lateral sides of the tanks. We can see in these pictures a proposal to fill the gallery connecting holes.

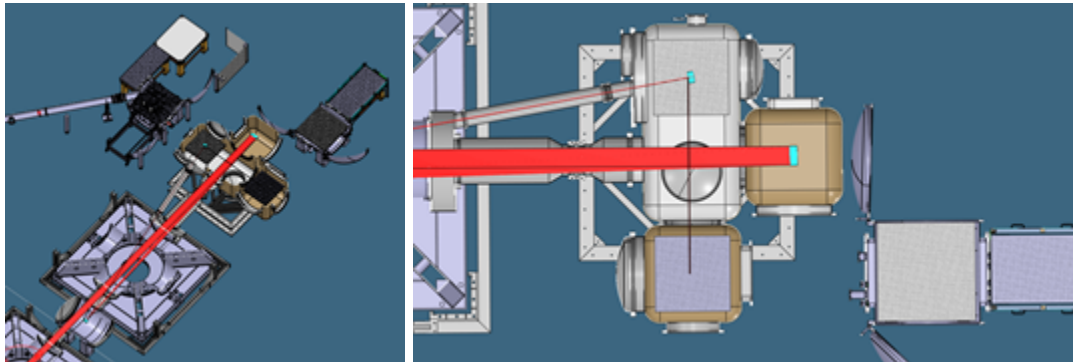


Figure 46 - DETECTION area

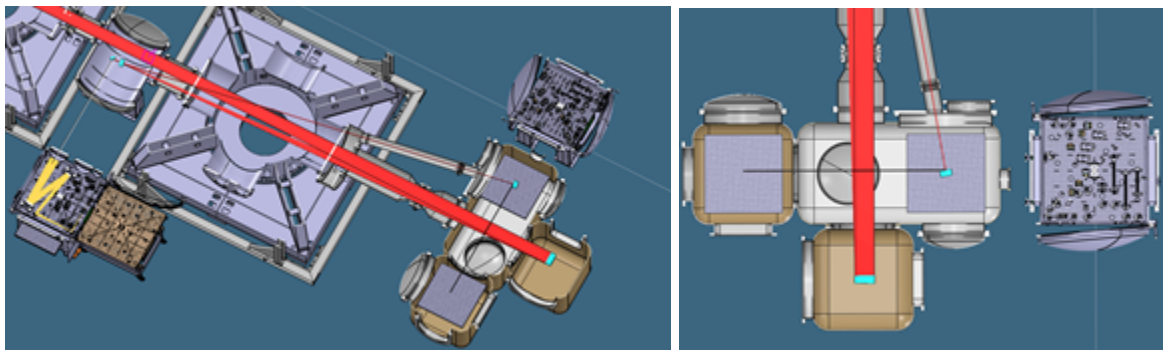


Figure 47 - INJECTION area

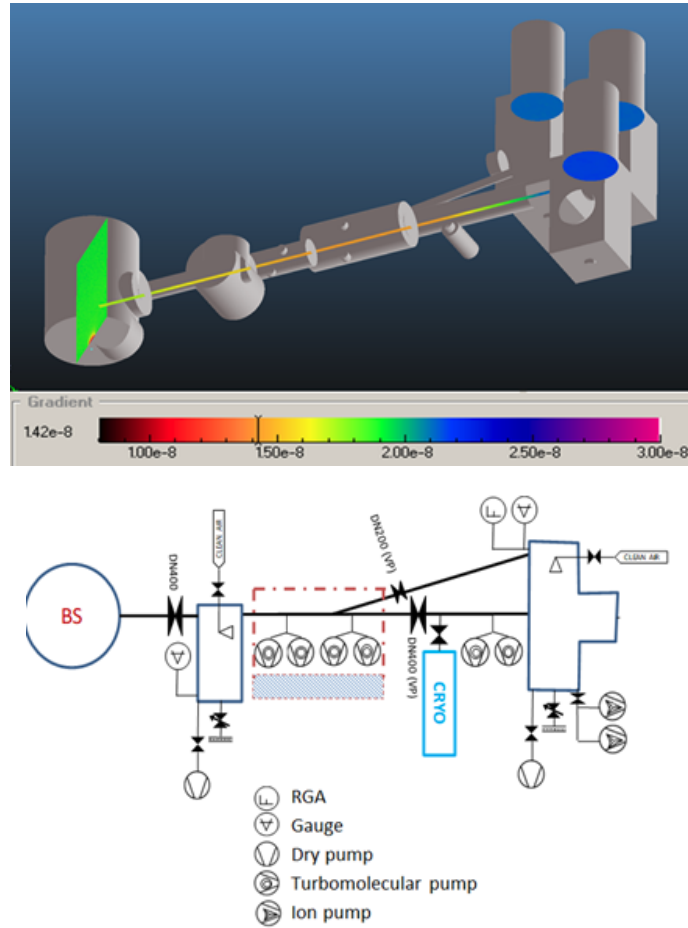


Figure 48 - calculated example for a typical case (scale in mbar): partial pressure of water vapor ($2E-5$ mbar.l/s from each of the new tower) . Results meet requirements. Bottom: sketch of equipment layout.

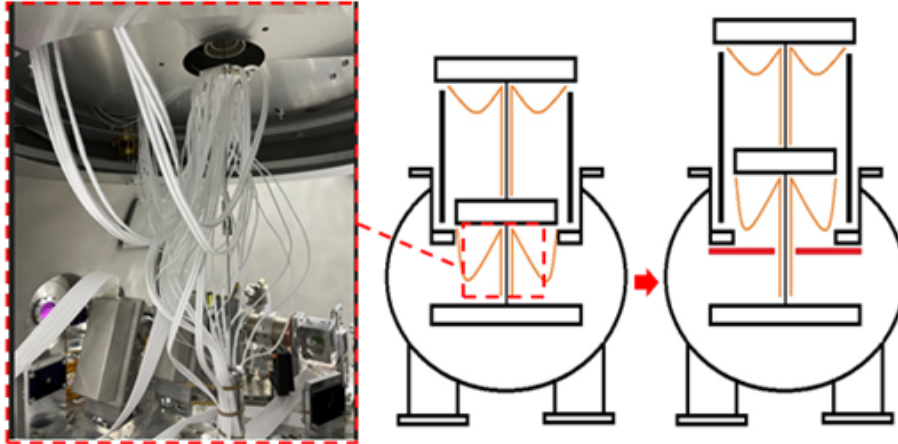


Figure 49 - picture of current cabling arrangement within a 'minitower' [eLog 52261] (Left). Sketch showing the minitower in its current state and a potential modification with an IVC, highlighted in red (right). Note that IVC aperture could be relatively large to ease the cable's passage while still safeguarding against fallout of dust particles, once providing a suitable overpressure in the lower compartment. This is just a conceptual picture, the design must be adapted to the 3 wires payload type. Additionally, an outer tent covering the upper part may be needed as well.



Figure 50 - Current clean areas (ISO6 / Class 1000) could be extended like in the picture. The blue lines are the potential expansion of the new cleanrooms, serving new chambers of DET and INJ, with a rationalized entrance: separate for personnel and for materials. PRM2, SRM2 and SPRB could have a portable clean room or light structure support with clean air box.



Short Stable Cavities Preliminary Design

Date 2024-05-22
VIR-0461A-24
Page 94 of 101

	Short Stable Cavities Preliminary Design	Date 2024-05-22 VIR-0461A-24 Page 95 of 101
---	--	---

2.14. Infrastructure

2.14.1. Introduction

This section describes the civil works required for the implementation of the Short Stable Cavities of the Virgo interferometer, for the adaptation of the existing spaces in CEB to accommodate the scientific equipment foreseen by the new layout, according to the information available at this time.

An essential point to consider for the CEB Hall, is the availability of complete and adequate information of the current state as a starting point for the most accurate and detailed design possible. In this sense the current situation is not optimal, due to the various phases of modifications and new installations that have taken place in Virgo over the years. In order to be able to fully assess all the necessary operations (including the study of protections to put in place) and evaluate their impact in terms of heavy works to be performed in an already structured experimental laboratory, it is necessary to have an integrated 3D drawing with all the equipment currently present in the CEB Hall (BIM model), which is currently not available or only partial and incomplete representations are available.

The problem of dust production, which is inevitable in this type of heavy activity for extremely impactful work in a crowded experimental area, is very significant and high risk. Safeguards will have to be made to confine the areas of operation, but due to the crowded scientific equipment present they are difficult to implement and not certain to be totally effective.

Although the civil works to be carried out are smaller in scale than the Long Option solution, they can be considered more impactful and difficult to carry out due to the experimental areas where the works will have to be executed.

The process of carrying out the civil works will have to evolve in a similar way through the different design phases (preliminary and executive) signed by the designers in charge who assume the legal responsibilities, and the related validation steps to verify the integration with the scientific equipment. The validated executive design is necessary for requesting the authorization permit for the planned structural works. Both the design and the realization of the works must be entrusted with contracts to external firms, for which separate tenders will have to be made in accordance with the regulations for the execution of public works in Italy (Code of Tenders, Legislative Decree. 36/2023). In the following section devoted to the program for the implementation of these works, the different timeframes required for the execution of these various phases have been hypothesized.

	Short Stable Cavities Preliminary Design	Date 2024-05-22 VIR-0461A-24 Page 96 of 101
---	--	---

2.14.2. Description of the needed modification works

As a very preliminary, although broad outline at this stage, some sketches were made to identify the areas of intervention, the actions to be done and also to get an idea of the protections needed for the execution of very impactful works in controlled contamination areas or in existing clean rooms, which have been shown in Figures 93 to 96 below ([VIR-1106A-23](#)).

The adjustment works to be carried out can be essentially grouped into:

- dismantling of the suspensions and removal of the existing IT and DT vacuum chambers, to make space for future installations (Figure 51 - see also paragraphs VAC, SUSP,...) ([VIR-1093A-23](#));
- structural adjustment of the reinforced concrete slab where the current openings are located below the existing INJ and DET vacuum chambers, to reduce the area of the opening from 2.5x2.5m to 1.0x1.0m, according to the new optical layout and the new smaller vacuum chambers (Figure 52 and 53); the existing wall coverings in the tower gallery clean room, for the two affected areas, will have to be dismantled and rebuilt from scratch after the structural works; these zones will have to be confined and sealed with temporary protections to contain dust during the structural works, both at the level of the towers and below, once INJ and DET towers will be removed from their current position;
- expansion of the existing INJ Lab and DET Lab clean rooms to install the new scientific installations (vacuum chambers and optical benches), including upgrading the dedicated HVAC, electrical and data distribution systems of the clean rooms (Figure 54).

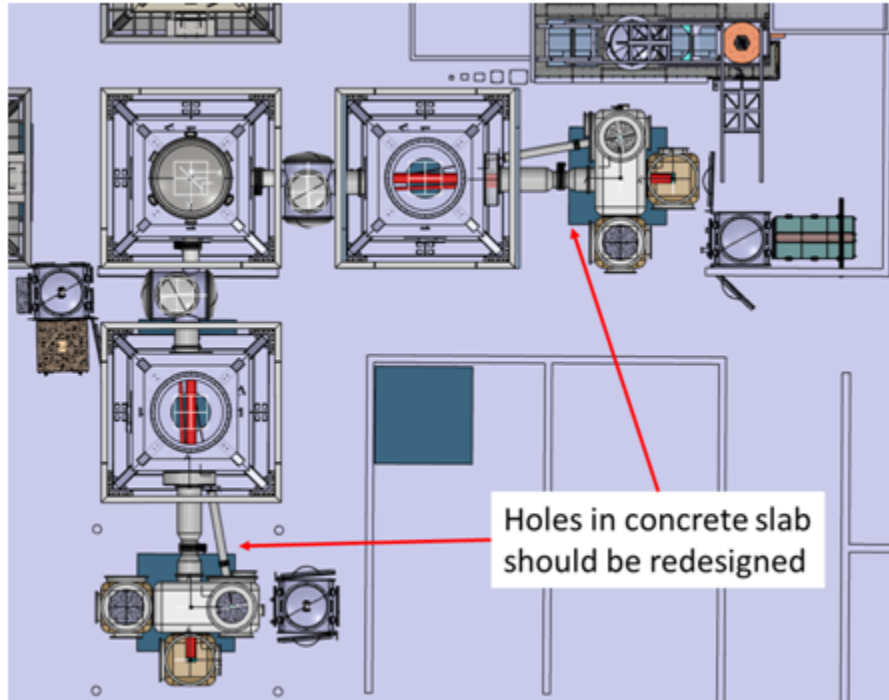


Figure 51 - Overview of the new scientific equipment to be placed in the INJ and DET Lab in place of the existing INJ and DET towers.

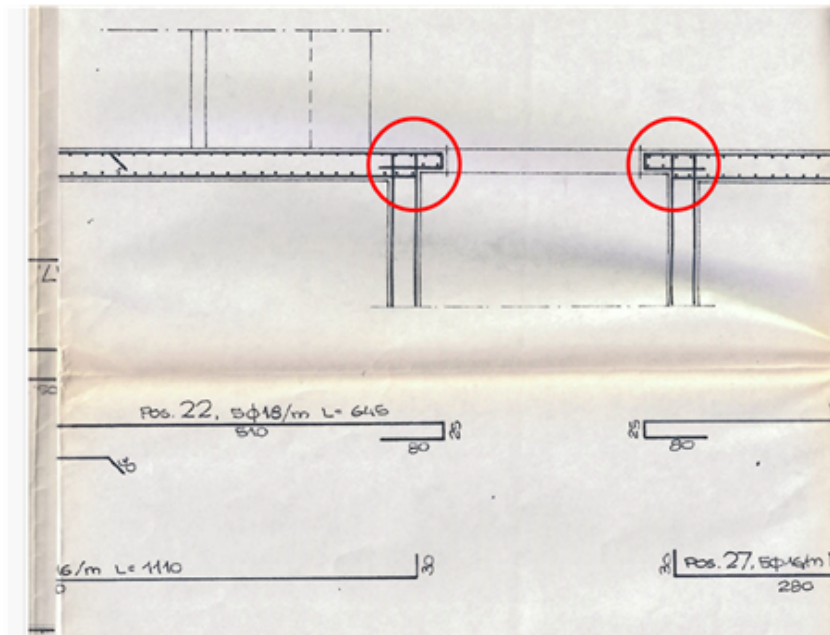


Figure 52 - Detail of the reinforced concrete structures to be modified for closure and partial restoration of the base slab in the affected areas below the existing INJ and DET towers.

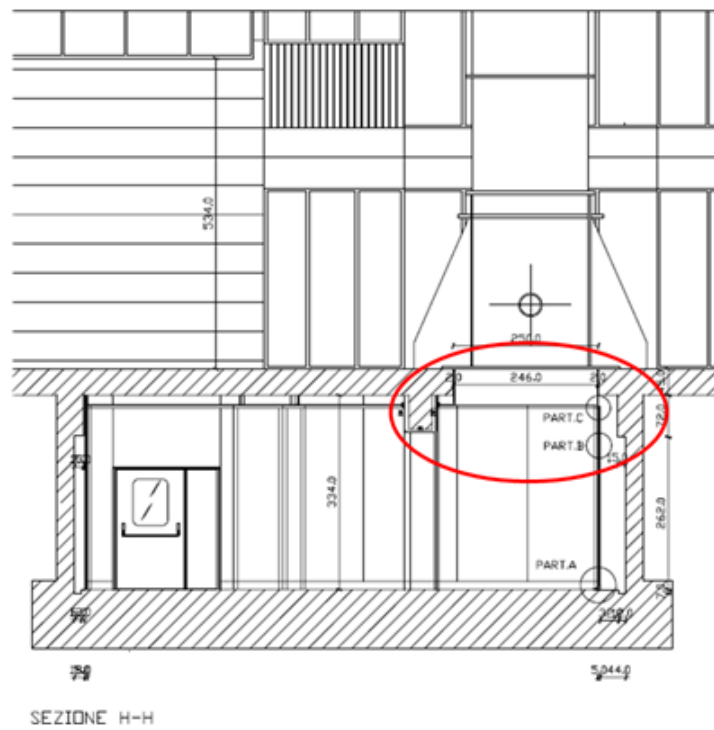


Figure 53 - Detail of the clean room zone underneath the current IT and DT towers affected by the disassembly, modification and restoration of the clean room walls and false-ceiling.

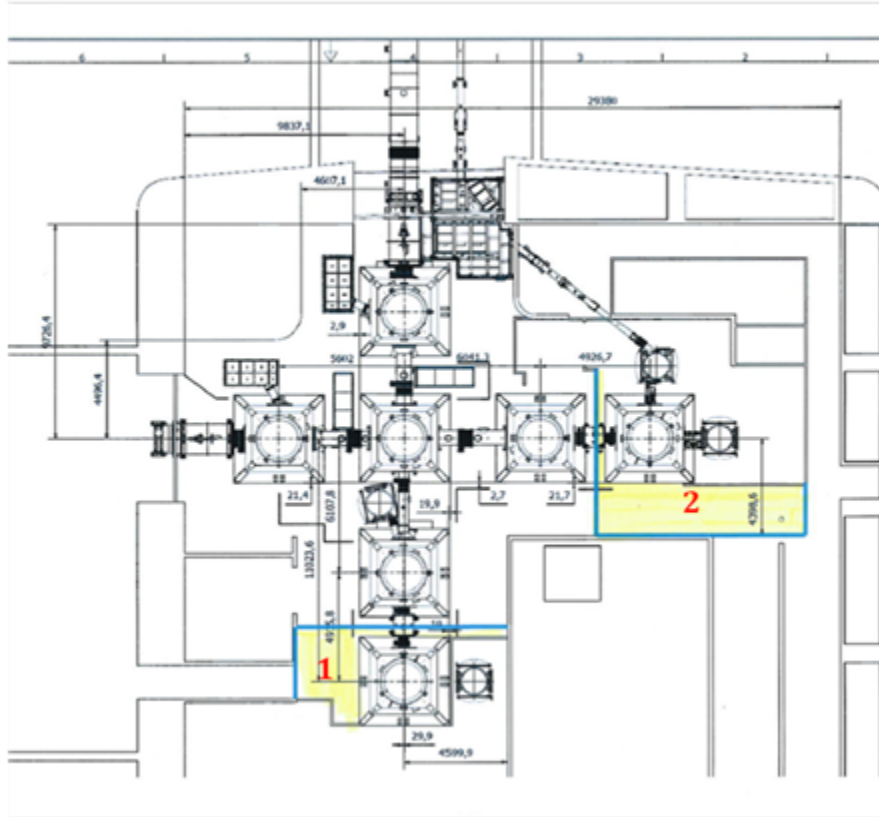


Figure 54 - Plan View of the CEB – INJ and DET Lab with highlighted the areas to be expanded for the installation of the new scientific equipment.

3. Costs

The preliminary estimate of the budget required to build the short recycling cavities is given in Figure 55. This estimate includes VAT and 20% of contingency.

	Stable cavities			
	Total	2024	2025	2026
INF	257	37	220	
INJ	278		200	78
DET	278		200	78
SLC	400		200	200
MIR	1500	1500		
TCS	150		100	50
Suspensions	3300	400	1500	1400
ALS	100		100	
DAQ	50		25	25
VAC	3030	360	2670	
Contingency	1869	459	1043	366
	11212	2756	6258	2197

Figure 55 - Budget for the short cavity solution and expenditure profile (2024-2026)

The table also shows the commitment profile. Please note that some of the works last for more than a year (e.g. mirrors) so the spending profile will be distributed over a slightly longer period.

Also in this case it should be noted that the commitments in 2024 concern the acquisition of components that are on the critical path. The EGO Council will deliberate on these urgent expenses in July 2024.

4. Schedule

The preliminary schedule (visible in Figure 56) includes all the elements of this configuration: vacuum system production and installation, together with the central hall preparation, and the production of the suspensions and mirrors, and the other equipment (DAQ, TCS, EMS...). The plan ends with the milestone “stable cavities ready for ITF commissioning”, approximately in mid 2027. The detailed plan can be

downloaded from the [Wiki](#). For the Short cavity option, the critical path is due to the realization and installation of the suspensions and the other equipment.

The installation plan of the other upgrades in view of O5, their pre-commissioning and the commissioning plan are not available at this stage. They will be assembled into a global Resource Loaded Schedule, based on the WBS of the different Subsystems, to be delivered with the overall TDR. Current best estimates roughly place the beginning of O5 for Virgo at fall 2028.

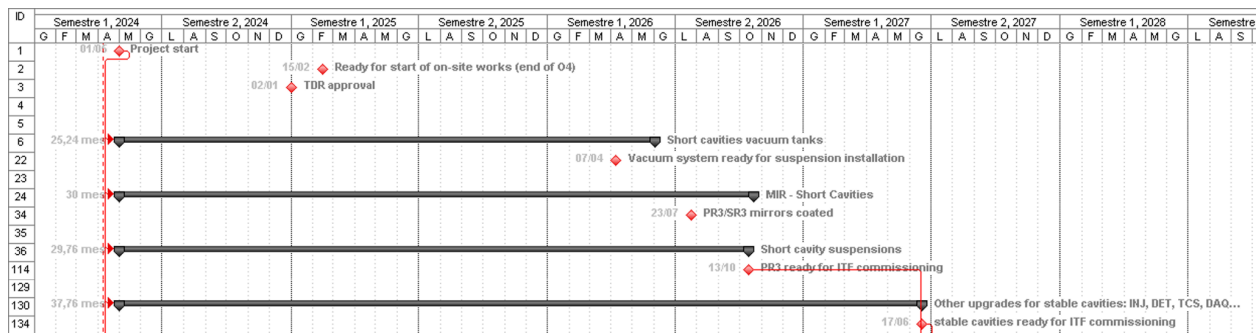


Figure 56 - preliminary production and installation planning for the short stable recycling cavities.

5. Risk assessment

During this initial design phase, aimed primarily at generating data for comparing short and long options, an initial risk assessment campaign has been conducted. A snapshot of the Risk Register, captured on January 23rd, 2024, can be downloaded from the AdV+ Wiki [page dedicated to stable cavities](#). Methods and criteria for evaluating the severity of various risks are outlined in documents [VIR-1088B-23](#) and [VIR-1112A-23](#). The outcomes of this initial assessment are detailed in document [VIR-0063B-24](#).

It's important to note that, at this stage, the complete risk management lifecycle outlined in the current Risk Management Plan ([VIR-1060A-23](#)) has not yet been implemented. This will be carried out during the production of the TDR.